Title

Analysis of the initiation, progression and therapy of BRAF(V600E) and KRAS(G12D)- driven non-small cell lung adenocarcinoma using conditional mouse models

Author

Trejo, Christy

Publication Date

2012

Peer reviewed|Thesis/dissertation

Analysis of the Initiation, Progression, and Therapy of BRAF(V600E) and KRAS(G12D) - driven Non-Small Cell Lung Adenocarcinoma Using Conditional Mouse Models

by

Christy L. Trejo

DISSERTATION

Submitted in partial satisfaction of the requirements for the degree of

DOCTOR OF PHILOSOPHY

in

Cell Biology

in the

GRADUATE DIVISION

of the

[redacted]

Acknowledgements

I would like to genuinely thank my advisor, Professor Martin McMahon, for allowing me the opportunity to work in his lab. I could not have asked for a better mentor to direct me through my various projects, presentations, and overall graduate school experience. Throughout my time in his lab, Martin has been very generous with his knowledge and very patient. His guidance has been the driving force of my success, and he is an overall fun guy to be around. I am honored to be the first graduate student to earn a Ph.D in his lab.

I owe a debt of gratitude to my thesis committee as well: Allan Balmain, Dean Sheppard, and Robert Blelloch. Their combined advice was invaluable in helping me achieve my many goals and hallmarks throughout graduate school. The enthusiasm and involvement they showed in my work was instrumental in helping me graduate on time and produce successful publications.

While in Martin's lab, I had the opportunity to work with many people. A big thanks goes to David Dankort, who advised me when I first settled into the lab for my thesis work. He taught me how to work with mice and got me started on the right foot. I would also like to thank Eric Collisson for his support and advice. He was a great help to me on my various projects and I am grateful that he included me in his. I would also like to thank every member of the McMahon Lab for their input and camaraderie, especially Shon Green, Joseph Juan, and Victoria Marsh for their direct contributions to my work. Furthermore, this work would not have been possible without collaborators such as Byron Hann for teaching me how to conduct bioluminescent imaging on mice, and Wayne Phillips for providing us with the *Pik3ca*$^{lat\text{-}H1407R}$ mouse.

Finally, I must thank my family- Gil, Cindy, and Adam Trejo, my boyfriend Jean-Francois Brazeau, my best friend Nicole Sangster, my dogs Myron and Elmo and my cat Bagheera. Without their love and support none of this would be possible.

Abstract

Analysis of the Initiation, Progression, and Therapy of $BRAF^{V600E}$ and $KRAS^{G12D}$ - driven Non-Small Cell Lung Adenocarcinoma Using Conditional Mouse Models

Lung cancer is the most prevalent malignancy in the industrialized world and is responsible for ~160,000 deaths/year in the USA. Genetic analysis indicates that activation of receptor tyrosine kinase signaling, through mutation of *EGFR, ALK, KRAS, BRAF* or *PIK3CA,* is common in non-small cell lung cancer (NSCLC), the most prevalent form of the disease. The use of genetically engineered mouse models allows for the evaluation of specific stages of disease and assessing the role of effector pathways downstream of driver mutations. Expression of mutationally activated $KRAS^{G12D}$ or $BRAF^{V600E}$ leads to lung tumorigenesis in genetically engineered mouse models. We have used models for the conditional activation of *KRas*, a gene commonly mutated in human non-small cell lung cancer, as well as *BRaf* and *Pik3ca*, two major downstream effectors of KRAS. In a head-to-head comparison of $KRAS^{G12D}$ vs. $BRAF^{V600E}$-induced tumorigenesis, $BRAF^{V600E}$ elicits an abundance of benign tumors that do not progress beyond low-grade adenomas while $KRAS^{G12D}$ driven tumors are fewer in number but often progress to adenocarcinoma. Despite this difference, both tumor types express the same distal lung cell type markers and remain sensitive to ERK1/2 pathway inhibition both in vivo and in vitro. In humans, *BRAF* and *KRAS* mutations are mutually exclusive in human lung cancer, but we found that activation of both oncogenes allows for the progression of tumors beyond

what is observed in the *KRas* model. Using a conditional mouse model for the activation of *Pik3ca* encoding the p110α^{H1047R} oncogene, we found that this oncogene is unable by itself to induce tumorigenesis in the mouse lung. However, when combined with the $BRAF^{V00E}$ or $KRAS^{G12D}$, $PIK3CA^{H1047R}$ expression greatly increases tumor growth, resulting in a dramatic decrease in survival. This effect is dependent of signaling through AKT. Finally, in cells isolated from $BRAF^{V600E}$- driven tumors, $PIK3CA^{H1047R}$ expressed both ectopically or endogenously promotes anchorage independent growth.

These studies demonstrate the importance of ERK1/2 activation in the establishment and maintenance of lung tumors, and mutational activation of $PIK3CA^{H1047R}$ is not sufficient to drive tumorigenesis but cooperates in a dramatic fashion with mutationally activated $BRAF^{V600E}$ or $KRAS^{G12D}$.

Table of Contents

List of Figures

List of abbreviations:

AAH- atypical adenomatous hyperplasia

AdCre – Adenovirus expressing Cre Recombinase

AQP5- Aquaporin 5

BrdU- Bromo-deoxy Uridine

CA- conditionally activated

CC3- Cleaved Caspase 3

CCA- Clara Cell antigen

COPD- Chronic obstructive pulmonary disease

DAB- Diaminobenzidine

DMSO- Dimethyl Sulfoxide

EH- Epithelial hyperplasia

EGF- Epidermal growth factor

EGFR- Epidermal growth factor receptor

EMT- Epithelial to mesenchymal transition

GEF- Guanine nucleotide exchange factor

GEMMs- Genetically engineered mouse models

GAP- GTPase activating protein

GTP- Guanosine tri-phosphate

LSL- lox-stop-lox

MAPK- Mitogen Activated Protein Kinase

NSCLC- Non-small cell lung cancer

OIS- Oncogene induced senescence

PCR – Polymerase chain reaction

PFU- Plaque forming units

PH- Pleckstrin homology

PI3'K- Phosphatidyl-Inositol 3' Kinase

PI- Propidium Iodide

SCLC- Small cell lung cancer

SH2- Src homology 2

SPC- Surfactant protein C

CHAPTER 1: Introduction

Non-small cell lung cancer

Lung cancer is the most prevalent malignancy in the industrialized world and was responsible for ~160,000 deaths in the USA in 2008 (CDC). It is the leading cause of cancer deaths worldwide. Despite its prevalence and strikingly high mortality rates, the cellular origins of lung cancer remain obscure and therapeutic approaches to treat the disease have proven disappointingly ineffective. Consequently, the 5-year survival rate for patients with advanced lung cancer remains low, emphasizing the need for new therapeutic approaches to treat this disease. Lung cancers are classified as either non-small cell lung carcinoma (NSCLC) or small cell lung carcinoma (SCLC), which account for 85% and 15% of cases, respectfully (1). NSCLC is further divided in three subtypes: large cell carcinoma, squamous cell carcinoma, and adenocarcinoma- the most common subtype for both smokers and non-smokers.

The standard therapeutic intervention for lung cancer is chemotherapy combined with radiation. Patient prognosis following this treatment regime is poor while toxicity and non-specificity remain a problem. Recently, the genetic heterogeneity of lung cancer has been understood in more detail and in a manner that has direct implications for generating targeted therapy (2). For example, mutational activation of *ERBB1*, encoding the EGF receptor (EGFR), predicts for a good clinical response to EGFR inhibitors such as Tarceva (3). Similarly, lung cancers expressing an oncogenic EML4-ALK fusion protein respond well to Crizotinib, an inhibitor of ALK and MET protein kinases (4). KRAS, a GTP-binding protein, is the most commonly

mutated gene in NSCLC with a frequency of ~25% (5). This mutation is mutually exclusive to other commonly found mutations such as EGFR and BRAF, does not respond to either EGFR or ALK inhibitors and, at least with Tarceva, the use of EGFR inhibitors is contra-indicated (6). KRAS activates a multiplicity of effector proteins including (but not limited to) RAF protein kinases, PI3'-lipid kinases and RAL-GDS, a guanine nucleotide exchange factor for RAL family GTPases (7). In addition, there are known mutational frequencies in KRAS effector pathways. *BRAF*, which encodes for a serine kinase immediately downstream of KRAS in the MAPK signaling cascade, has a mutational frequency of 1-3% in lung cancer (8). The phosphatidyl-inositol 3' kinase (PI3'K) pathway is also often deregulated in human tumors through activating mutations in the *PIK3CA* gene encoding the catalytic subunit of PI3'K. A recent study found that 2% of human lung adenocarcinoma harbor mutations in *PIK3CA* (9). *AKT*, the most studied effector of PI3'K, is often found to be over-expressed or amplified in a variety of human tumors (10). Furthermore, loss of heterozygosity of negative regulator *PTEN* has been found in ~50% of cases (11). PTEN is a lipid phosphatase that directly counteracts the effects of PI3'K signaling.

Since mutationally activated KRAS remains an intractable pharmacological target, defining the relevant roles of RAS effector pathways in lung cancer is of critical importance. All the more so since potent and specific inhibitors of protein or lipid kinases that serve as RAS effectors are being clinically tested for a number of different cancers (12). Examples of compounds that have entered clinical trials include inhibitors targeting members of the MAPK pathways (such as RAF, MEK, and ERK), as well as the PI3'K signaling arm (such as PI3'K, AKT and mTOR). Predicting the success of targeted therapy in the clinic can be made possible with the

use of mouse models that recapitulate human disease based on specific mutations.

RAS signaling

RAS relays extracellular stimuli to the nucleus to alter gene expression and promote a wide variety of cellular processes such as proliferation and differentiation. Growth factor- bound receptor tyrosine kinase dimers cross phosphorylate to create docking sites for intracellular signaling proteins containing SH2 domains. Grb-2, an adaptor protein, binds to the activated receptor and is then bound by SOS, a Guanine nucleotide exchange factor (GEF). Once in proximity to membrane associated RAS, SOS promotes the exchange of hydrolyzed GDP for GTP, thereby activating Ras.

Active, GTP-bound RAS signals downstream to the MAPK and PI3'K to promote growth and survival of the cell (Fig. 1-1). RAS has a low intrinsic GTPase activity that hydrolizes GTP to render itself inactive, hence RAS-GTP inactivation is promoted by GTPase activating proteins (GAPs). The most common mutation in *KRAS* encodes for a glycine to aspartic acid substitution in codon 12, rendering it insensitive to GAPs, and thus constitutively active, promoting cell proliferation and inhibiting apoptosis.

The most studied effector pathway of RAS is the MAP Kinase (MAPK) signaling cascade. This highly conserved pathway is responsible for relaying extracellular signals throughout the cell to regulate gene expression. RAF is recruited to the plasma membrane by RAS where it is then activated by other kinases and phosphatases. RAF then phosphorylates and activates MEK 1 and MEK 2. These are dual-specificity kinases, which then activate ERK 1 and ERK 2 by Dual threonine and tyrosine phosphorylations. Activated ERK 1/2 then translocate to the nucleus

and phosphorylate a host of effectors, including transcription factors that regulate the expression of G1 Cyclins. The requirement for multiple phosphorylation events on MAP Kinases ensure specificity and despite short-lived extracellular stimuli, cascade activation results in a sustained cellular response. Because this pathway promotes cell proliferation, deregulation has pathological consequences. The most prevalent mutation in this pathway occurs in gene encoding the RAF protein family member, *BRAF*. The most commonly occurring mutation in *BRAF* (90% of all *BRAF* mutations) is a T1799A transversion that encodes a valine to glutamic acid substitution within the activation segment of the kinase domain (13). This mutation obviates the need for activation by upstream kinases on Thr 599 and Ser 602 and leads to constitutive kinase activity. *BRAF* mutations most commonly occur in melanoma but are found in a wide variety of human cancers including lung, colon, and thyroid. The mutational frequency of *BRAF* in human cancers implies that its activation promotes cell growth and it is a major oncogenic effector pathway in *RAS*- driven cancers.

Another major effector pathway of RAS that regulates cell growth and survival is the PI3'K signaling pathway. PI3'K catalyzes the phosphorylation of the 3' OH of cytosolic phosphatidylinositol 4,5 bisphosphate (PI[3,4]P2) to produce phosphatidyl-inositol 3,4,5 triphosphate (PI[3,4,5]P3). This modified lipid serves as a docking site for a number of signaling molecules that can then become activated to promote survival of the cell. PI3'K can either bind activated receptor tyrosine kinases directly through a pair of SH2 domains in its p85 regulatory subunit, or can be activated by GTP-bound RAS through a RAS-binding domain in the catalytic subunit. Both interactions relieve an intrinsic negative feed-back which allows PI3'K to phosphorylate its lipid substrate. The activity of PI3'-kinase is antagonized by the action of the PTEN tumor suppressor, which encodes a PI3'-lipid phosphatase.

PI(3,4,5)P3 serves as a docking site on which intracellular proteins containing pleckstrin homology (PH), phox homology (PX), or FYVE domains may bind and activate downstream signals. One such protein, AKT (PKB), binds and is then phosphorylated and activated by PDK. Activated AKT can inhibit the pro-apoptotic BCL family members and phosphorylate Mdm2 to inhibit p53, thus promoting cell survival. Furthermore, active AKT can promote growth through its effects on the mTOR pathway. AKT inhibits the TSC complex, thereby activating mTORC1 and ribosomal S6 Kinase. Activated mTOR also phosphorylates 4EBP1, causing it to release of eIF4E and allow for Cyclin D and Myc translation. AKT signaling also promotes cell proliferation through its inhibitory effects on negative regulators of the cell cycle such as FOX01, GSK3ß, (an inhibitor of cyclin D), p27, and p21.

Many cancers have hyperactivation of PI3'K> AKT signaling. One of the most common mechanisms is through loss of PTEN. Germline mutations in PTEN have been discovered in a number of familial cancer sydromes such as Cowdens. Patients with this syndrome have an increased susceptibility to cancers in the thyroid, breast, and endometrium (14). Loss of expression of PTEN can occur through point mutations, epigenetic silencing, or post-translational modifications. Furthermore, activating mutations are commonly found in the *PIK3CA* gene. Mutations in *PIK3CA* predominantly occur in two hotspots, the helical and catalytic domains. These mutations are common in a wide variety of cancers, including about 2% non-small cell lung carcinomas (9). AKT, the most studied effector of PI3'K, is often found to be over-expressed or amplified in a variety of human tumors (10).

Genetically engineered mouse models of human cancer

Genetically engineered mouse models (GEMMs) for human cancer have allowed

for the analysis of cancer phenotypes driven by specific genetic lesions. Such systems serve as preclinical platforms for the evaluation of novel therapeutics. The sequencing of the mouse genome has revealed genetic similarities with humans and has made mice the most widely used model for cancer. Early mouse models relied on spontaneous tumors in inbred strains or carcinogen-induced disease. Later, the ability to manipulate mouse embryonic stem (ES) cells revolutionized the field and paved the way for a vast number of specific cancer models to be developed. Eventually, the development of transgenic mice involving over-expression of viral or cellular oncogenes, and knockouts- in which tumor suppressor function is lost- allowed for a better ability to relate genotype to phenotype. Gene targeting strategies such as the knock-in approach prevented variability in phenotype associated with random integration of exogenous DNA into the genome. One problem commonly encountered through germ line manipulation is embryonic lethality. Additional limitations of such approaches include the inability to target mutations to specific tissues and the complications of cell non-autonomous effects. Thus, conditional mouse models, in which somatic mutations may be induced in specific cell types in an investigator-controlled manner to better mimic sporadic human tumors, were developed.

The most widely used conditional models rely on chemically induced transcription factors, such as the tetracycline-dependent regulatory system, which allows for the switching on and off of transgenes at specific times. Another popular inducible system involves a fusion product consisting of an oncogene of interest and the hormone binding domain of the estrogen receptor in which the protein is rendered inactive until hormone binding activates it. These systems allow for gene expression in a time controlled manner and evaluating effects of tumors upon loss of oncogene

expression. Two potential downfalls include poor inducibility, or expression in the absense of an inducer (leakiness).

Site-specific recombination using the Cre-*lox*P system is a way to alter DNA in a tissue and time specific manner without genomic integration, leakiness, or overexpression. It allows for the expression of an oncogene from its endogenous promoter and does not alter protein structure, allowing for interaction with binding partners in the cell. Cre Recombinase from P1 bacteriophage recognizes two 34 base pair sequences and catalyzes recombination between them. A common example of this strategy involves inserting a DNA segment flanked by loxP sites (floxed) between a promoter and a mutated gene. Expression of Cre recombinase results in deletion of the DNA segment containing a stop element, and the oncogene can then be expressed. Constructs can be targeted to the proto-oncogene to avoid the use of transgenic promoters and allow for oncogene expression at the physiological level in specific cell types. In the Cre-*lox*P system, controlling the recombination event is what determines how and when the oncogene is expressed. Crosses can be performed with transgenic mice in which Cre Recombinase is expressed from a tissue specific promoter or Cre can be delivered through an exogenous source controlled by the investigator. An example of this is using viral vectors such as retrovirus, adenovirus, or lentivirus. Additional advantages of this delivery system include the ability to control tumor multiplicity by tittering the virus. Additionally, the investigator can control the onset of tumor initiation and thus follow tumor progression through time.

Conditional Mouse Models of KRAS- and BRAF- induced lung tumorigenesis

Conditional mouse models are the preferred method to study KRAS or BRAF

oncogenesis since small changes in activity of RAS and RAF can dramatically alter biological outcome (15, 16). One of the most widely used tools to explore $KRAS^{G12D}$ driven tumorigenesis is the $KRAS^{LSL}$ conditional mouse model. Intranasal instillation of Adenovirus expressing Cre Recombinase (AdCre) causes recombination of the conditional allele in the distal lung epithelium. This allows from the expression of mutated exon 1 by the removal of an upstream stop element. $KRAS^{G12D}$ is then expressed from its endogenous promoter at physiological relevant levels (Fig. 1-2A), (17). At early time points (2-6 weeks), mice develop atypical adenomatous hyperplasias (AAH) and epithelial hyperplasias (EH). After six weeks, low-grade adenomas are present, and at later time points (16+ weeks), a fraction of tumors can be classified as high-grade adenocarcinomas (Fig 1-2B). The majority of tumors found at late time points are low grade and not highly proliferative, suggesting that progression requires a stochastic event to bypass a growth arrest phenotype. Loss of p53 in these tumors greatly increases the likelihood of tumor progression, and in this case local invasion and metastasis may occur (18).

Our lab has developed a conditional mouse models for $BRAF^{V600E}$ driven tumorigenesis that is analogous to the $KRAS^{G12D}$ model. In the $BRaf^{CA}$ mouse model, normal BRAF is expressed from a conditional allele prior to Cre mediated recombination. *Lox*P sites flank human cDNA encoding wild type exons 15-18, followed by a strong stop element. Cre mediated recombination removes this and allows for the expression of mutated exon 15, encoding the $BRAF^{V600E}$ oncoprotein. $BRaf^{CA}$ express normal BRAF from the $BRaf^{CA}$ alele and Cre mediated recombination allows for expression of the V600E oncoprotein at physiological levels with normal patters of splicing and exon usage (Fig 1-3A). $BRaf^{CA}$ mice infected with AdCre developed a high multiplicity of lesions in the lung. Similar to what is observed in

KRas^{LSL} mice, early time points present small hyplerplasias, however at mid to late time points, only benign adenomas were found (Fig1-3B). All tumors had normal papillary structure and nuclear morphology, and low levels of proliferation (Fig 1-3), (19). Loss of key tumor suppressors such as p53 (deleted conditionally through Cre-mediated recombination) allows for tumor progression to high- grade adenocarcinoma. These tumors have a greatly increased proliferation index and widespread nuclear abnormalities.

PD0325901 is a potent and specific inhibitor of MEK 1/2 that binds adjacent to the ATP pocket to interfere with kinase activity in an allosteric manner (20). Use of this small molecule inhibitor has demonstrated the requirement for MAPK signaling in BRAF^{V600E} - driven tumorigenesis. Treatment of *BRaf*^{CA} mice with PD0325901 starting four weeks after AdCre infection were largely tumor free after six weeks of treatment.

Use of genetic tools such as conditional mouse models as well as biochemical tools such as small molecule inhibitors allow for the analysis of specific pathways and the roles they may play in the initiation and progression of non-small cell lung cancer. The aim of this study is to further interrogate the role of the MAPK signaling pathway in both KRAS- and BRAF- mediated lung tumorigenesis. *KRas*^{LSL} and *BRaf*^{CA} mice allow for the comparison of oncogene expression in a manner that is physiologically relevant and correlative of human NSCLC. I have compared and contrasted both tumor types in a head to head manner, which had not been conducted before. Specific pathway activation was assessed using small molecule inhibitors of MAPK signaling in both *KRas*^{LSL} and *BRaf*^{CA} mice. An in vitro system using cell lines isolated from tumors in each mouse also serve as a means to interrogate pathway activation downstream of each oncogene.

A mouse model for the conditional activation of mutated PI3'K was also analyzed. Following Cre mediated recombination, *Pik3ca*$^{lat\text{-}H1047R}$ mice express the p110α^{H1047R} mutation in the catalytic domain of PI3'K from the endogenous promoter. This mouse was used to determine if hyperactive PIK3CA^{H1047R} could drive lung tumor initiation much like KRAS and BRAF. Furthermore, the affects of expressing PIK3CA^{H1047R} alongside KRAS^{G12D} and BRAF^{V600E} were assayed. The aim of this study was to determine the importance of PI3'K>AKT signaling in the mouse lung on its own, as well as in the context of tumors driven by KRAS and BRAF.

I have also explored the effects of inducing a pro-inflammatory environment in BRAF^{V600E} tumors. It is possible that progression observed in the KRAS^{G12D} lung tumor model is a result of inducing inflammation in the microenvironment. Inducing inflammation in *BRAF*^{CA} mice through knockout of genes that inhibit inflammation, as well as intranasal challenge with an antigen could potentially mimic what is observed in KRAS tumors and cause BRAF^{V600E} tumors to progress to adenocarcinoma.

Fig 1-1

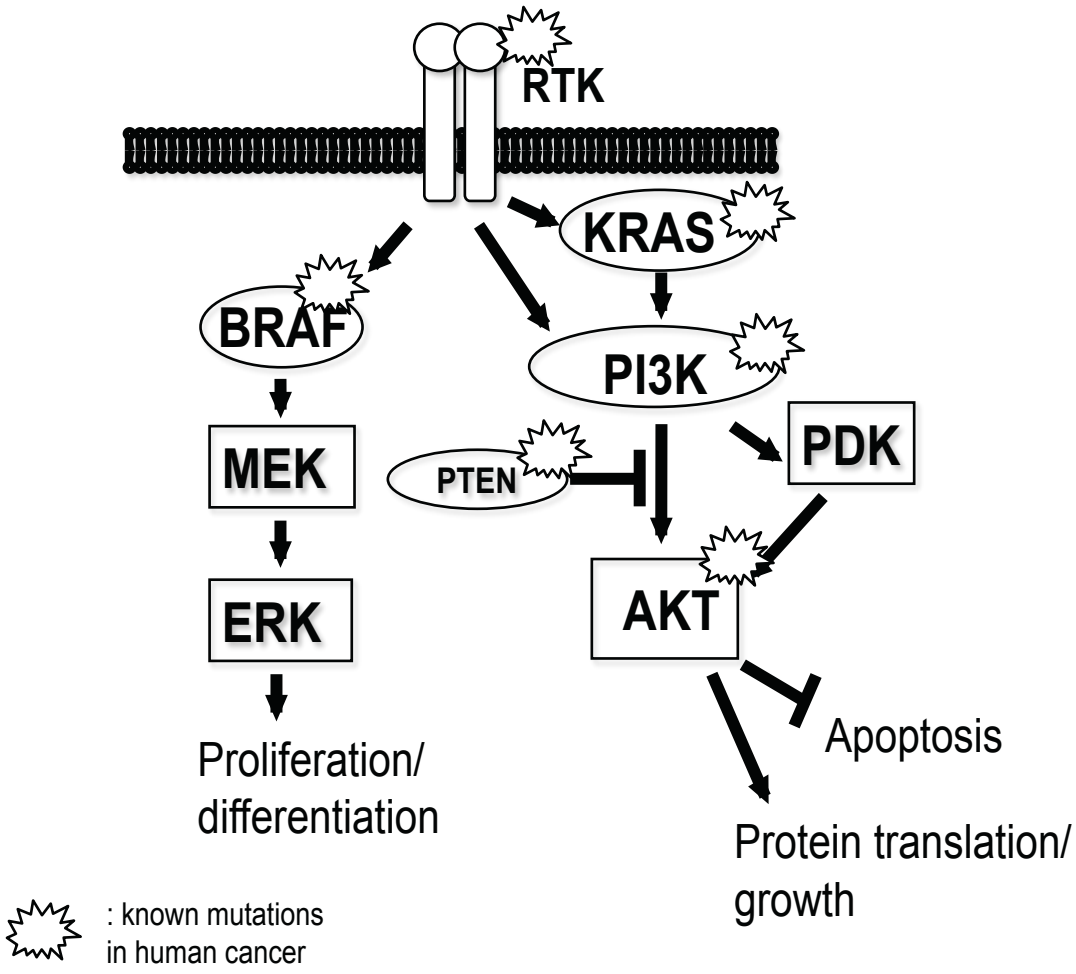
RTK
KRAS
BRAF
PI3K
MEK
PTEN
PDK
ERK
AKT
Apoptosis
Proliferation/
differentiation
Protein translation/
growth
: known mutations
in human cancer

Fig. 1-2

A

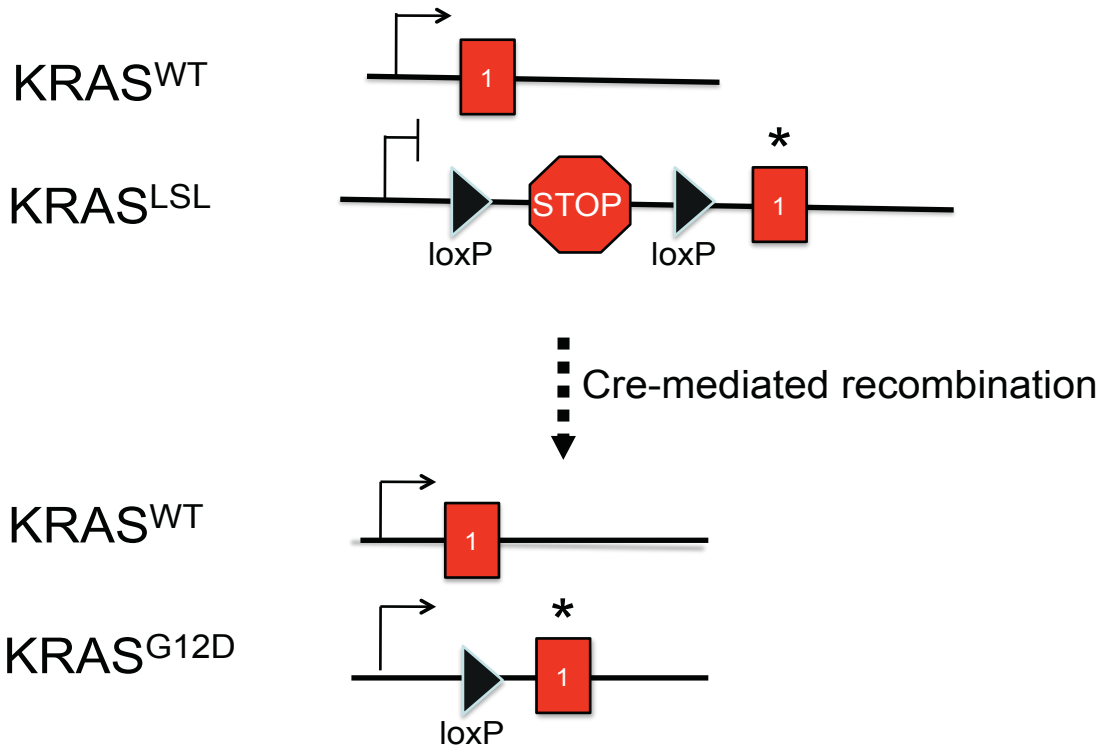
KRAS^WT
KRAS^LSL
1
STOP
1
*
loxP
loxP
Cre-mediated recombination
KRAS^WT
KRAS^G12D
1
1
*
loxP

B

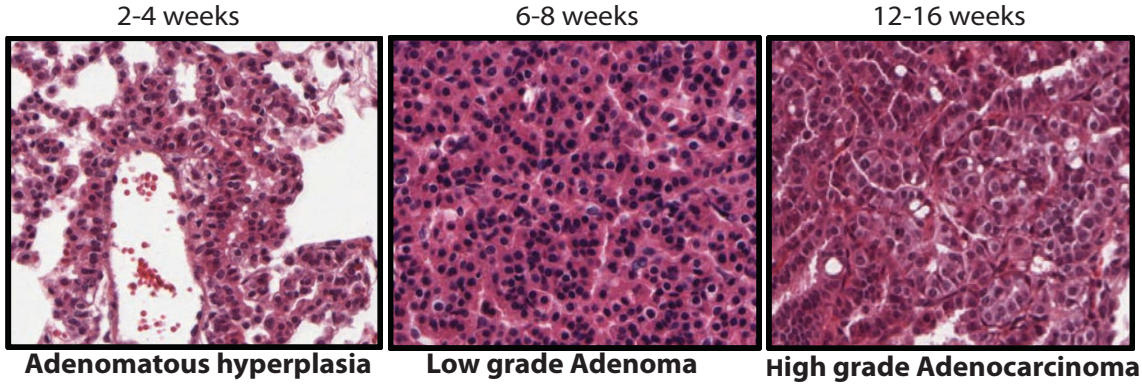
2-4 weeks
6-8 weeks
12-16 weeks
Adenomatous hyperplasia
Low grade Adenoma
High grade Adenocarcinoma

Fig 1-3

A

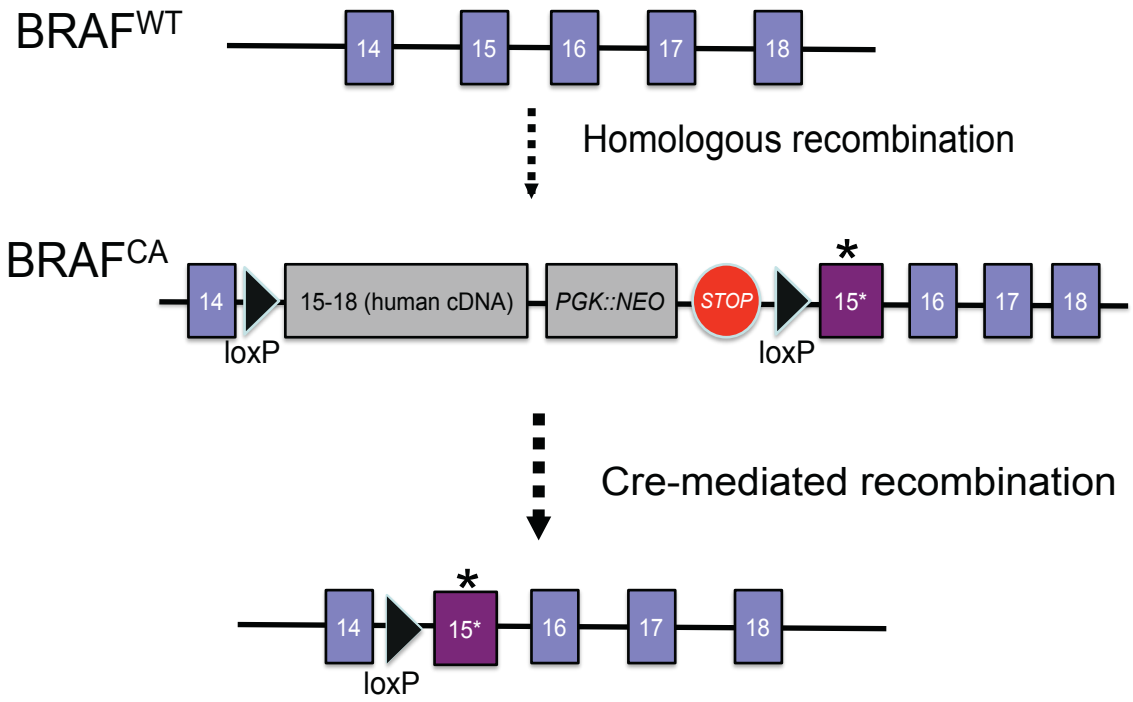
BRAF^WT
14
15
16
17
18
Homologous recombination
BRAF^CA
14
loxP
15-18 (human cDNA)
PGK::NEO
STOP
loxP
15*
16
17
18
Cre-mediated recombination
14
15*
loxP
16
17
18

B

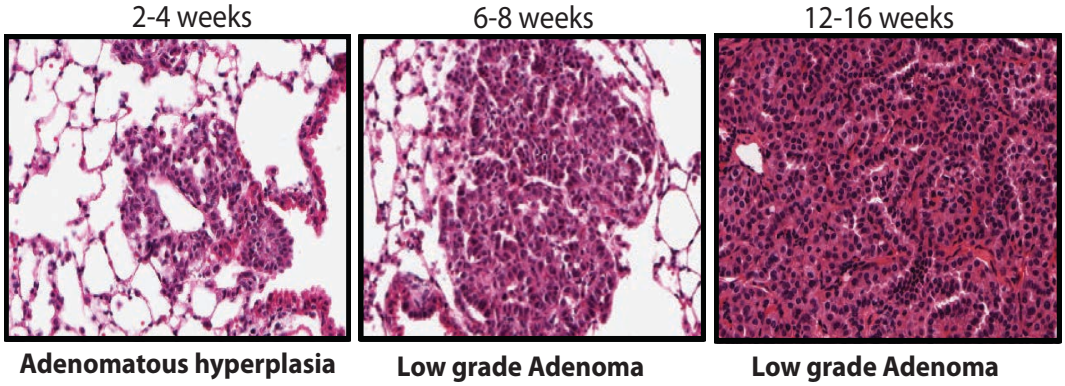
2-4 weeks
6-8 weeks
12-16 weeks
Adenomatous hyperplasia
Low grade Adenoma
Low grade Adenoma

CHAPTER 2: Autochthonous KRAS^{G12D}- or BRAF^{V600E}-induced lung tumors are sensitive to the anti-tumor effects of MEK1/2 inhibition

BRaf^{CA} mice display an earlier onset and higher multiplicity of lung tumors than *KRas*^{LSL} mice

Genetically engineered *KRas*^{LSL} or *BRaf*^{CA} mice carrying knock-in alleles of *KRas* or *BRaf* respectively at the normal chromosomal loci allow for conditional expression of either oncogenic KRAS^{G12D} or BRAF^{V600E} in response to Cre recombinase (17, 19). In both of these mouse strains intranasal instillation of Cre expressing Adenovirus (Ad-Cre) elicits oncogene expression in the lung epithelium in a manner in which the timing and frequency of oncogene expressing cells can be investigator controlled. Lung epithelium expression of KRAS^{G12D} is reported to lead initially to atypical alveolar hyperplasia (AAH) and then to the development of benign lung adenomas and ultimately to development of malignant non-small cell lung cancers (17). Lung epithelium expression of BRAF^{V600E} also leads initially to AAH and then to benign lung adenomas but progression to frank malignancy is rare and appears to be constrained by cellular senescence (19). Despite their similarities, a thorough side-by-side comparison between these two models of lung tumorigenesis has not yet been conducted.

To minimize the influence of genetic modifiers of lung tumorigenesis on our experiments, *BRaf*$^{CA/+}$ and *KRas*$^{LSL/+}$ mice were bred into an FVB/N genetic background for a minimum of four generations and were then bred together to generate compound *BRaf*$^{CA/+}$; *KRas*$^{LSL/+}$ mice. These mice were further intercrossed for at least three generations. Experimental mice were generated by breeding compound *BRaf*$^{CA/+}$; *KRas*$^{LSL/+}$ heterozygous mice with FVB/N mice resulting in

progeny heterozygous for either *BRaf*^{CA} or *KRas*^{LSL} alleles on a predominantly FVB/N genetic background.

The lung epithelium of *BRaf*$^{CA/+}$ or *KRas*$^{LSL/+}$ littermates was infected with 10^7 pfu of Ad-Cre to initiate expression of BRAF^{V600E} or KRAS^{G12D} oncoproteins respectively. Mice were euthanized at 6 or 17 weeks following initiation of oncogene expression at which time lungs were processed for tumor analysis. Average tumor number and size was quantified and percentage tumor burden was calculated as the area occupied by tumors/total lobe area as described in Materials and Methods.

6 weeks post-initiation, BRAF^{V600E} expression led to numerous detectable lung tumors whereas very few lung tumors were detected in mice with KRAS^{G12D} expression in lung epithelium (Figs. 2-1 A & B). 6 weeks after Ad-Cre infection of *BRaf*^{CA} mice they had an average of ~23 lesions/lobe whereas similarly treated *KRas*^{LSL} mice had an average of ~3 lesions/lobe (*p =.0017*, Figs. 2-1 A & B). In addition, individual tumors in the lungs of initiated *BRaf*^{CA} mice were approximately 8 times larger than lesions initiated in *KRas*^{LSL} mice (50,370.3μm^2 vs. 6,231.8μm^2, Figs. 2-1 A & B), (*p<.0001*). At 6 weeks overall lung tumor burden was significantly higher in *BRaf*^{CA} mice (average of 7.3% of lung area was tumor bearing), whereas lung tumor burden in *KRas*^{LSL} mice was ~0.28% (*p<.0006*, Figs. 2-1 A & B).

At 17 weeks post-initiation, lung tumors in *BRaf*^{CA} mice were confluent in many areas of the lung lobes, making individual tumor number and size difficult to quantify. For this reason, only tumor burden was quantified. Lungs of *BRaf*^{CA} mice displayed approximately 26% tumor burden while *KRas*^{LSL} mice had a burden of approximately 9% (p = .0009, Figs. 2-1 A & B). It was not possible to compare lung tumor burden between Ad-Cre treated *BRaf*^{CA} or *KRas*^{LSL} mice at later time points due to the extensive tumor burden in the *BRaf*^{CA} mice, which led to respiratory distress and weight loss such that these mice had to be euthanized. By contrast, at a time when

all of the Ad-Cre treated *BRaf*^{CA} had been euthanized all of the similarly treated *KRas*^{LSL} mice appeared healthy and maintained a normal weight despite the obvious lung tumor burden that they presented at euthanasia.

BRAF^{V600E}*-induced lung tumors fail to progress beyond low-grade, benign adenomas*

To better characterize KRAS^{G12D}- or BRAF^{V600E}- induced lung tumors, lesions were classified as epithelial hyperplasia (EH), adenomatous hyperplasia (AH) or adenomas. EH was classified as regions of hyperplasia originating from or directly associated with airways. Adenomatous hyperplasias were defined as hyperplasias originating from the alveoli and measuring 100μm in diameter or less. Adenomas (lesions >100μm) were classified as being high or low grade depending on the degree of cellular atypia. Percentage of each tumor type per lobe was calculated as area of specific lesion type/area of total lesion area. The statistical significance of differences in lung tumorigenesis between *BRaf*^{CA} versus *KRas*^{LSL} mice was assessed using the exact Wilcoxon rank sum test.

At six weeks, the lungs of Ad-Cre treated *BRaf*^{CA} or *KRas*^{LSL} mice had a similar percentage of EH (9% and 12.5%, respectively, p = 0.23, Fig. 2-1C*)*. The majority (~74%) of lesions in *BRaf*^{CA} mice were fully formed, low-grade adenomas, compared to only 5% of such lesions in the *KRas*^{LSL} mice (p =0.002). Indeed, at six weeks, the vast majority (85%) of the lesions in the *KRas*^{LSL} mice were adenomatous hyperplasias compared to only 17% of such lesions in *BRaf*^{CA} mice (p =0.04).

At 17 weeks, there was no significant difference in the percentage of epithelial hyperplasias between *BRaf*^{CA} and *KRas*^{LSL} mice, (1.3% vs. 4% respectively, p= 0.52). Adenomatous hyperplasias were more prevalent in *KRas*^{LSL} mice compared to *BRaf*^{CA} *mice* (30% vs. 11% respectively, p = .0005). The percentage of low-grade

adenomas remained significantly higher in *BRaf*^{CA} mice compared to *KRas*^{LSL} mice (88% vs. 56% respectively, p= 0.002). Importantly, high-grade adenomas were only observed in *KRas*^{LSL} mice, where they comprised 10% of the total lung lesions (p=0.02, Fig. 2-1C).

The majority of BRAF^{V600E}-induced lung tumors appeared benign and adenomatous with a structured papillary pattern made up of seemingly well-differentiated, cuboidal epithelial cells and did not display characteristics of high-grade tumors (Fig. 2-1D). These observations are in accord with our previous studies demonstrating the benign nature of BRAF^{V600E}- induced lung tumors and their low rate of spontaneous malignant progression (19). By contrast, despite the overall lower tumor burden, lung tumors in *KRas*^{LSL} mice frequently appeared to be of higher grade, as evidenced by nuclear atypia such as prominent nucleoli and an increased nucleus to cytoplasm ratio (Fig. 2-1D). Finally, we observed no evidence of either local invasion, pleural effusion or distant metastatic spread in lung tumors arising in either *BRaf*^{CA} or *KRas*^{LSL} mice, which is consistent with our previous observations and those of others (19, 21).

To determine if there was a difference in proliferation rate of KRAS^{G12D}- versus BRAF^{V600E}-induced lung tumors 17 weeks after initiation, appropriate mice were injected with BrdU ~20 hours prior to euthanasia. Lung sections were stained with antibodies against BrdU and Surfactant Protein (SP-C), a marker for alveolar type 2 pnuemocytes expressed in KRAS^{G12D}- and BRAF^{V600E}-induced lung tumor cells (17, 19). Tumor cell specific proliferation was assessed by measuring the percentage of SP-C+ cells that stained for BrdU incorporation by double label immunofluorescence. By these criteria, 0.98% of BRAF^{V600E} expressing tumor cells and 1.67% of KRAS^{G12D} expressing tumor cells were BrdU positive respectively (p = 0.12, Fig. 2-2). These data were confirmed by double label immunofluorescence for Ki67/SP-C positive

cells. By these criteria, 2.35% of $BRAF^{V600E}$ expressing and 4.53% of $KRAS^{G12D}$ expressing tumor cells were Ki67/SP-C double positive (p = 0.08, Fig. 2B). Hence, at 17 weeks $KRAS^{G12D}$- and $BRAF^{V600E}$-expressing tumors display a low proliferative index that is not significantly different from one another.

We next assessed signal pathway activation downstream of oncogenic $KRAS^{G12D}$ or $BRAF^{V600E}$ by immunohistochemical staining for phospho-ERK1/2 (pERK1/2) or phospho-S6 (pS6) in low- or high-grade adenomas. In general, the levels of pERK1/2 and pS6 were low but detectable in both $BRAF^{V600E}$ and $KRAS^{G12D}$-induced low-grade adenomas. Moreover, we did not detect a substantial elevation in pERK1/2 in $KRAS^{G12D}$-induced high-grade adenomas although elevated pS6 was detected in these tumors (Fig. 2-3). These data are consistent with the previous observations that neither $KRAS^{G12D}$ nor $BRAF^{V600E}$ induce high-level signal pathway activation during the early stages of lung tumorigenesis (22).

$BRAF^{V600E}$- and $KRAS^{G12D}$- induced lung tumors express markers of Alveolar type 1 and type 2 pneumocytes

To further characterize lung tumors arising in Ad-Cre treated $BRaf^{CA}$ or $KRas^{LSL}$ mice we stained for expression of markers of epithelial cells of the terminal bronchioles and alveoli: Clara Cell Antigen (CCA); Surfactant Protein-C (SP-C) and Aquaporin 5 (AQP5). Clara cells are CCA positive but negative for SP-C and AQP5. Alveolar type 2 (AT2) pneumocytes are SP-C positive but negative for CCA and AQP5. Alveolar type 1 (AT1) pneumocytes are AQP5 positive but negative for CCA and SP-C. As previously reported, adenomas arising in both the $BRaf^{CA}$ and $KRas^{LSL}$ mice were uniformly CCA negative (data not shown). However, both $BRAF^{V600E}$- and $KRAS^{G12D}$-induced lung tumors were double positive for both SP-C and AQP5, a combination of marker expression not readily detected in the normal

mouse lung epithelium. SP-C was localized in a punctate manner inside tumor cells consistent with its sequestration into lamellar bodies that are characteristic of AT2 cells (23). AQP5, an integral membrane water channel, localization appeared membranous and expressed asymmetrically on tumor cells consistent with its normal expression on the apical surface of AT1 cells (Fig. 2-4A). To rule out the possibility that the apparent double positivity of lung tumor cells for both SP-C and AQP5 was not simply due to the close juxtaposition of two different cell types, we analyzed $BRAF^{V600E}$-induced lung tumors by electron microscopy. This analysis revealed that $BRAF^{V600E}$-induced tumors were comprised of cuboidal AT2-like cells with prominent lamellar bodies (Fig. 2-4B, red arrow) and were not infiltrated by normal AT1-like cells. To further analyze the extent of tumor cell expression of AT1 markers, we stained for RAGE (Receptor for Advanced Glycosylation End Products) and Podoplanin. However, neither $BRAF^{V600E}$- nor $KRAS^{G12D}$-induced lung tumors expressed either of these proteins (data not shown). To test whether this combination of marker expression is observed in human lung cancer, we stained sections of eight lung cancers with documented $BRAF^{T1799A}$ mutation with antisera against CCA, SP-C or AQP5 (24). However, these lung cancers were uniformly negative for the expression of these markers (data not shown).

To allay concerns regarding the specificity of the anti-AQP5 antibody and to test for a possible role of AQP5 in lung tumorigenesis, we generated $BRaf^{CA}$ mice homozygous for a null allele of *Aqp5* (25). $BRAF^{V600E}$ expression was initiated in the lung epithelium of $BRaf^{CA}$; $Aqp5^{+/+}$ or $BRaf^{CA}$; $Aqp5^{-/-}$ mice with mice analyzed for lung tumor formation 11 weeks later. Loss of AQP5 expression had no discernable effect on tumor frequency or the extent of tumor burden initiated by $BRAF^{V600E}$. Indeed, $BRaf^{CA}$; $Aqp5^{-/-}$ mice developed benign adenomas that were indistinguishable from those that formed in control $BRaf^{CA}$; $Aqp5^{+/+}$ mice. As

expected, lung tumors arising in *BRaf^{CA}; Aqp5$^{+/+}$* mice were double positive for both SP-C and AQP5 expression, whereas lung tumors arising in *BRaf^{CA}; Aqp5$^{-/-}$* mice were SP-C positive but negative for AQP5 (Fig. 2-4C). These data confirm the specificity of the AQP5 antiserum and indicate that BRAF^{V600E}- (and by extension KRAS^{G12D}-) induced lung tumors are indeed positive for at least one marker of AT1 cells. However, based on their cuboidal morphology and the presence of lamellar bodies, tumor cells appear most similar to AT2 cells. Finally, these data unequivocally demonstrated that AQP5 is dispensable for BRAF^{V600E}-induced lung tumorigenesis.

BRAF^{V600E}- initiated lung tumors regress upon MEK1/2 inhibition

BRAF^{V600E}-initiated lung tumorigenesis is prevented by the potent and specific MEK1/2 inhibitor PD0325901 (19), (20). However, others have reported that inhibition of KRAS^{G12D}-initiated lung tumorigenesis requires blockade of both RAF→MEK→ERK and PI3'-kinase→AKT→mTorc signaling (26). Consequently, we sought to test the ability of single agent PD0325901 to promote regression of established BRAF^{V600E}- or KRAS^{G12D}-induced lung tumors. As a first step we generated compound *BRaf^{CA}; LucRep* mice carrying the conditional *BRaf^{CA}* allele in combination with a Cre-activated Luciferase transgene (27). Hence, Ad-Cre infection of the lung epithelium will initiate oncogenic BRAF^{V600E} expression and the expression of Luciferase, which can be used to image tumorigenesis and response to pathway-targeted therapy using a Xenogen In Vivo Imaging System (IVIS).

Bioluminescence (in photons/second, p/s) was measured in compound *BRaf^{CA}; LucRep* mice at different times after initiation with Ad-Cre (10^7 pfu). Baseline signal was determined to be $2x10^6$ photons/second by measuring *LucRep* expressing littermates lacking the Cre-activated *BRaf^{CA}* allele. Starting five weeks after Ad-Cre

infection, bioluminescence was observed to increase in one representative mouse and at nine weeks had increased 30-fold to $6x10^7$ p/s. At this time oral PD0325901 was administered daily for five weeks. Over this period the Luciferase signal gradually decreased until it was below baseline (Fig. 2-5). In addition, at the time of drug administration, this mouse appeared hunched, had lost body weight and was displaying the signs of respiratory distress that typify the end-stage of confluent $BRAF^{V600E}$-induced benign lung tumorigenesis. Following five weeks of drug treatment the mouse appeared healthy, had gained 8.7 grams (a ~40% increase in body weight) and no longer displayed signs of respiratory distress. Upon euthanasia of similarly treated $BRaf^{CA}$ mice we could find little or no evidence of residual tumors following five weeks of MEK1/2 inhibition (Data not shown). This experiment was repeated with an additional group of 5 $BRaf^{CA}$; *LucRep* mice, all of which displayed robust tumor regression in response to MEK1/2 inhibition (Data not shown). These data indicate that MEK→ERK signaling is required for both the initiation and maintenance of $BRAF^{V600E}$-induced lung tumors.

We next assessed the effect of MEK inhibition on $KRAS^{G12D}$-induced lung tumorigenesis. $KRAS^{G12D}$ expression was initiated in a cohort of $KRas^{LSL}$ mice by infection with Ad-Cre and four weeks later, a time prior to the onset of tumorigenesis, mice were treated with either vehicle or PD0325901 for six weeks at which time they were euthanized and lung tumor burden assessed. MEK1/2 inhibition with PD0325901 treatment was highly effective in the prevention of $KRAS^{G12D}$-driven lung tumors (Fig. 2-6A). Whereas vehicle treated mice had 12.5 tumors/lobe, PD0325901 treated mice had an average of 1.4 lung tumors/lobe – a 9-fold decrease in lung tumor incidence ($p = .0012$, Fig. 2-6A). In addition, we observed a 9-fold difference in the size of individual lesions when comparing control versus PD0325901 treated mice (9,111 μm^2 in vehicle treated mice compared to 69,354μm^2 for drug treated

mice, (*p*= *.0002*, Fig. 2-6A). The differences in tumor number and size contributed to an overall 47-fold lower tumor burden in PD0325901 treated mice compared to vehicle treated littermates (.072% vs. 3.4%, *p* = *.0005*, Fig. 2-6A). These data indicate that RAF→MEK→ERK signaling is essential for the onset of $KRAS^{G12D}$-induced lung tumorigenesis.

Next we assessed the efficacy of PD0325901 in promoting regression of pre-existing $KRAS^{G12D}$-initiated lung tumors. Ten weeks after initiating $KRAS^{G12D}$ expression, mice were treated with either vehicle or PD0325901 for a further four weeks at which time they were euthanized and lung tumor burden assessed. Mice treated with PD0325901 showed significantly fewer tumors per lobe compared to vehicle treated littermates (7.6 vs. 25.3, *p* = *0.01*). Moreover, whereas vehicle treated mice displayed mostly high-grade lung adenomas, lesions in PD0325901 treated mice were predominantly epithelial and adenomatous hyperplasias and thus generally smaller than tumors observed in vehicle treated mice. However the difference in overall lesion size between PD0325901 and vehicle treated mice was not significant (129,679 μm^2 vs. 305,584 μm^2, *p* = *.08*). This is likely due to the presence of residual large adenomas (boxed) remaining after the full course of drug treatment, which were presumably resistant to the effects of MEK inhibition. Importantly, overall tumor burden was decreased approximately eight-fold in PD0325901 treated $KRas^{LSL}$ mice compared to control (19% compared to 2.2%, *p* = *.0002*, Fig. 2-6B).

To unequivocally demonstrate regression of pre-existing $KRAS^{G12D}$-induced lung tumors, we treated a representative $KRas^{LSL}$*; LucRep* mouse with 10^8 pfu Ad-Cre and monitored tumor growth by bioluminescent imaging as described above (Fig. 2-6C). Baseline signal ($2.6x10^6$ p/s) was determined as the average signal of $KRas^{+/+}$*; LucRep* mice treated with the same does of Ad-Cre. 11.5 weeks after initiation of

KRAS^{G12D} expression, this *KRas$^{LSL/+}$ LucRep* mouse displayed a consistent bioluminescent signal ~17-fold above baseline at which time PD0325901 was administered. After 8.5 weeks of PD0325901 treatment, the bioluminescent signal from lung tumor burden was reduced ~6-fold ($4.5x10^7$ to $8x10^6$ p/s) however MEK1/2 inhibition did not result in the reduction of the bioluminescent signal to baseline. As with BRAF^{V600E}-induced lung tumors, cessation of PD0325901 treatment led to rapid re-growth of KRAS^{G12D} expressing lung tumors requiring that this mouse be euthanized two weeks later (Fig. 2-6C). Cumulatively, these data provide compelling evidence that inhibition of RAF→MEK→ERK signaling both prevents the growth and promotes the regression of pre-existing of KRAS^{G12D}-induced lung tumors. However, the presence of adenomas at the end of the drug treatment period may explain the incomplete tumor regression observed in *KRas^{LSL}* mice and thus why KRAS^{G12D}-driven lung tumors appear less sensitive to MEK1/2 inhibition than their BRAF^{V600E} expressing counterparts.

BRAF^{V600E}; p53$^{-/-}$ tumors remain sensitive to MEK inhibition

Intact tumor suppressors such as p53 may be required for response to MEK inhibitor PD0325901. In the previous experiments, p53 was functional. Evidence from patients in the clinic suggests that status of tumor suppressor genes such as *TP53* and *PTEN* may influence response to therapy. Furthermore, in vivo studies using mice demonstrate the requirement of p53 for apoptosis induced by anti cancer agents (28). We sought to determine if the dramatic tumor regression observed in BRAF^{V600E} tumors when treated with MEK inhibitor depends on a p53- mediated response. *BRaf$^{CA/+}$; Trp53$^{-/-}$* mice were aged to 6 weeks and then infected with $5x10^6$ pfu AdCre. Six weeks later, mice were split into two groups and dosed with 12.5 mg/kg PD0325901 or vehicle control. Mice were dosed for an additional four weeks

and euthanized two hours after the final drug treatment. Lungs were isolated and tumor burden was analyzed. *BRaf*$^{CA/+}$*; Trp53*$^{-/-}$ mice remained sensitive to the affects of MEK inhibition. Vehicle treated mice had an overall tumor burden of 19%. Many of these tumors appeared to be progressed beyond a benign stage, as loss of cell polarity was noted as well as an increase nucleus/cytoplasm size ratio. In contrast, PD0325901-treated mice had a significantly lower tumor burden of 1.2% (p= <.0001). These mice had only around 3-4 lesions per lobe, the majority of which were small alveolar or airway hyperplasia (Fig. 2-7). This finding indicates that the mechanism of action by PD0325901 does not depend on intact p53 within tumor cells.

BRAF*^{V600E} *or KRAS*^{G12D} *expressing lung tumor derived cell lines are sensitive to MEK inhibition in vitro

The anti-tumor effects of PD0325901 against BRAF^{V600E}- or KRAS^{G12D}- induced tumors *in vivo* could be mediated either by tumor cell autonomous or non-autonomous mechanisms or some combination thereof. Hence, to determine if there is a tumor cell autonomous response to MEK inhibition, we utilized cell lines isolated from either BRAF^{V600E} or KRAS^{G12D}- induced lung tumors. Whereas lung tumor lines can be generated from Ad-Cre infected *KRas*^{LSL} mice, this is not the case for similarly treated *BRaf*^{CA} mice. This may reflect the fact that BRAF^{V600E}-induced lung tumor cells undergo senescence and therefore are irreversibly arrested in the cell division cycle. Consequently, we infected compound *BRaf*$^{CA/+}$*; Trp53*$^{lox/lox}$ mice with Ad-Cre to initiate BRAF^{V600E} and silence p53 expression. These mice develop abundant high-grade lung tumors with a propensity for malignant lung cancer progression (19). 10 weeks later mice were euthanized and independent BRAF^{V600E}; p53$^{-/-}$ lung cancer-derived cell lines were established as described in Materials and Methods. Cre-mediated recombination of the *BRaf*^{CA} and *Trp53*^{lox} alleles in the

various cell lines was confirmed by PCR. Independent $KRAS^{G12D}$ expressing lung tumor derived cell lines were similarly derived from Ad-Cre infected $KRas^{LSL/+}$ mice in which spontaneous progression to NSCLC is observed. Immunoblot analysis revealed that $KRAS^{G12D}$ expressing cell lines express detectable p53.

Treatment of $BRAF^{V600E}$- or $KRAS^{G12D}$- expressing lung tumor cells with 1μM PD0325901 for 48 hours led to almost complete inhibition of proliferation compared to vehicle (DMSO) control (Fig. 2-8A) with comparable effects of PD0325901 observed on both $BRAF^{V600E}$- and $KRAS^{G12D}$-expressing lung tumor cells. Analysis of the cell cycle profile of control versus PD0325901 treated cells revealed an accumulation of both $KRAS^{G12D}$ and $BRAF^{V600E}$ expressing lung tumor cells in G1 (Fig. 2-8B) consistent with the observed inhibition of cell proliferation. In parallel, control versus PD0325901- treated cells were stained for a marker of apoptosis (Annexin V) and cell death (PI). Whereas there was a modest increase of apoptotic and dead cells in PD0325901 treated cultures, the majority of cells remained Annexin 5 and PI negative (Data not shown).

In parallel, cell extracts were analyzed to assess the effect of MEK inhibition on signal pathway activation. As expected, PD0325901 treatment led to increased phospho-MEK1/2 but decreased phospho-ERK1/2 consistent with the mechanism of action of this agent (Fig. 2-8C). Both cell lines also displayed decreased expression of Cyclin D1 consistent with the known role of ERK1/2 signaling in Cyclin D1 regulation (29). We also detected modest induction of the pro-apoptotic BCL-2 family member BIM, consistent with its regulation by ERK signaling, and the presence of cleaved-Caspase-3 (CC3) in PD0325901 treated cells. Cumulatively, these data suggest that the anti-tumor effect of PD0325901 in mouse models of $KRAS^{G12D}$- or $BRAF^{V600E}$-induced lung tumorigenesis results, at least in part, from

direct anti-proliferative effects of the agent on tumor cells that is accompanied by a modest induction of apoptosis.

BRAF^{V600E} and KRAS^{G12D} cooperate in the progression of lung adenocacinoma

Mutations in BRAF and KRAS are mutually exclusive in human tumors (30). This is likely due to the redundancy of these mutations. Since both are found in the MAPK pathway and are sufficient to induce tumorigenesis, mutational activation of both BRAF and KRAS likely serves no additional growth advantage to the cell. Such potent signaling in a case where both BRAF and KRAS are mutated may even induce growth arrest due to high MAPK signaling output, similarly to what has been observed in human fibroblasts (15). Because we have established that activated KRAS signals through the MAPK pathway, we wanted to determine what effect additional activation in the form of mutated BRAF would have. We crossed *BRaf^{CA}* and *KRas^{LSL}* mice together to generate littermates that contained one copy of each conditional allele, as well as *BRaf^{CA}*; *KRas^{LSL}* compound mice. Mice from all three genotypes were infected with 10^7 pfu AdCre and euthanized 11 weeks later when lesion number and size, and overall tumor burden was assessed.

BRaf^{CA} mice had the highest number of lesions, with an average of 103 per lobe. This number was significantly different when compared to *KRas$^{LSL/+}$* and compound *BRaf$^{CA/+}$*; *KRas$^{LSL/}$*mice (p = .004 and .001, respectfully, Fig 2-9A).

KRas^{LSL} mice and compound *BRaf^{CA}*; *KRas^{LSL}* had 32 and 29 lesions per lobe respectfully, and the difference between these two groups was not significant (p= .8). Compound *BRaf^{CA}*; *KRas^{LSL}* had the largest lesions on average compared to either of the single mutants (214,186.9 μM^2 compared to 83,751.13μM^2 for *BRaf^{CA}* and 90,291.06μM^2 for *KRas^{LSL}* (p = <.001 for both cases.) The average size of lesions at this time point between KRas and BRaf mice was not significantly different (p = .65).

Overall, tumor burden was highest in *BRaf*^{CA} mice due to the high number of lesions found in these mice. 21% of the lung in these mice were occupied by adenomas compared to 7.3% for *KRas*^{LSL} mice (p = .005) and 12.6% in compound *BRaf*^{CA}; *KRas*^{LSL} mice (p = .01). Overall, tumor burden was not significantly different when comparing *KRas*^{LSL} and compound mice at this time point (p= .22, Fig 2-9A).

We next assessed the grade of tumors found in these mice. As expected, tumors driven by BRAF^{V600E} alone were benign and low grade with normal papillary structure and nuclear to cytoplasmic ratio. Tumors driven by KRAS^{G12D} at this time point were slightly less organized in their papillary structure and had a reduced nuclear polarity compared the BRAF^{V600E} tumors (Fig 2-9B). In the case of the compound mutant mice, many tumors possessed characteristics of advanced tumor grade including condensed chromatin, enlarged nuclear to cytoplasmic ratio, loss of polarity, and distinct mitotic figures within the abnormal nuclei (Fig 2-9B). These hallmarks were found more commonly in the larger tumors of these mice. Compound mutant mice also had tumors situtated within the airway in addition to the large adenomas found in the distal lung. These airway lesions appeared anaplastic in nature, and in some cases obliterated the airways in which they were found. This phenotype was not found in the single mutant mice, and likely contributed the relative diminished health at this time point compared to *BRaf*^{CA} littermates despite the decreased overall tumor burden. Tumors in compound mutant mice were also more proliferative that the single mutant tumors, as determined by KI67 immunostaining (Fig 2-9B).

DISCUSSION

Mutationally activated *KRAS* is a feature common to ~25% of all cancers and is particularly prevalent in pancreas, colon and lung cancer (1, 2, 31, 32). Consistent with its purported importance in human lung cancer, expression of oncogenic $KRAS^{G12D}$ in the mouse lung epithelium leads to the development of non-small cell adenocarcinomas, some of which have a propensity for metastasis (18, 21). However, it remains unclear, which of its various effector pathways are critical for $KRAS^{G12D}$-induced lung tumor initiation and maintenance.

Here, we show that RAF/MEK/ERK signaling is both necessary and sufficient for the early stages of $KRAS^{G12D}$- induced tumorigenesis up to the formation of low-grade adenomas. Consistent with this, the expression of oncogenic $BRAF^{V600E}$ in the lung epithelium leads to the development of benign lung tumors with many of the same histological features but with enhanced efficiency compared to $KRAS^{G12D}$. At early time points following conditional activation of either oncogene, $BRaf^{CA}$ mice generally have larger and more abundant lesions than their $KRas^{LSL}$ littermates. This highly reproducible observation may be due to higher levels of MEK1/2→ERK1/2 pathway activation in $BRAF^{V600E}$ driven tumors, which may promote faster proliferation of initiated cells. Differences in MEK1/2→ERK1/2 pathway activation by $KRAS^{G12D}$ versus $BRAF^{V600E}$ may be ascribed to negative feedback on RAF→MEK→ERK signaling in tumors driven by $KRAS^{G12D}$ (22, 33). Another explanation for this difference may be the efficiency of Cre-mediated recombination of the conditional $BRaf^{CA}$ and $KRas^{LSL}$ alleles, which is not readily measurable in the lung epithelium. Another possibility is that there may be more cells with tumorigenic potential that express BRAF compared with KRAS. Finally, the efficiency of lung tumorigenesis may reflect a better ability of $BRAF^{V600E}$ to elevate MEK/ERK signaling compared with $KRAS^{G12D}$. Although we did not see a difference in pERK between

$KRAS^{G12D}$- or $BRAF^{V600E}$-induced lung tumors, we were not able to assess pERK levels in single initiated cells to determine whether there may be differences between the 2 oncogenes in signal pathway engagement. Although this highly reproducible difference in the efficiency of $BRAF^{V600E}$- versus $KRAS^{G12D}$- induced lung tumorigenesis was surprising, it is not without precedent. For example, whereas $BRAF^{V600E}$ elicits papillary thyroid cancer when expressed in mouse thyrocytes, $KRAS^{G12D}$ xpression had no effect in the thyroid unless combined with PTEN silencing (34, 35).

Although lung lesions induced by $KRAS^{G12D}$ or $BRAF^{V600E}$ are very similar at early time points, lung tumors driven by $BRAF^{V600E}$ remain low-grade and benign, whereas $KRAS^{G12D}$-driven tumors display a greater propensity for malignant progression. Whereas evidence suggests that high-grade lesions emerge from more benign tumors, it remains possible that these lesions emerge from a different cell of origin. To explore the possibility that cell of origin may differ between the $KRAS^{G12D}$- or $BRAF^{V600E}$-induced lung tumors, we stained tumors for markers of cells of the distal lung epithelium.

Whereas both $KRAS^{G12D}$- and $BRAF^{V600E}$- induced lung tumors types lacked CCA expression, they were uniformly double positive for SP-C and AQP5, markers of AT2 and AT1 pneumocytes, respectively, and a combination of markers not detected in normal lung. However, by most other criteria, $KRAS^{G12D}$- and $BRAF^{V600E}$- induced lung tumor cells resembled AT2 cells. Consequently, it is unclear why the AT2-like cells in $KRAS^{G12D}$- or $BRAF^{V600E}$- driven lung tumors express an AT1 marker such as AQP5, but increased signaling through the MEK pathway may influence expression of this protein in AT2 cells. Overall, the data stress the similarity of the cellular phenotype of both $KRAS^{G12D}$- or $BRAF^{V600E}$- induced lung tumors and suggest that the ability of $KRAS^{G12D}$ to promote malignant progression at late time points may be a

result of differences in signaling caused by this oncogene perhaps reflected by the elevated phospho-S6 detected in high-grade $KRAS^{G12D}$-induced tumors. KRAS activates PI3'K through a RAS binding domain present on the catalytic domain of the kinase, and activation of PI3'K signaling may allow $KRAS^{G12D}$ driven tumors to progress. This pathway is not important and likely not active in $BRAF^{V600E}$ driven tumors, as treatment of *BRaf*^{CA} mice with AKT inhibitor MK-2206 did not have an effect of tumorigenesis (Chapter 3). Finally, It has been proposed that the cell of origin of $KRAS^{G12D}$- driven lung tumors is a bronchioalveolar stem cell (BASC), which coexpresses both CCA and SP-C (36). Although we detected small numbers of double CCA/SP-C–positive cells in $BRAF^{V600E}$- driven tumors, not all tumors contained such cells and their frequency was less than 1% of the total tumor cells (data not shown). To explore the importance of MEK/ERK signaling in $BRAF^{V600E}$- or $KRAS^{G12D}$- driven tumors, we used PD0325901, a highly selective and potent inhibitor of MEK1/2 (20, 37). In vivo bioluminescent imaging showed the ability of this agent, not only to prevent the onset of $BRAF^{V600E}$-induced tumorigenesis (19) but also to promote dramatic regression of pre-existing lung tumors. PD0325901 treatment also effectively prevented the formation of $KRAS^{G12D}$- driven tumors and promoted the regression of preexisting lung tumors, consistent with the work of others (26, 38). However, the magnitude of tumor regression in the $KRas^{LSL}$ mice was less dramatic than that observed in $BRaf^{CA}$ mice and, at euthanasia, we detected fully formed adenomas in the lungs of PD0325901-treated mice, which were presumably resistant to the cyto-toxic effects of MEK inhibition. In addition, despite the striking effects of MEK1/2 inhibition on $BRAF^{V600E}$- induced lung tumorigenesis, we were unable to eradicate tumor-initiating cells from the lungs of these animals, which rapidly regrew lung tumors upon cessation of drug treatment. The reasons for these observations are the subject of ongoing investigation.

Tumor cell autonomous effects of MEK1/2 inhibition were established using cultured cells isolated from $BRAF^{V600E}$- or $KRAS^{G12D}$-driven lung tumors. Although such cell lines were sensitive to the anti-proliferative effects of MEK inhibition and displayed some evidence of apoptosis, we did not observe substantial involution of these cell cultures. This leaves open the possibility that MEK1/2 inhibition has both tumor cell autonomous and non-autonomous effects that contribute to the regression of $BRAF^{V600E}$- and $KRAS^{G12D}$- induced lung tumors in vivo. However, these data emphasize the central importance of RAF/MEK/ERK signaling in $KRAS^{G12D}$- induced lung tumorigenesis in the mouse. Because mutationally activated KRAS remains an intractable pharmacologic target, it is possible that targeting MEK1/2, either alone or in combination chemotherapy, may represent a viable approach for targeting KRAS-induced lung cancer (12).

The effectiveness of PD0325901 on $BRAF^{V600E}$- driven tumorigenesis could also be extended to tumors lacking p53. This finding demonstrates that the mechanism of tumor prevention and regression by MEK inhibition does not depend on the intact tumor suppressor. This does not rule out the possibility that $BRAF^{V600E}$; $p53^{-/-}$ cells are sensitive to MEK inhibition in the tumor microenviroment or vasculature and some degree of drug response was due to cell non-autonomous effects.

Our comparative analysis of $BRAF^{V600E}$- and $KRAS^{G12D}$- induced tumorigenesis allowed us to explore the effects of combining both oncogenes using *BRaf*^{CA}*; KRas*^{LSL} (compound mice). These mice display advanced grade, anaplastic tumors that are highly proliferative. Since elevated levels of MAPK signaling tends to cause growth arrest in vitro, this may be due to cooperation between MAPK activated by both oncogenes and additional signaling pathways driven predominantly by KRAS, such as the PI3'K signaling pathway. Only a fraction of tumors driven by $KRAS^{G12D}$ have a tendency to reach high grade, and the proliferative indices of the tumors

remains relatively low. This may be due to negative feedback effect acting at the level of RAF**.** The $BRAF^{V600E}$ mutation may override such feedback and thus allow for progression to high-grade lesions which maintain proliferation. Spry2 is a negative regulator of the MAPK pathway, associating directly with RAF Kinases to inhibit their activity. It is upregulated in $KRAS^{G12D}$ driven lung tumors and studies using shRNA knockdown of Spry2 enhanced KRAS- driven tumorigenesis, implicating its role as a tumor suppressor (22). Induction of Spry by RAS may be the mechanism of negative feedback. Spry 2 is unable to associate with $BRAF^{V600E}$ due to its altered conformation (39), and this may explain why tumors with both KRAS and BRAF mutations have a high rate of progression and proliferation.

Interestingly, the multiplicity of these lesions is the same as in $KRas^{LSL}$ mice, significantly less than $BRaf^{CA}$ mice. This indicates that a lower tumor multiplicity is a dominant effect of $KRAS^{G12D}$ expression. It is possible that expression of this oncoprotein in a subset of cells does not lead to proliferation and may result in quiescence or even apoptosis. Another possibility explaining to decreased multiplicity of tumors in compound mutant mice is aberrant recombination. Both *BRaf* and *KRas* genes are located on mouse chromosome six, so the presence of four *lox*P sites, with Cre mediated recombination may result in the removal of a large span of DNA, making the cell nonviable. This would be difficult to ascertain in vivo, but recombination status of both alleles in compound tumors could be assessed with PCR.

Figure 2-1. Comparison of $BRAF^{V600E}$ and $KRAS^{G12D}$ initiated lung tumorigenesis.

A: H & E staining of lungs from $BRaf^{CA/+}$ or $KRas^{LSL/+}$ mice 6 or 17 weeks after intranasal infection with 10^7 pfu Ad-Cre. Scale bar represents 500μm.

B: Multiplicity and size of $BRAF^{V600E}$ or $KRAS^{G12D}$ initiated lung tumors.

Tumor number and size were quantified for $BRAF^{V600E}$ or $KRAS^{G12D}$ -initiated lung tumors at 6 weeks. Tumor number and size were quantified for $BRAF^{V600E}$ or $KRAS^{G12D}$ -initiated lung tumors at 6 weeks. Tumor burden was calculated as tumor area per total area lobe at 6, and 17 weeks.

D: H & E stainings from $BRaf^{CA/+}$ and $KRas^{LSL/+}$ at high magnification demonstrate divergent tumor phenotypes at 17 weeks. $KRAS^{G12D}$ tumors are present with enlarged nuclei with prominent nucleoli. Bar represents 50 microns.

Figure 2-2. Quantification of proliferating cells in $BRAF^{V600E}$ and $KRAS^{G12D}$ driven lung tumors.

A: BrdU (green) /SP-C (red) and Ki67 (green) /SPC (red) staining of $BRAF^{V600E}$ and $KRAS^{G12D}$ driven tumors at 17 weeks. Double positive cells within fully formed adenomas were classified as proliferating. Bar represents 25 microns. Images are 40x magnification.

B: Quantification of percentages of proliferating cells per tumor type marked with KI67 or BrdU.

***Figure 2-3.* Immunohistochemical staining of $BRAF^{V600E}$ and $KRAS^{G12D}$ driven lung tumors.**

Antibodies against pErk 1/2 (Thr 202/ Tyr204) and phospho-S6 (Ser 235/236) were used to stain low grade adenomas from both $BRaf^{CA}$ and $KRas^{LSL}$ mice and high grade adenomas from $KRas^{LSL}$ mice.

Figure 2-4. Both $BRAF^{V600E}$ and $KRAS^{G12D}$ driven tumors express Alveolar Type 1 pneumocyte marker Aquaporin 5 (AQP5).

A: Immunofluorescent staining of $BRAF^{V600E}$ and $KRAS^{G12D}$ driven lung tumors using antibodies against Surfactant Protein C (SP-C, red) and Aquaporin 5 (AQP5, green).

B: Electron microscopy image of $BRAF^{V600E}$ –driven tumor demonstrating AT2-like cells with prominent lamellar body (red arrow). Bar represents 2μm.

C: AQP5 Immunofluorescent staining of $BRAF^{V600E}$- driven tumors in mice either wild type or null for AQP5.

Figure 2-5. $BRAF^{V600E}$- driven tumors regress upon treatment with MEK inhibitor PD0325901.

Luciferase imaging of $BRaf^{CA/+}$ and $BRaf^{+/+}$ luciferase reporter mice following infection with 10^7 pfu Ad-Cre. Mice were administered 12.5 mg/kg PD032901 at nine weeks post infection and dosed five days a week for five weeks. Bioluminescent signal was measured in photons/ second (p/s).

Figure 2-6. MEK inhibitor PD0325901 is effective in the prevention and regression of $KRAS^{G12D}$ driven lung tumors.

For both A and B, tumor number and size were quantified and tumor burden was calculated as disease area per total area lobe. H and E stained sections of PD0325901 and vehicle treated mice. Bar represents 500 μm.

A: $KRas^{LSL/+}$ mice were administered 12.5 mg/kg PD0325901 four weeks after infection with 10^7 pfu Ad-Cre. Mice were dosed 5 times a week for six weeks.

B: Mice were administered 12.5 mg/kg PD0325901 10 weeks after infection with 10^7 pfu Ad-Cre and dosed for six weeks.

C: Luciferase imaging of $KRas^{LSL/+}$ and $KRas^{+/+}$ luciferase reporter mice following infection with 10^8 pfu Ad-Cre. Mice were administered 12.5 mg/kg PD032901 at 11.5 weeks post infection and dosed five days a week for 7.5 weeks. Bioluminescent signal was measured in photons/ second (p/s).

Figure 2-7. $BRAF^{V600E}$; $p53^{-/-}$ tumors remain sensitive to MEK1/2 inhibition.

Mice were dosed with 12.5 mg/kg PD0325901 or vehicle control six weeks after intranasal infection with $5x10^6$ pfu AdCre and dosed for four weeks. Lung sections were removed and H and E stained and percent tumor burden was calculated for both groups. The top bar represents 500 microns, and the bottom bar represents 100 microns.

Figure 2-8. Cells isolated from $BRaf^{V600E}$ and $KRas^{G12D}$- driven tumor are sensitive to MEK inhibition in vitro.

Cells isolated from tumor bearing mice were cultured in 10% serum and treated with 1μM PD0325901 or vehicle control for 1, 24, and 48 hours.
A: Cell number of drug treated cells relative to vehicle controls were determined by percent reduction using Alamar Blue viability assay.
B: lung tumor–derived cell lines described in A were treated for 24 hours with either PD0325901 (PD) or vehicle control, at which time permeabilized cells were stained with PI to assess the percentage of cells in the G0–G1, S, or G2–M phases of the cell-cycle division.
C: Western blot analysis of lysates from 24 hour drug treated cells using antibodies against phospho-MEK 1/2 (Ser 221), total ERK 1/2, phospho-ERK 1/2 (Thr202/Tyr204), BIM, Cleaved Caspase 3 (CC3), and Cyclin D.

Figure 2-9. $BRAF^{V600E}$ and $KRAS^{G12D}$ cooperate in lung tumor progression.
$BRaf^{CA/+}$, $KRas^{LSL/+}$, and $BRaf^{CA/+}$; $KRas^{LSL/+}$ mice were infected with 10^7 pfu AdCre and euthanized 11 weeks later.
A: H and E staining of lungs from mice and quantification of tumor number, size, and percent tumor burden.
B: High magnification of H and E stained lung tumors demonstrating advanced grade in $BRaf^{CA/+}$; $KRas^{LSL/+}$ mice. KI67 staining of lung tumors demonstrating an increase in proliferating cell number in $BRaf^{CA/+}$; $KRas^{LSL/+}$ mice.

Fig 2-1

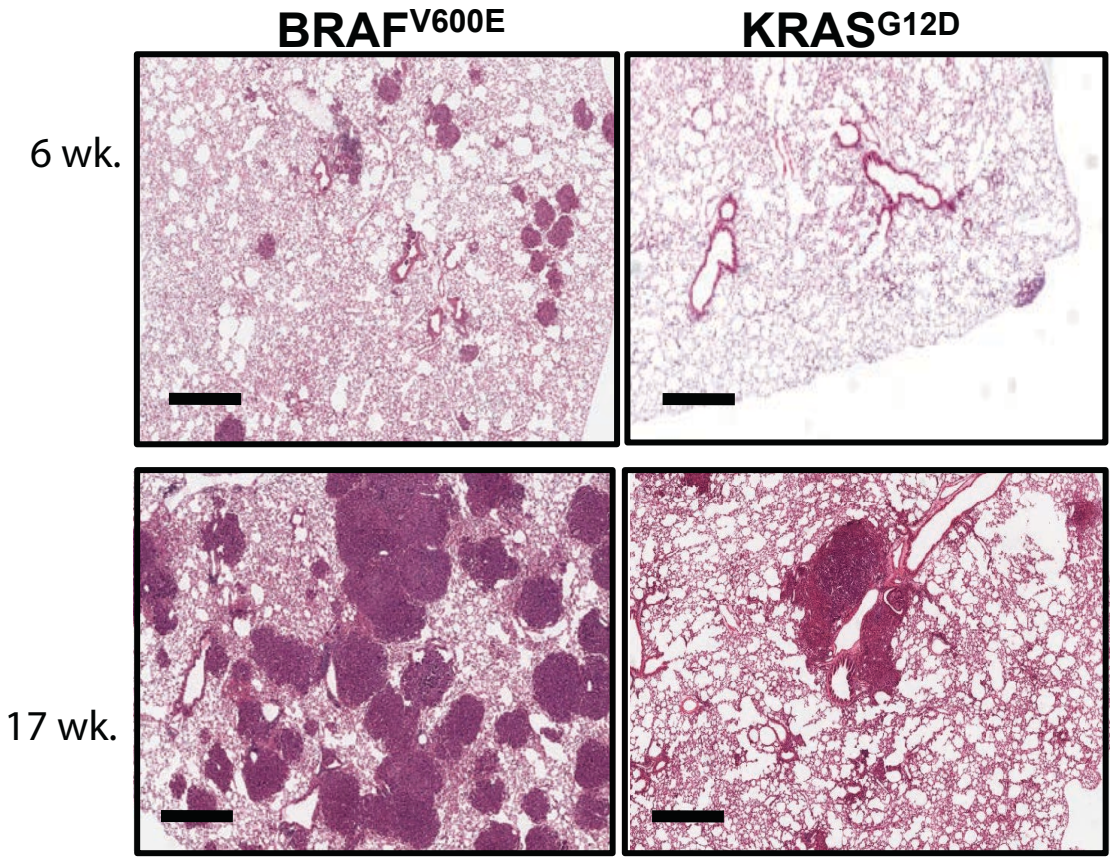
A
BRAF V600E
KRAS G12D
6 wk.
17 wk.

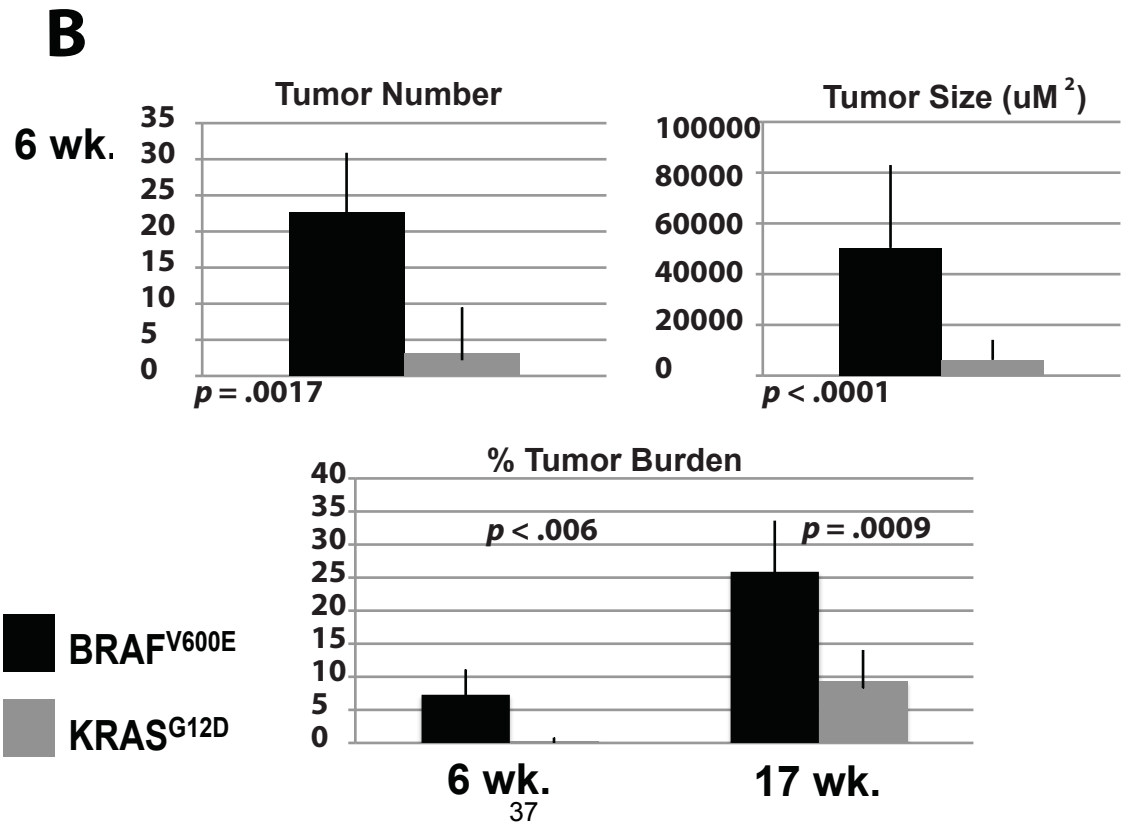
B
6 wk.
Tumor Number
35
30
25
20
15
10
5
0
p = .0017
Tumor Size (uM 2)
100000
80000
60000
40000
20000
0
p < .0001
% Tumor Burden
40
35
30
25
20
15
10
5
0
p < .006
p = .0009
6 wk.
17 wk.
BRAF V600E
KRAS G12D

C

Fig 2-1

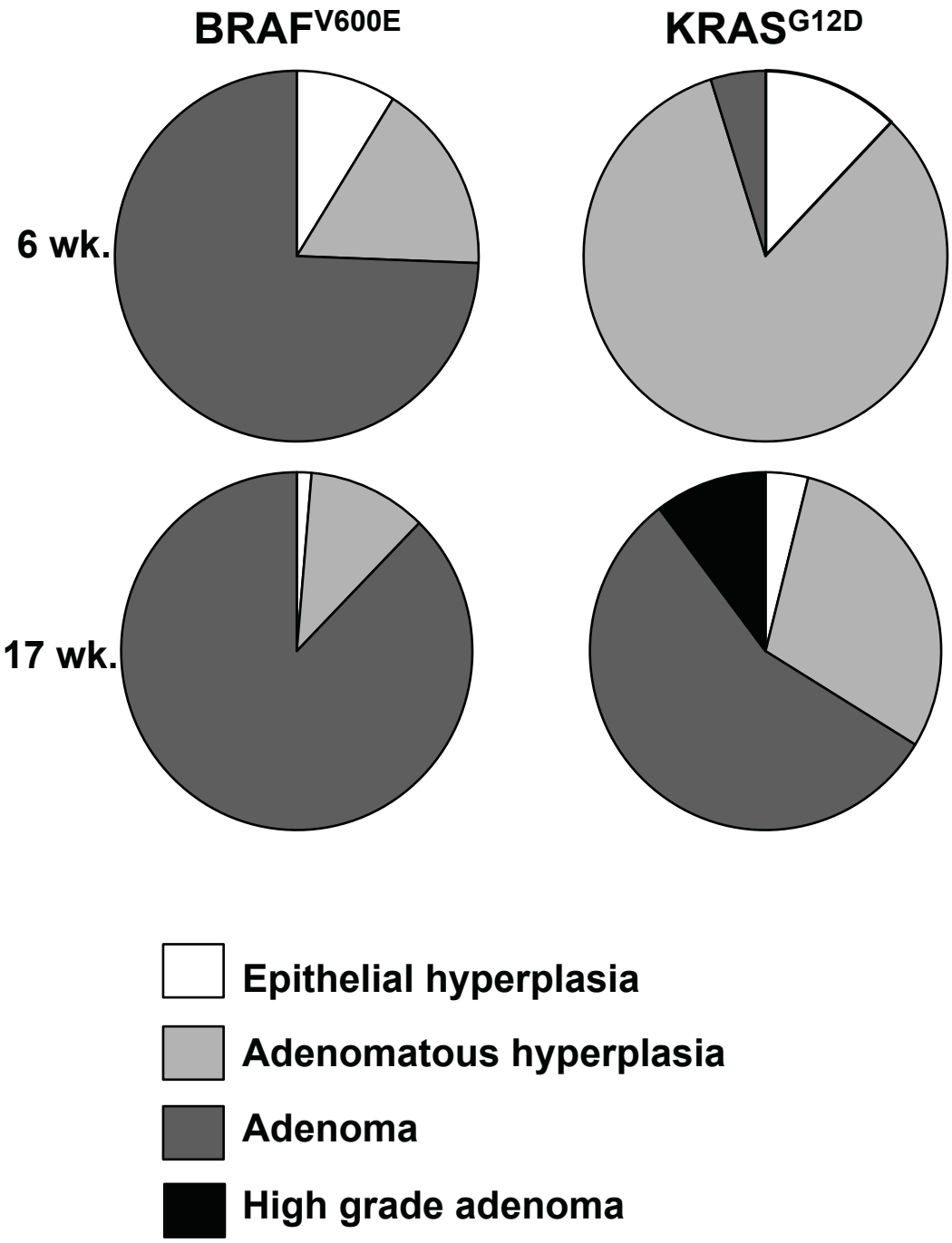
BRAF V600E
KRAS G12D
6 wk.
17 wk.
Epithelial hyperplasia
Adenomatous hyperplasia
Adenoma
High grade adenoma

Fig 2-1

D

BRAF^{V600E}

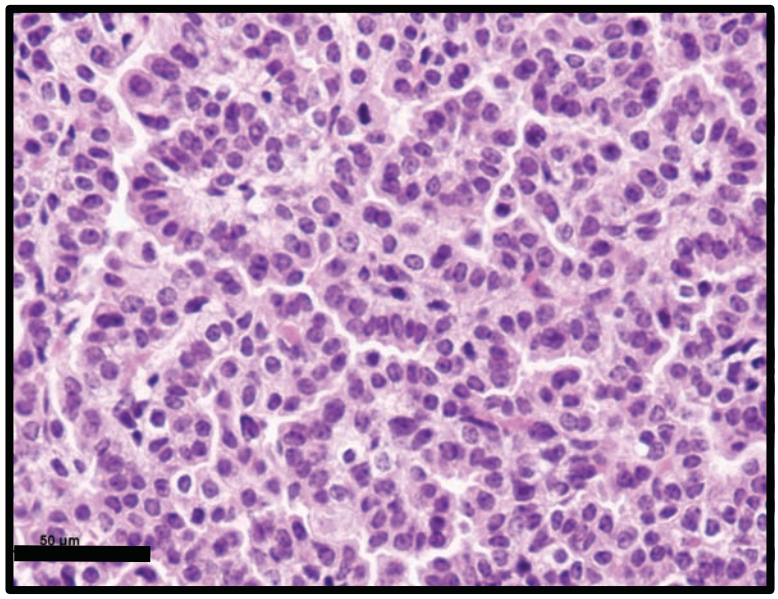

KRAS^{G12D}

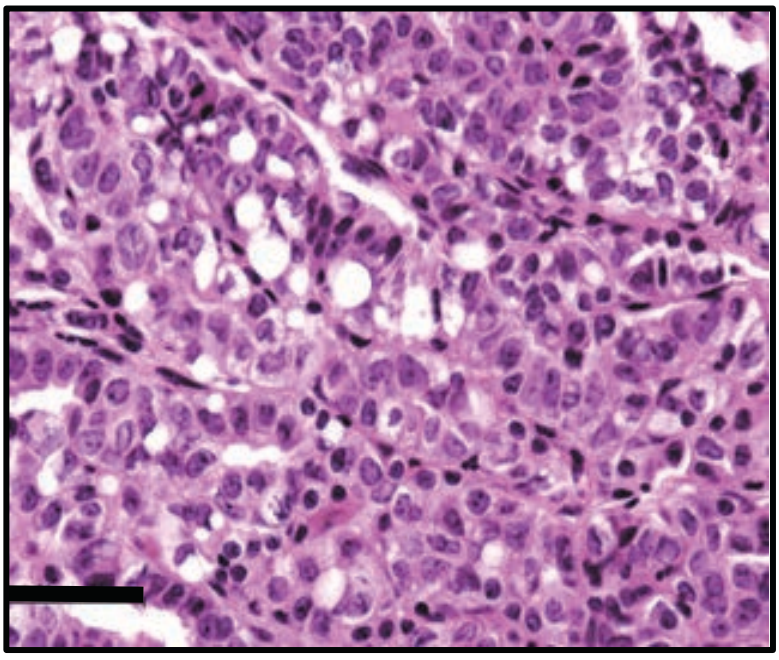

Fig 2-2

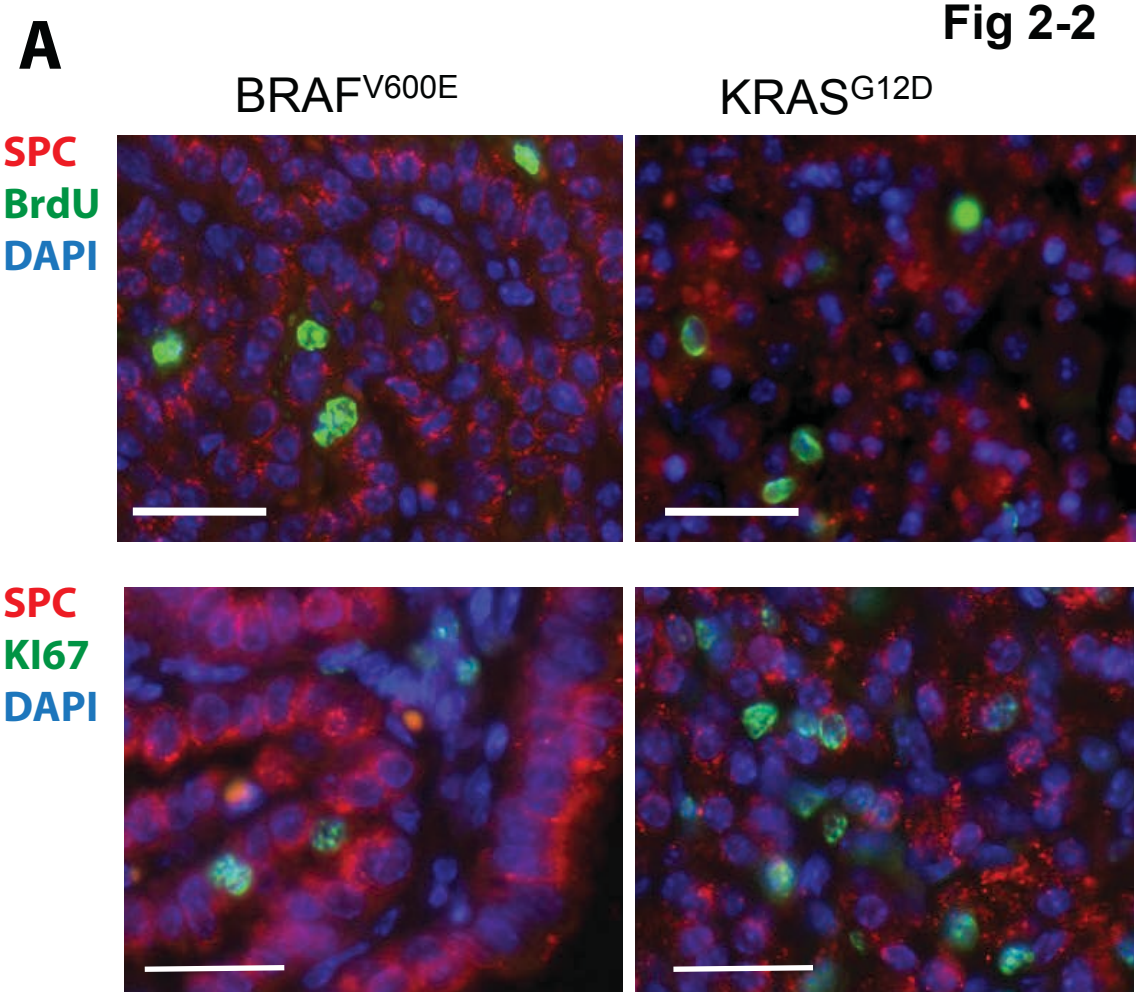
A
BRAFV600E
KRASG12D
SPC
BrdU
DAPI
SPC
KI67
DAPI
B
Percent BrdU+/SPC+ cells
3
2.5
2
1.5
1
0.5
0
BRAFV600E
KRASG12D
p = .12
Percent KI67+/SPC+ cells
8
7
6
5
4
3
2
1
0
p = .08

Fig 2-3

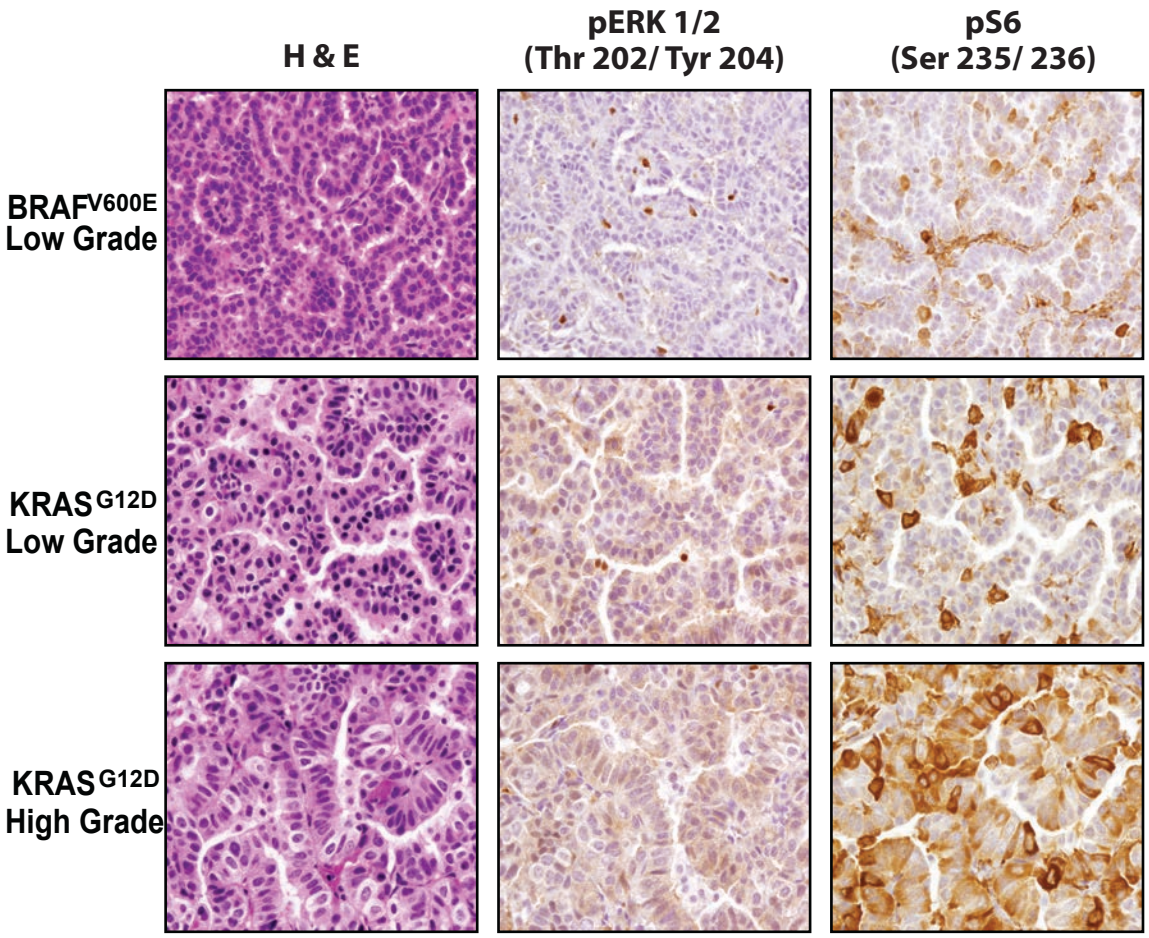
H & E
pERK 1/2
(Thr 202/ Tyr 204)
pS6
(Ser 235/ 236)
BRAF V600E
Low Grade
KRAS G12D
Low Grade
KRAS G12D
High Grade

Fig 2-4

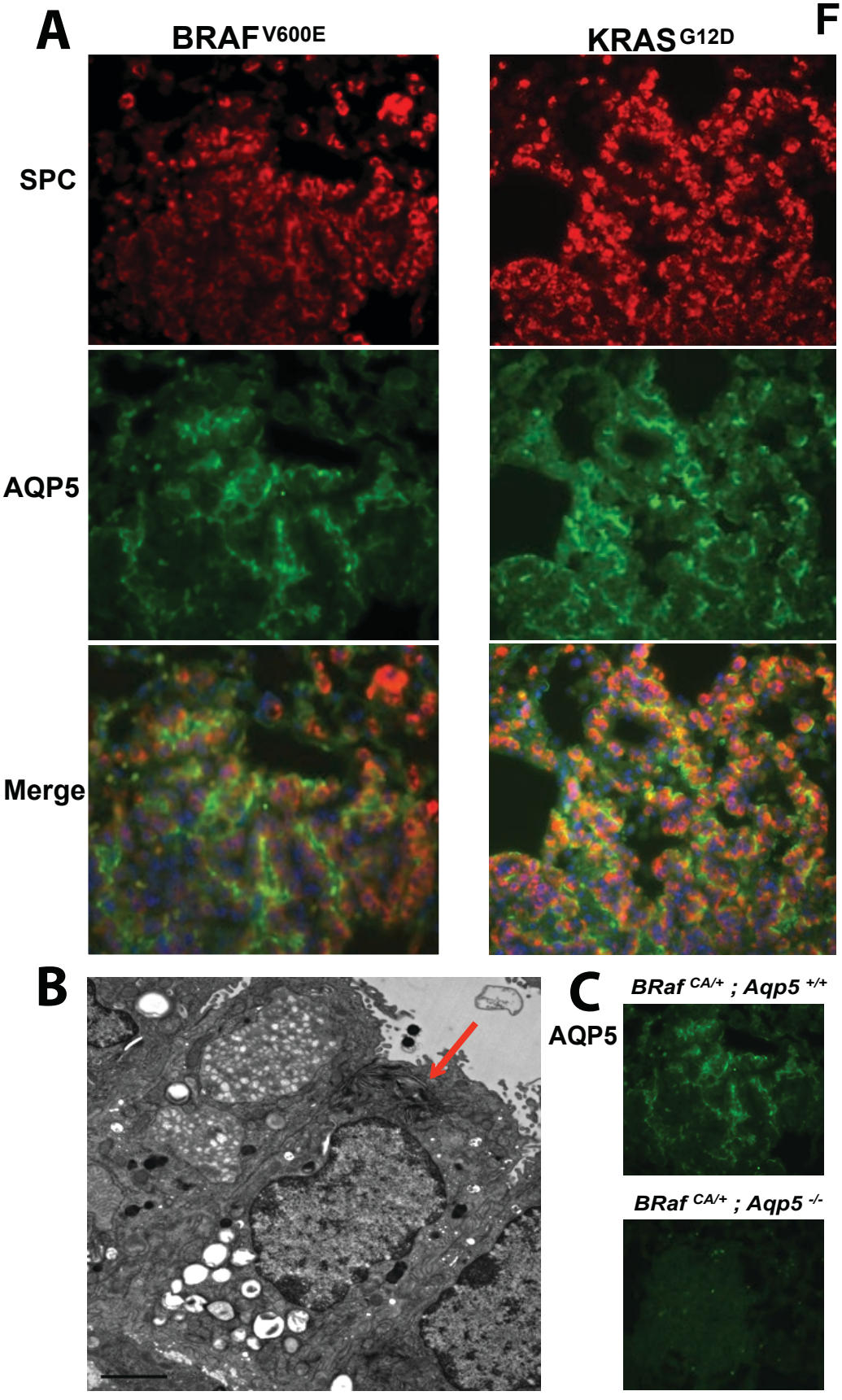
A
BRAF V600E
KRAS G12D
SPC
AQP5
Merge
B
C
AQP5
BRaf CA/+ ; Aqp5 +/+
BRaf CA/+ ; Aqp5 -/-

Fig 2-5

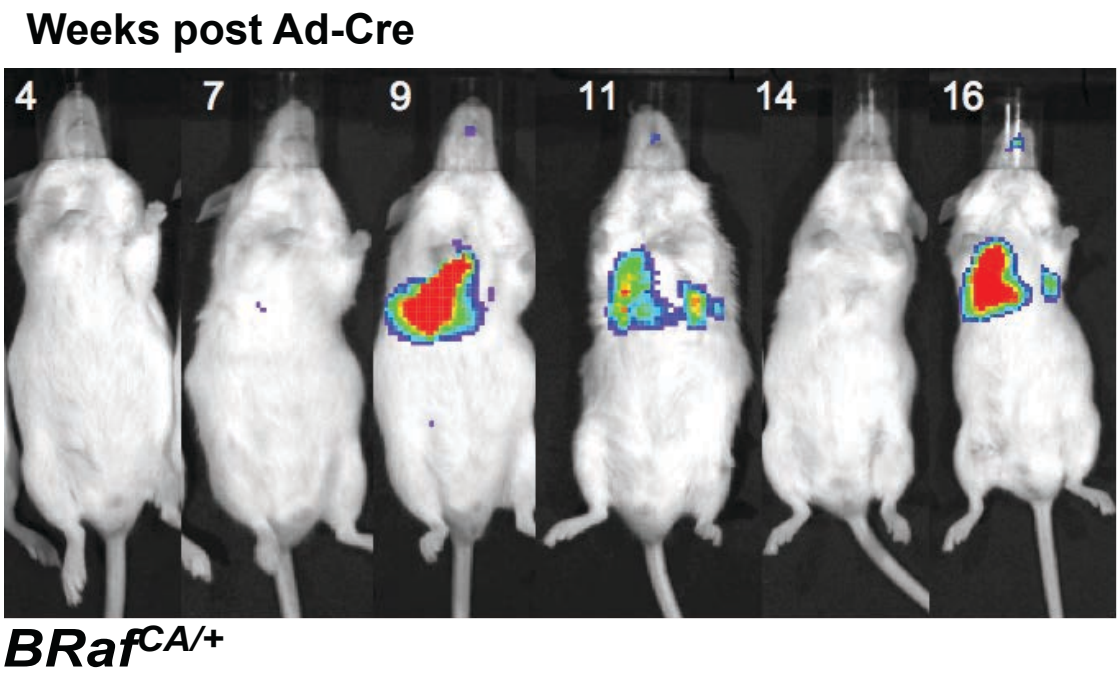
Weeks post Ad-Cre
4
7
9
11
14
16
BRaf^CA/+

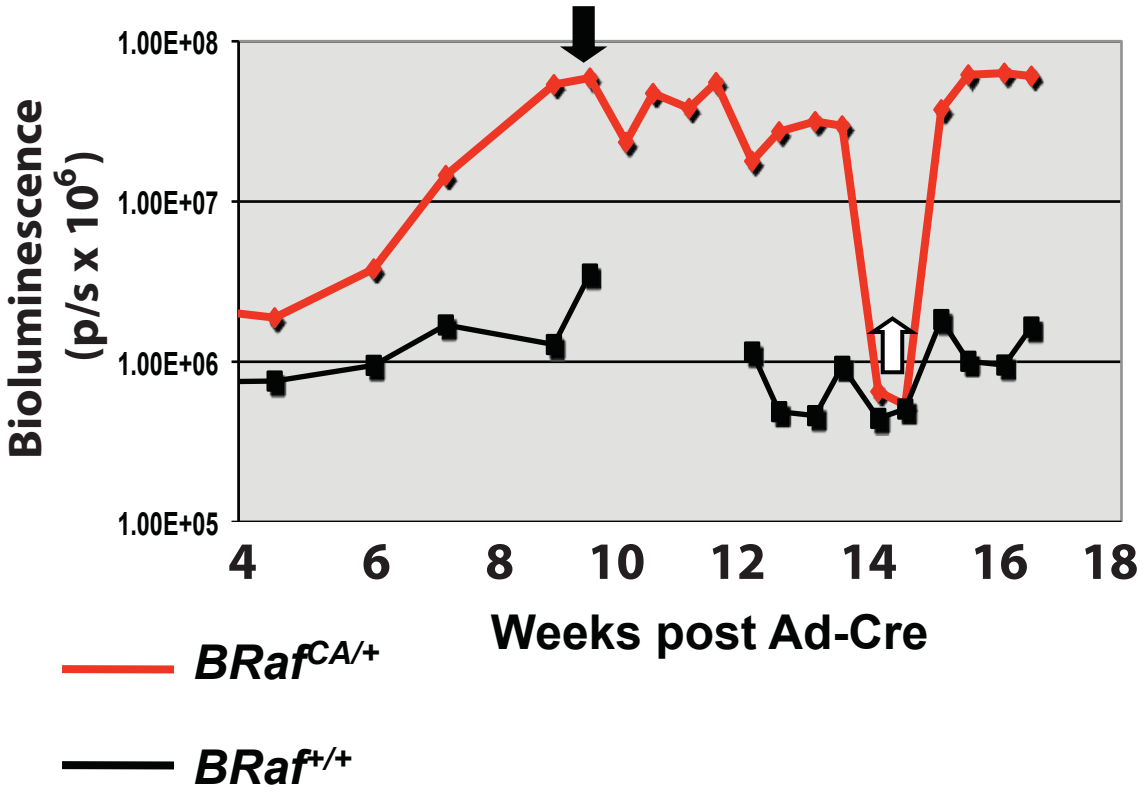
Bioluminescence (p/s x 10^6)
1.00E+08
1.00E+07
1.00E+06
1.00E+05
4
6
8
10
12
14
16
18
Weeks post Ad-Cre
BRaf^CA/+
BRaf^+/+

A $KRAS^{G12D}$

Fig. 2-6

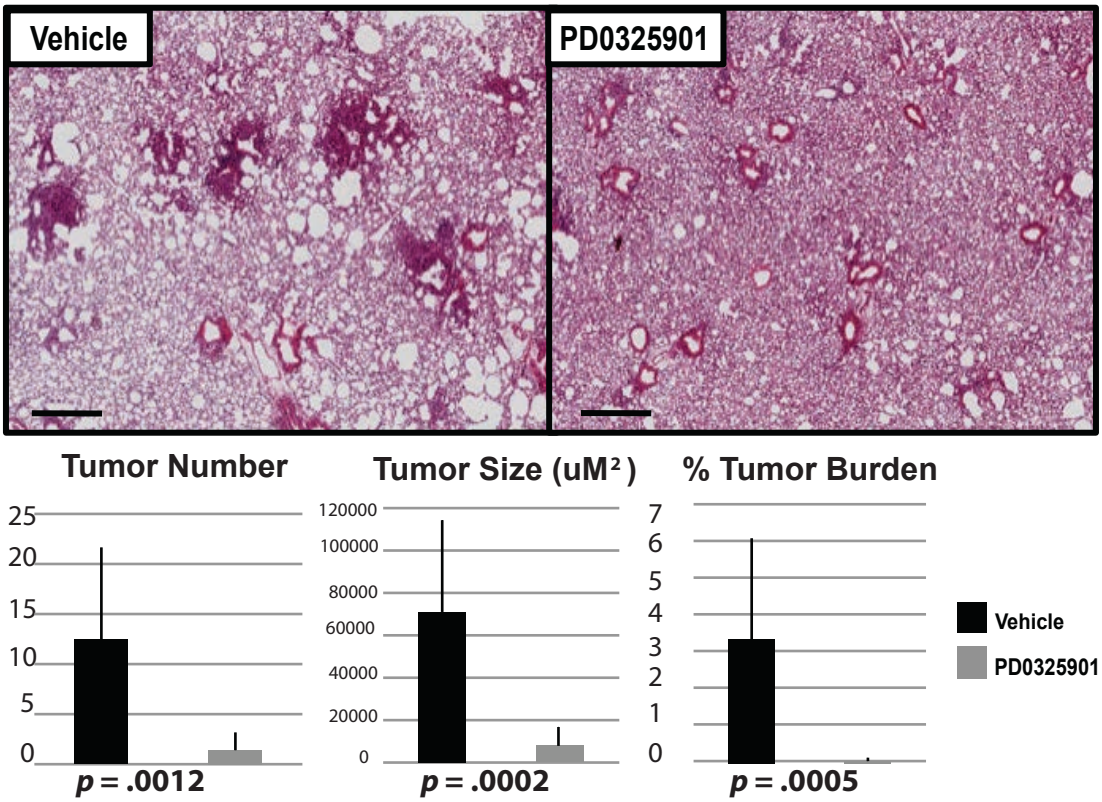

B $KRAS^{G12D}$

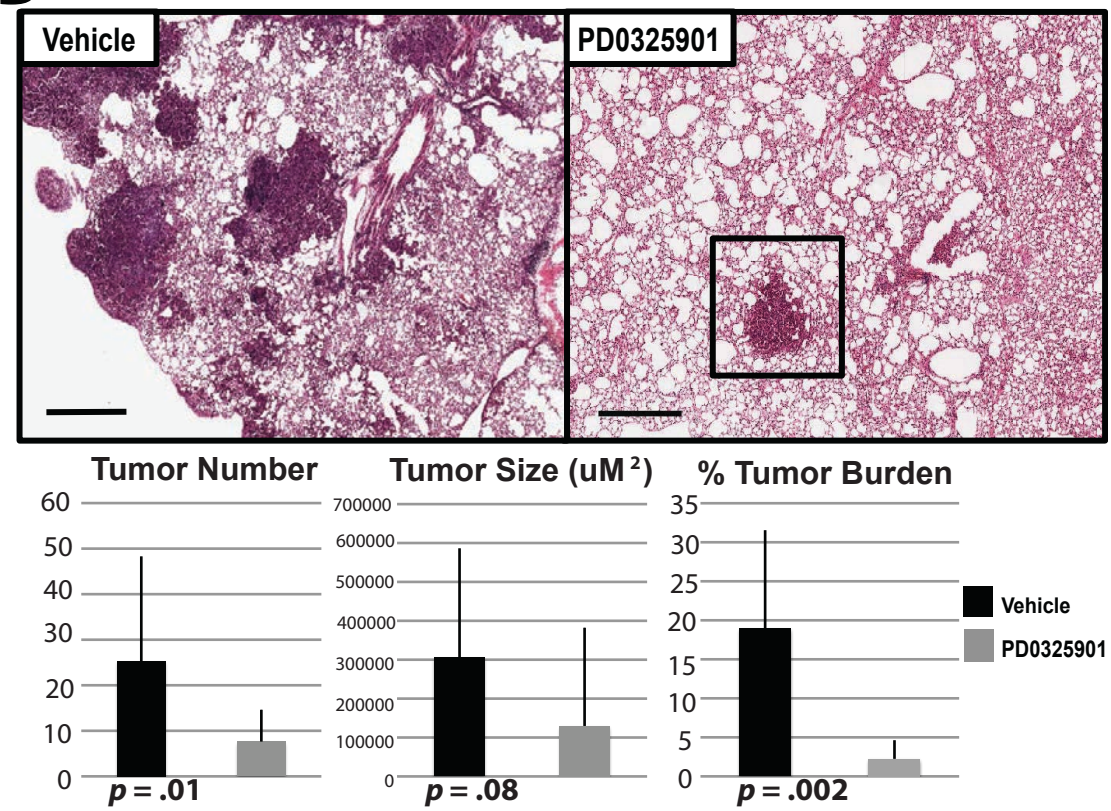

C

Fig 2-6

Weeks post Ad-Cre

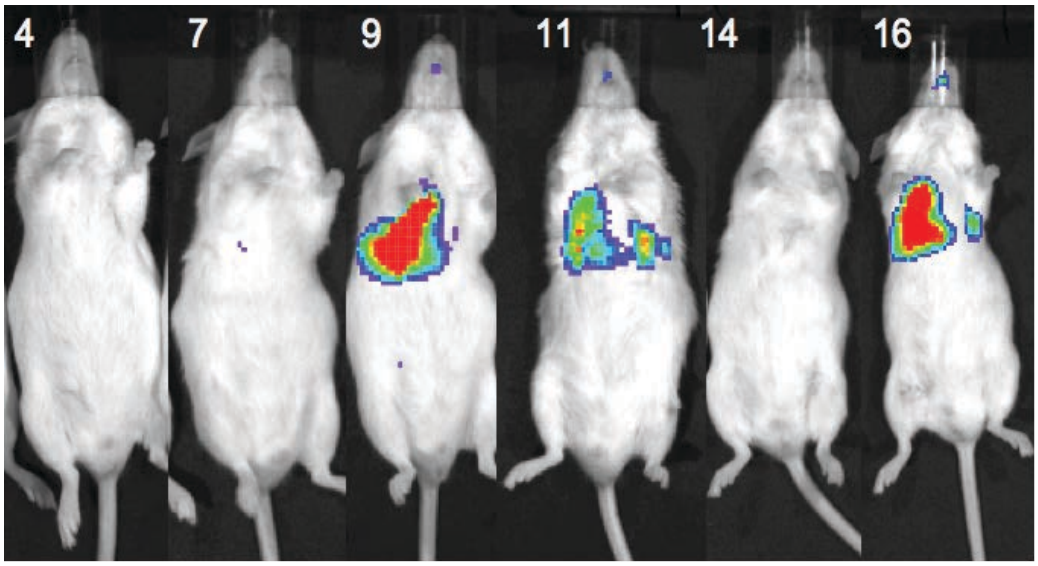

KRas$^{LSL/+}$

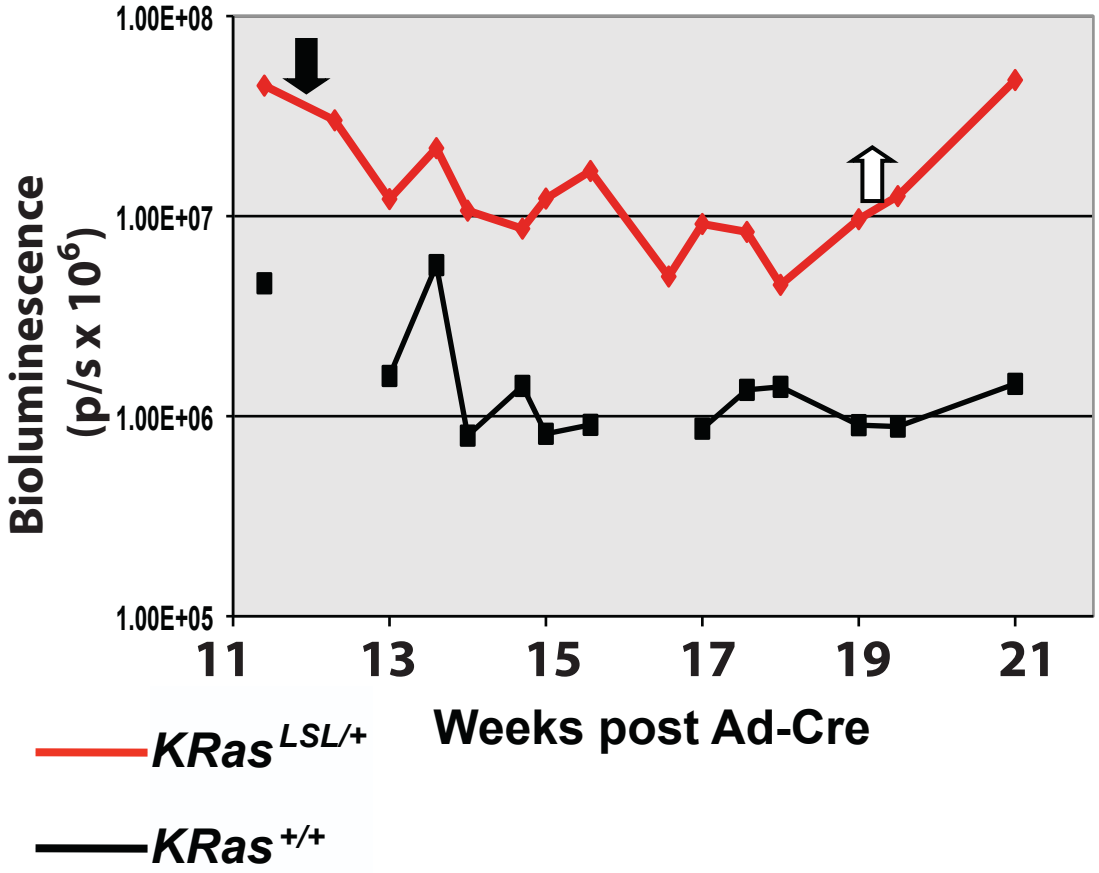

Fig. 2-7

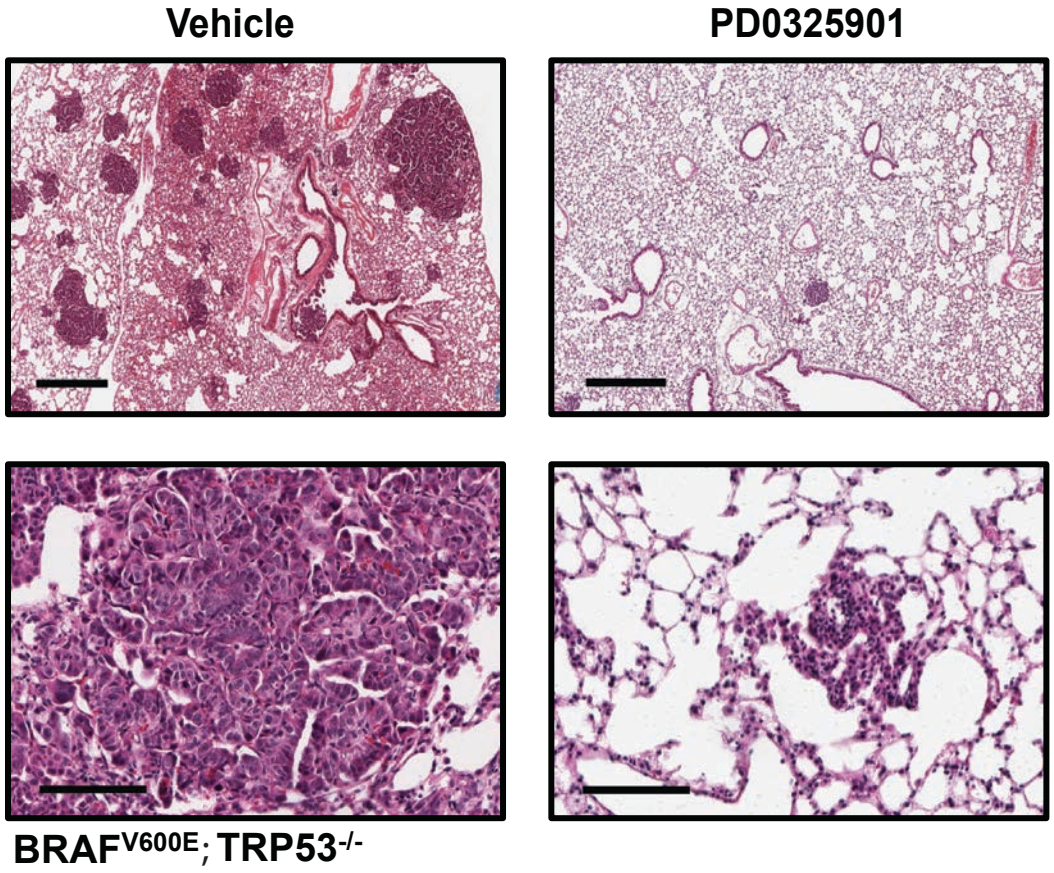
Vehicle
PD0325901
BRAF^{V600E}; TRP53$^{-/-}$

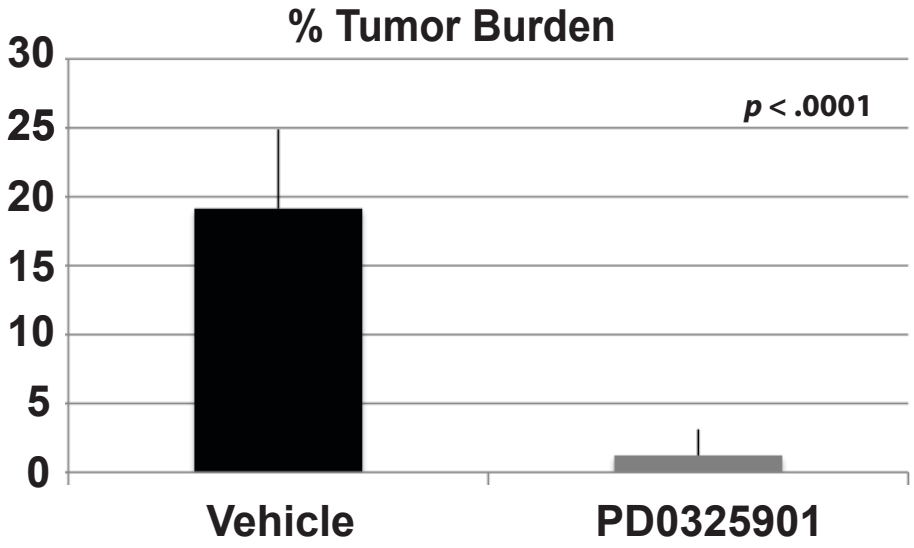
% Tumor Burden
30
25
20
15
10
5
0
p < .0001
Vehicle
PD0325901

Fig 2-8

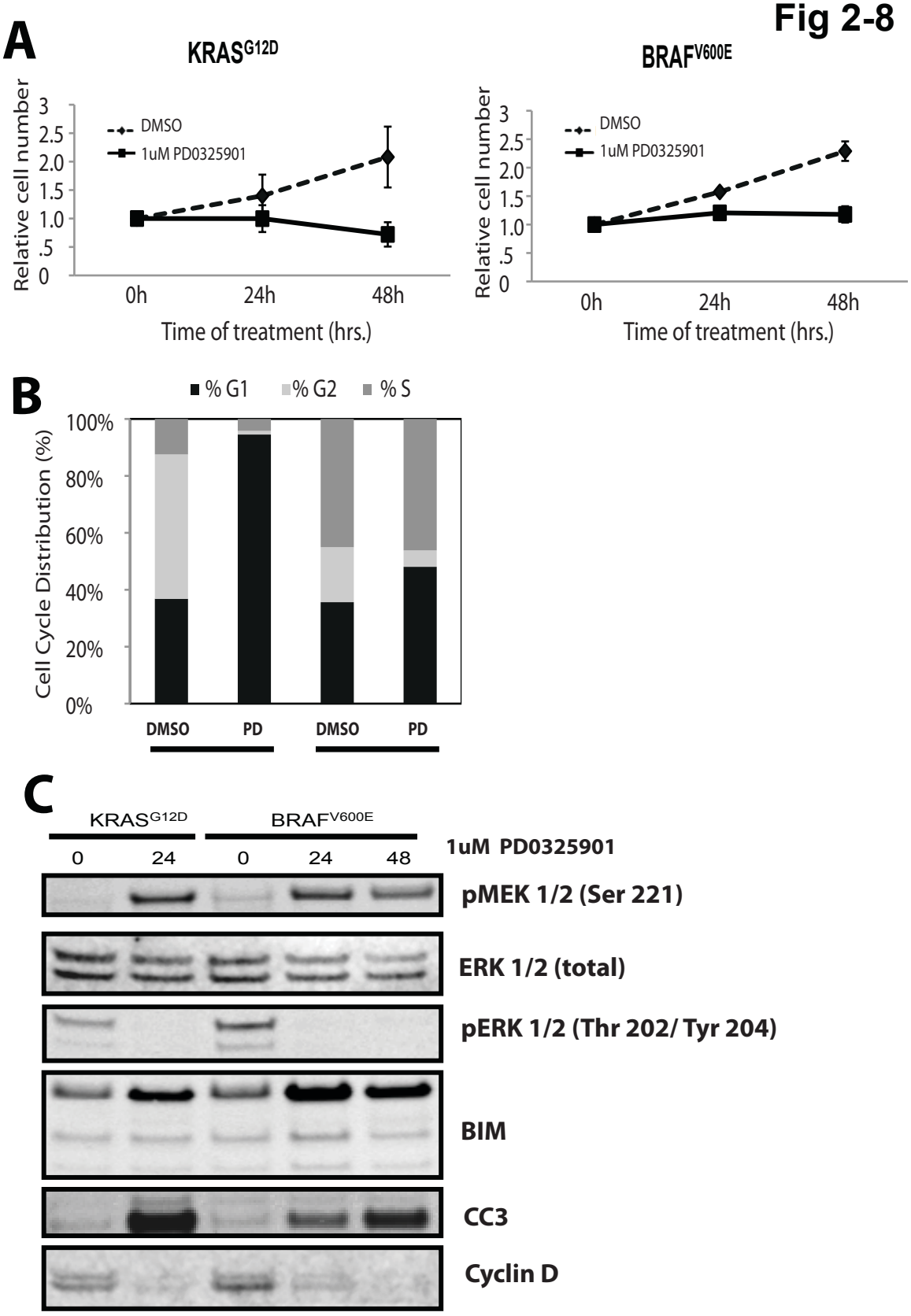
A
KRASG12D
BRAFV600E
Relative cell number
DMSO
1uM PD0325901
Time of treatment (hrs.)
0h
24h
48h
B
% G1
% G2
% S
Cell Cycle Distribution (%)
DMSO
PD
C
KRASG12D
BRAFV600E
1uM PD0325901
pMEK 1/2 (Ser 221)
ERK 1/2 (total)
pERK 1/2 (Thr 202/ Tyr 204)
BIM
CC3
Cyclin D

Fig 2-9

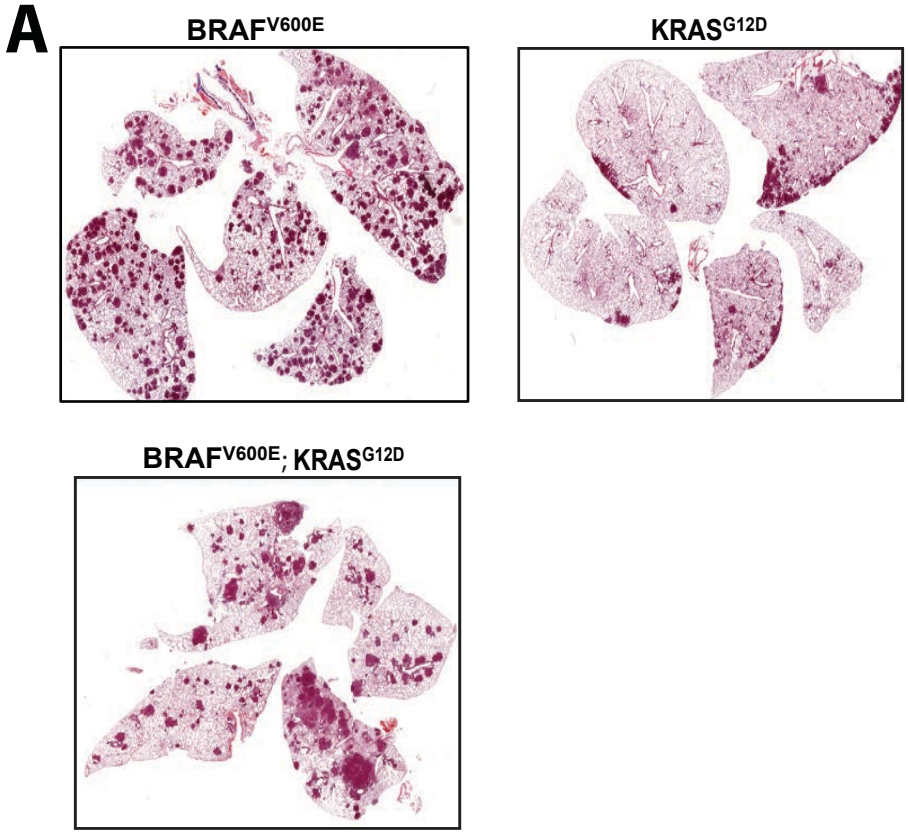

* : $p \leq .01$

B

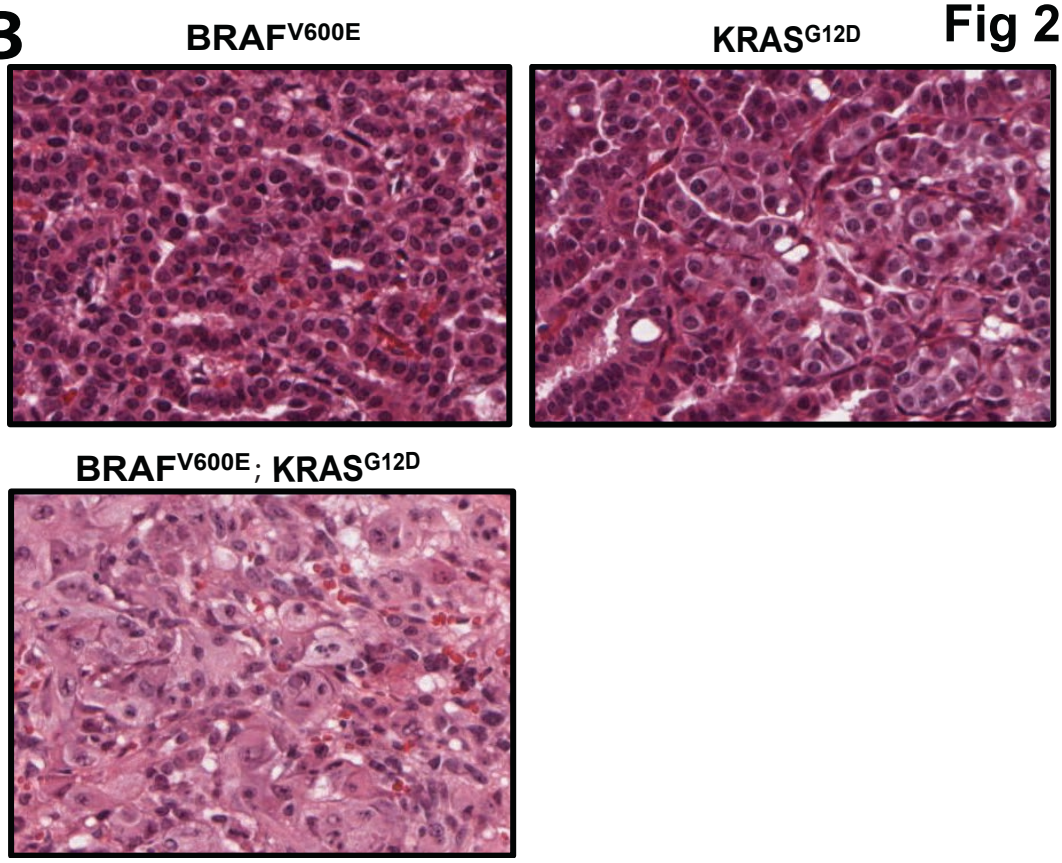
BRAF^{V600E}
KRAS^{G12D}
BRAF^{V600E}; KRAS^{G12D}
BRAF^{V600E}
KRAS^{G12D}
KI67
KI67
BRAF^{V600E}; KRAS^{G12D}
KI67

CHAPTER 3: Mutational activation of PIK3CA^{H1047R} dramatically accelerates BRAF^{V600E} and KRas^{G12D} induced lung tumorigenesis

Activation of the *PIK3CA* kinase domain mutant p110α^{H1047R} is insufficient to induce tumorigenesis in the mouse lung.

It has not been explored whether physiological activation of mutant PI3'K could initiate lung tumorigenesis in a mouse model, although others have claimed that transgenic expression of PIK3CA^{H1047R} is pro-tumorigenic in the lung epithelium (26). We obtained a conditional mouse in which Cre Recombinase leads to the expression of the *Pik3ca* gene encoding the PI3'K catalytic domain mutant p110α^{H1047R} (40). Mice heterozygous or homozygous for the conditional *Pik3ca$^{lat\text{-}H1047R}$* allele and also combined with floxed PTEN alleles were dosed with 10^7 pfu AdCre intranasally and euthanized at 3 months, 6 months, and 12-15 months. Adenomas were only found at the latest time point and only in *Pik3ca$^{lat\text{-}H1047R/lat\text{-}H1047R}$; Pten$^{flox/flox}$* mice at a frequency of less than 1 tumor per mouse. All adenomas in these mice were determined to be pAKT (-), PTEN (+) by immunostaining, suggesting that they arose from a spontaneous mutation and were not induced by Cre-mediated recombination of conditional alleles. In genotypes with at least one conditional *Pik3ca* and one or two floxed *PTEN* alleles, small hyplerplasias were found in patchy areas in the airways, and were most prevalent in the *Pik3ca$^{lat\text{-}H1047R/lat\text{-}H1047R}$; Pten$^{flox/flox}$* genotype. These stained positive for pAKT, and levels of signal correlated with genotype: mice homozygous for both the conditional *Pik3ca* and floxed *Pten* alleles had the brightest signal (Fig 3-1). Such hyperplasias in mice homozygous for the floxed *Pten* allele were negative for PTEN expression through immunostaining (data not shown),

indicating these lesions are a product of recombination. Few of these hyperplasias were proliferative by staining with KI67, and none were larger than 50 μm, indicating an arrest in development. This demonstrates that hyperactive signaling of the PI3'K pathway is insufficient in the formation of tumors in the mouse lung. This is in contrast to mutations in the MAPK pathway such as KRAS and BRAF, known to robustly induce tumors.

Mutational activation of PI3'Kα dramatically accelerates BRAF^{V600E} driven tumorigenesis in the mouse lung

To determine the effects of mutational activation of the PI3'K pathway on BRAF^{V600E}– driven tumorigenesis, we crossed the *Pik3ca$^{Lat\text{-}H1047R}$* and *BRaf^{CA}* mice to generate a cohort of littermates with either *BRaf^{CA}* alone, or both *Pik3ca$^{Lat\text{-}H1047R}$* and *BRaf^{CA}* alleles (compound). At 8 weeks of age, mice were infected with 10^7 pfu AdCre. Three weeks after infection, *Pik3ca$^{Lat\text{-}H1047R}$; BRaf^{CA}* mice began to show labored breathing and weight loss. At this time point, all mice from both groups were euthanized and lung tumor burden was quantified. *Pik3ca$^{Lat\text{-}H1047R}$; BRaf^{CA}* mice presented with significantly more tumors than *BRaf^{CA}* mice (96 vs. 54, p=.025), and had tumors that were on average larger (52,516 μm^2 vs. 6,782.5μm^2, p=.004). Tumors in compound mutant mice appeared as fully formed adenomas, whereas *BRaf^{CA}* mice had mostly small alveolar and airway hyplerplasias. Overall, compound mutant mice had a 14-fold higher tumor burden at three weeks post AdCre infection (16.8% vs. 1.2%, p= .01) (Fig 3-2A). This experiment was repeated with 10^6 pfu AdCre. At this titer, *Pik3ca$^{Lat\text{-}H1047R/+}$; BRaf^{CA}* survived until 7 weeks and had greater than 6 times the percent tumor burden compared to *BRaf^{CA}* littermates (34% vs. 5%, p = <.001), (data not shown).

To compare long term survival of single and compound mutant mice, mice were infected with 5 x 10^6 pfu AdCre and aged out until heavy tumor burden necessitated euthanasia. On average, *BRaf*^{CA} mice lived 2.5x longer than *Pik3ca*$^{Lat\text{-}H1047R/+}$*; BRaf*^{CA} mice after AdCre infection (100 days vs. 39, p = 1.25 x 10^{-5}), (Fig. 3-3). Mice carrying only the conditional *Pik3ca* allele, even when combined with floxed *Pten* alleles survived well beyond the time at which all mice harboring the *BRaf* allele had died. These mice died of old age rather than a lung tumor phenotype (Data not shown).

Inhibition of PI3'K >AKT signaling has no effect on BRAF^{V600E} induced tumorigenesis

To address the effects of PI3'K signaling inhibition on the cooperation observed in compound mutant mice, we initially sought to determine if inhibition of AKT interfered with the development of tumors driven by BRAF^{V600E} alone. *BRaf*^{CA} mice were infected with 10^6 pfu AdCre. At 5 weeks post infection, mice were split into two groups and dosed with either vehicle or 120 mg/kg of AKT inhibitor MK-2206 by oral gavage daily for five weeks. All mice were euthanized and tumor burden was assessed five weeks later. Mice treated with MK-2206 had diminished pAKT levels in whole-lung lysates compared to vehicle treated mice, demonstrating the effectiveness of the drug (Figure 3-4B). There was no difference in average tumor burden between the vehicle and MK-2206- treated *BRaf*^{CA} mice (vehicle- 25%, MK-2206- 22%, p =.63). This demonstrates that blockade of PI3'K>AKT signaling had no effect on tumorigenesis driven by BRAF^{V600E} alone (Fig 3-4 A), and that MK-2206 does not effect the normal stroma in a manner that interferes with tumor growth.

Inhibition of PI3'K > AKT signaling prevents cooperation in *Pik3ca*$^{Lat\text{-}H1047R}$*; BRaf*^{CA} mice

To assess the role of signaling downstream of PI3'K in tumor cooperation, *Pik3ca*$^{Lat\text{-}H1047R/+}$*; BRaf*$^{CA/+}$ mice were infected with 10^6 pfu AdCre and were dosed with 120 mg/kg MK-2206 or vehicle starting two weeks post infection. After four weeks of dosing, mice were euthanized and lung tumor burden was quantified. Tumor number did not differ between mice treated with vehicle and mice treated with MK-2206 (vehicle = 31.8; MK-2206 = 28.7; p = .76, Fig 3-5A & C). The drug treated groups showed a significant decrease in tumor size. (Vehicle= 121,413 μm^2, MK-2206= 30,083 μm^2, p = <.0001, Fig 3-5A & C). Overall, decrease in tumor size led to a significant decrease in tumor burden in mice treated with AKT inhibitor when compared to vehicle treated mice (vehicle = 20.7% , MK-2206 = 5%, p = .004, Fig 3-5A & C). The effect on tumor size but not number may be attributed to time of dosing- at two weeks post infection, compound mutant mice show a difference in tumor burden between *BRaf*^{CA} mice, and at this time point, a significant number of tumors are already initiated in compound mutant mice (data not shown).

To test whether cooperation was prevented by AKT inhibition, tumor burden was compared in *Pik3ca*$^{Lat\text{-}H1047R/+}$*; BRaf*^{CA} mice treated with MK-2206, and *BRaf*^{CA} mice treated with vehicle. Vehicle treated mice expressing BRAF^{V600E} alone had a similar tumor burden to compound mutant mice treated with drug (*BRaf*^{CA} vehicle= 7.3%, *Pik3ca*$^{Lat\text{-}H1047R}$*; BRaf*^{CA} MK2206= 5%, p = .33, Fig 3-5A & C). Tumor number was not significantly different between both groups (*BRaf*^{CA} vehicle = 22.6, *Pik3ca*$^{Lat\text{-}H1047R}$*; BRaf*^{CA} MK2206= 28.7, p = .42, Fig 3-5A & C). There was no significant difference between *BRaf*$^{CA/+}$ mice and MK-2206 treated *Pik3ca*$^{Lat\text{-}H1047R/+}$*; BRaf*$^{CA/+}$ mice in terms of tumor size. Taken together, this data indicates that treatment of *Pik3ca*$^{Lat\text{-}H1047R}$*; BRaf*^{CA} mice with AKT inhibitor prevented cooperation by affecting the growth of tumors, rather than the initiation of new lesions, and that the effect of the drug is largely cytostatic. (Fig. 3-5 A & C).

Past studies using MEK inhibitor PD0325901 have shown that $BRAF^{V600E}$ driven lung tumors require MAPK signaling for initiation and progression (19),(41). Additionally, experiments using a panel of cell lines from lung, pancreas, and colon cancers show resistance to MEK inhibition when harboring mutations in *PIK3CA*. In these experiments, resistance was conferred by sustained expression of Cyclin D in *PIK3CA* mutant cells (42, 43).

We sought to determine if mutational activation of PI3'K in $BRAF^{V600E}$- driven tumors could cause resistance to MEK inhibition in vivo. $Pik3ca^{Lat\text{-}H1047R}$; $BRaf^{CA}$ mice were infected with 10^6 pfu AdCre to initiate tumors. At two weeks, mice were dosed with PD0325901. After four additional weeks of dosing, mice were euthanized and lung tumor burden was assessed. PD0325901 treated mice had an average of two lesions/ lobe, 15x less than vehicle treated compound mutant mice (p = .005). PD0325901 treated mice presented with only few small alveolar and airway hyperplasias. No fully formed adenomas were present in these mice. This resulted in a greater than 100 fold reduction in average tumor size (10,914 μm^2 for drug treated mice, p < .0001). Overall, $Pik3ca^{Lat\text{-}H1047R}$; $BRaf^{CA}$ mice treated with PD0325901 had only .001% lung tumor burden: 20,000-fold less than vehicle treated mice (p = .004). This data indicates that tumors with activating mutations in both MAPK and PI3'K pathways remain sensitive to the anti-tumor effects of MEK inhibition, and highlight the importance of MAPK signaling in the initiation and maintenance of these tumors. (Figure 3-5 A & C).

Activation of $PIK3CA^{H1047R}$ does not cause $BRAF^{V600E}$ tumors to progress to adenocarcinoma

Due to the rapid onset of tumorigenesis in $BRaf^{CA/+}$; $PIK3ca^{lat\text{-}H1047R}$ mice and decreased survival, we could not assess malignant progression of tumors in these

mice. Euthanasia of mice occurred at a relatively early time points, when confluent tumor burden was comprised of low-grade adenomas, histopathologically similar in grade to what is observed in mice expressing the $BRAF^{V600E}$ oncoprotein by itself. In order to age the mice to appropriate time points to observe any possible progression, mice were dosed with a significantly lower titer of AdCre to induce fewer tumors. Compound mutant mice and their *BRaf*^{CA} littermates were infected with 10^3 pfu AdCre and aged to 20 weeks, at which point they remained outwardly healthy. On average, *BRaf*^{CA} mice had 4.5 lesions throughout the lungs while *BRaf*^{CA}; *Pik3ca*$^{lat\text{-}H1047R}$ mice had 8 lesions on average, for a total 46 lesions found in these mice, collectively. All lesions in compound mutant mice were benign adenomas, and histopathologically indistinguishable both in grade and size from tumors driven by $BRAF^{V600E}$ alone (Fig. 3-6).

Lungs from *KRas*^{LSL} mice infected with AdCre display about 10% of tumors classified as high-grade or adenocarcinoma at 17 weeks. The complete lack of advanced grade lesions in $BRAF^{V600E}$*;* $PIK3CA^{H1047R}$ lungs 20 weeks after infection indicates that mutational activation of PI3'K in the context of $BRAF^{V600E}$- driven tumorigenesis does not drive progression. This means that activating the MAPK and PI3'K pathway in parallel through mutations does not phenocopy mutant KRAS driven lung tumorigenesis.

Activation of $PIK3CA^{H1047R}$ accelerates the development of adenocarcinoma in $BRAF^{V600E}$; $p53^{-/-}$ tumors.

It has been established that loss of p53 causes $BRAF^{V600E}$- driven tumors to progress to adenocarcinoma. High grade, invasive tumors are typically seen at late time points (12+ weeks) in *BRaf*$^{CA/+}$ *Trp53*$^{-/-}$ mice. We sought to determine if $PIK3CA^{H1047R}$ expression had an effect of the incidence or rate of tumor progression in this model.

We generated a mouse that was *BRAF*$^{CA/CA}$*; Trp53*$^{-/-}$; *PIK3CA*$^{lat\text{-}1047R}$ and infected it with 10^7 pfu AdCre along side a *BRaf*$^{CA/+}$; *Trp53*$^{-/-}$ littermate control mouse. After four weeks, the *BRaf*$^{CA/CA}$*; Trp53*$^{-/-}$*; Pik3ca*$^{lat\text{-}1047R}$ mouse began to display weight loss and labored breathing, as expected. Lungs were dissected and found to have confluent tumors. Overall, tumor burden in this mouse was 41% while the *BRaf*^{CA}*; Trp53*$^{-/-}$ control mouse had a tumor burden of only .2%. The control mouse had mostly hyperplasias, and the one adenoma present was small and benign (Fig 3-7). On the other hand, lungs of the *BRaf*$^{CA/CA}$*; Trp53*$^{-/-}$*; PIK3CA*$^{lat\text{-}1047R}$ mouse were full of high grade, anaplastic adenocarcinoma. In some regions, cells lost polarity and took on spindle formations, indicating an epithelial to mesenchymal transition (EMT). This was verified with positive staining for Vimentin, a marker of EMT. Regions expressing Vimentin had lost expression of TTF-1, a lung epithelial marker. Also, such regions were highly proliferative as determined by KI67, and expressed high levels of pS6, which is often found in high-grade lesions (Fig 3-7B). One lobe was removed from this mouse and used to establish a cell line for further analysis. This is the earliest example of tumor progression beyond grade three in any lung cancer model we have ever worked with. In our hands, BRAF^{V600E}; p53$^{-/-}$ tumors do not progress to adenocarcinoma until after at least 12 weeks and the dramatic onset of high-grade lesions within four weeks due to PIK3CA^{H1047R} expression strongly indicates that PIK3CA activation not only speeds up tumor initiation, but progression a well. The presence of a second conditional *BRaf* allele likely did not contribute to the phenotype, as past experiments have shown no significant difference in tumor grade between *BRaf*$^{CA/+}$ and *BRaf*$^{CA/CA}$ mice (data not shown).

Loss of PTEN tumor suppressor cooperates with BRAF^{V600E} in lung tumorigenesis

Experiments have shown that loss of both copies of PTEN does not lead to the development of tumors in the lung, but PTEN loss accelerated tumorigenesis driven by $KRAS^{G12D}$ (44). We have further shown that PTEN on its own does not induce tumorigenesis, even when combined with the $PIK3CA^{H1047R}$ mutation. Due to the dramatic cooperation in tumorigenesis when combining PIK3CA and BRAF mutations, we next sought to determine if PTEN loss would have a similar effect. PTEN is a phosphatase which counteracts the PI3'K pathway by the removal of the 3' phosphate of PI(3,4,5)P3 and is often found deregulated in human cancer through epigenetic silencing, point mutation, or deletion (10). This allows for activation of effectors downstream of PI3'K which confer a growth advantage to the cell. We obtained a mouse for conditional loss of *Pten* to determine if PTEN silencing might lead to increased multiplicity of $BRAF^{V600E}$ tumors in the mouse lung such as observed with the PIK3CA mutation. $Pten^{flox/flox}$ mice were bred for at least 5 generations with FVB/N mice, the same genetic background as $BRaf^{CA}$ and $Pik3ca^{lat\text{-}H1047R}$ mice. Mice that were $BRaf^{CA/+}$, $BRaf^{CA/+};Pik3ca^{lat\text{-}H1047R}$, and $BRaf^{CA/+};Pten^{flox/flox}$ were infected with 10^6 pfu AdCre, and euthanized four weeks post infection. PTEN loss cooperated with $BRAF^{V600E}$ in lung tumorigenesis, but not to the same degree as the PIK3CA catalytic domain mutation. At four weeks, $BRaf^{CA}$ mice had an overall tumor burden of 2.8% while $BRaf^{CA};Pten^{flox/flox}$ had an average tumor burden of 10.8% (p = .028). As expected, $BRaf^{CA}$; $Pik3ca^{lat\text{-}H1047R}$ had significantly higher tumor burden than $BRaf^{CA}$ mice (31.2%, p = <.001), but also had significantly higher tumor burden than $BRaf^{CA}; Pten^{flox/flox}$ mice (p = .007). This data supports our initial findings that hyperactivation of PI3'K signaling contributes to enhanced tumorigenesis and demonstrates that this can also occur through the mechanism of PTEN loss.

Activation of $PIK3CA^{H1047R}$ enhances tumorigenesis driven by $KRAS^{G12D}$

Due to the high number of human tumors with *KRAS* mutations, and the known co-mutational frequency with *PIK3CA* mutations, we next sought to determine if PI3'K activation had a similar cooperative effect in tumors driven by $KRAS^{G12D}$. The conditional $Pik3ca^{Lat\text{-}H1047R}$ mouse was bred with the $KRas^{LSL}$ mouse, in which the $KRAS^{G12D}$ oncoprotein is expressed following Cre-mediated recombination (17). These mice develop tumors that are phenotypically similar to $BRAF^{V600E}$ driven tumors at early time points, but have a significantly decreased onset and multiplicity of tumorigenesis (41). We generated a cohort of compound mutant mice with both conditional alleles of *KRas* and *Pik3ca*, along with littermates with the $KRas^{LSL}$ allele alone. Five weeks after infection with 10^7 pfu AdCre, compound mice began to show signs of heavy tumor burden and all mice from both groups were euthanized. Upon examination of lungs, tumors in compound mutant mice were confluent, fully formed adenomas, whereas littermates with only *KRas* mutated had few lesions, which were mostly epithelial hyperplasias. Compared to that with $BRAF^{V600E}$, cooperation between $PIK3CA^{H1047R}$ and $KRAS^{G12D}$ was even more dramatic, with a 92- fold greater tumor burden in the double mutant mice (46% vs. .5%, p= <.0001, Fig. 3-9).

Cell lines isolated from $PIK3CA^{H1047R}$; $BRAF^{V600E}$; $TRP53^{-/-}$ tumors are sensitive to the combined effects of MAPK and PI3'K pathway inhibition

Cells were isolated from lungs of a $BRaf^{CA}$; $Trp53^{flox/flox}$; $Pik3ca^{latH1047R}$ mouse four weeks after 10^7 pfu AdCre infection. This mouse presented with high-grade, anaplastic adenocarcinoma upon euthanasia (Fig. 3-7). Mixed population cells were cultured in DMEM and a number of clones were selected and grown out. Recombination of both the *BRaf* and *Pik3ca* alleles was verified with PCR (Data not shown). Recombination of the *BRaf* allele was further validated through the loss of resistance to G418. Prior to Cre-mediated recombination, the $BRaf^{CA}$ allele contains

a G418 resistance cassette that is lost upon recombination. A subset of cells cultured in media containing G418 died while control cells treated with vehicle survived. Finally, expression of $BRAF^{V600E}$ was determined through western blotting using an antibody specific to the oncoprotein (Data not shown).

Baseline signaling levels were assessed by isolating protein from a number of lung tumor derived cell lines growing in culture. Protein expression was compared to previously described $BRAF^{V600E}$; $TP53^{-/-}$ cells. In the line expressing mutant PIK3CA, activation of pathways downstream of PI3'K signaling was increased relative to control cells expressing wild-type PIK3CA. Phosphorylation of AKT at serine 473, as well as phosphorylated PRAS40 and S6 were for the most part elevated relative to PIK3CA wild type clones. (Fig 3-10 A). Clone 5 from the $BRAF^{V600E}$; $TRP53^{-/-}$; $PIK3CA^{H1047R}$ cell line was chosen for further analysis.

Next we sought to assess if inhibition of MAPK, PI3'K or both signaling pathways would have an affect on the growth of the $BRAF^{V600E}$; $TRP53^{-/-}$; $PIK3CA^{H1047R}$ cell line. A proliferation assay was set up in which cells were seeded in triplicate at 10^4 cells/mL and treated the following day with a range of inhibitors: vehicle control, 1μM- 15.6nM MEK inhibitor PD0325901 and ERK inhibitor SCH772984, 5μM- 7.8nM AKT inhibitor MK-2206 and PI3'K inhibitor GDC-0941, and combinations of PD0325901 + GDC-0941 and SCH772984 + MK-2206. 72 hours after initial treatment, a CellTitre-Glo viability assay was performed. In this assay, cells are lysed and a luminescent signal is generated which is proportional to the amount of ATP present, which itself is directly proportional the amount of metabolically active cells. PD0325901 and GDC-0941 were effective in decreasing cell viability after 72 hours, while the combination of the drugs had the strongest effect, demonstrating potential synergy particularly at higher concentrations of both drugs (Fig. 3-10B). MK-2206 had the weakest effect on this cell lines, demonstrating a cytostatic effect even at the

highest concentrations of drug. SCH772984 also had mostly a cytostatic effect, showing only a decrease in cell viability at the high concentrations of drug. The combination of MK-2206 and SCH772984 was more effective then both drugs by themselves, though synergy was difficult to demonstrate in this case due to the lack of effect by MK-2206 (Fig. 3-10B).

Cells were relatively sensitive to MEK inhibition, showing a steady decrease in cell viability as PD0325901 concentration was increased. PI3'K inhibition was somewhat effective at high concentrations, but cell viability was increased in low concentrations of GDC-0941. The combination of PD0325901 and GDC-0941 was the most effective in reducing cell viability, showing a significant decrease in cell viability at the smallest concentrations of drugs, and having the lowest GI_{50} value of all treatments (Fig. 3-10B).

We then chose the maximum dose of all drugs and performed 24 hours treatments in 10cm dishes for protein extraction. Cells were imaged 24 hours after drug edition before lysis and protein extraction. At this time point, the combination of PD0325901 and GDC-0941 was still the most effective, resulting in the presence of dead and floating cells (Fig 3-10C). Either drug by itself was not effective in resulting in cell death, but GDC-0941 appeared to have the strongest cytostatic effect, preventing cell growth relative to the vehicle-treated control plate. PD0325901, SCH772984, and MK-2206- treated cells did not appear strikingly different than vehicle treated cells at this time point (Fig 3-10C).

Western blot analysis was then performed on these cell lysates to verify effectiveness of drug and examine signaling pathway alterations. For this experiments, we performed 24 hour drug treatments with 1μM PD0325901 and SCH772984, and 5μM GDC-0941 and MK-2206. For drug combinations, PD0325901 and SCH772984 were both combined with MK-2206. Effectiveness of drug was

verified with loss of pERK 1/2 from PD035901 and SCH772984 and loss of pAKT and pPRAS40 with GDC-0941 and MK-2206 (Fig. 3-10D). pS6 levels were not effected by single agents but was decreased when combinations of drugs were used. This makes sense because both MAPK and PI3'K signaling pathways activate mTORC1 through the inhibition of TSC. Cyclin D expression was not decreased significantly in single agent treatments, but was reduced upon combination treatment. Cdk4 and Cdk2 expression followed the same pattern, indicative of G_1 arrest. Cleaved Caspase 3 was greatly induced upon inhibition of both MAPK and PI3'K pathways. There was also a slight elevation in $p27^{KIP1}$, an inhibitor of cell cycle progression regulated by AKT.

To further explore the mechanism by which $PIK3CA^{H1047R}$ and $BRAF^{V600E}$ may cooperate to transform cells, we sought to evaluate anchorage independent growth in cell lines generated from tumor bearing mice. $BRAF^{V600E}$; $p53^{-/-}$ cells were infected with retroviruses containing constructs expressing puromycin resistance along with mCherry, bovine PI3'K $p110\alpha^{H1047R}$, and HA- tagged, myrisolated AKT (AKT^{myr}). After infection, cells were selected in DMEM containing 2ug/uL puromycin. PI3'K pathway activation was affirmed by Western blotting cell lysates for known effectors of (Fig 3-11-B). Cells were plated at 10^4 cells/mL in soft agar, and three weeks later colony formation was assessed. $BRAF^{V600E}$; $p53^{-/-}$ cell lines expressing mCherry did not form a single colony in soft agar, even when left for up to two months. Cells infected with $PIK3CA^{H1047R}$ and AKT^{myr} formed numerous colonies within three weeks. (12.5 and 17.5 colonies per imaged field, respectfully, Figure 3-11A). This demonstrates that activation of the PI3'K pathway by expression of the kinase domain mutant has a transforming effect on BRAF- driven cell lines and allows for anchorage independent growth. This effect is likely due to signaling through AKT, as the constituitively activate form of AKT also confers anchorage independent growth.

Because changes in expression levels of an oncogene can greatly influence cell transformation, we performed the soft agar colony formation assay with PIK3CA^{H1047R}; BRAF^{V600E}; p53$^{-/-}$ cells. This allowed us to test anchorage-independent growth in cells where the PIK3CA^{H1047R} mutation is expressed at physiological levels from the endogenous promoter. These cells were capable of forming colonies in soft agar, unlike BRAF^{V600E}; p53$^{-/-}$ cells with wildtype PIK3CA. To test the role of signaling through AKT in colony formation, we prepared the soft agar with 5 μM AKT inhibitor MK-2206, 5uM PI3'K inhibitor GDC-0941 and 1 μM MEK inhibitor PD0325901. Inhibition of both AKT and PI3'K entirely prevented colony formation in these cells. As expected, MEK inhibition also had this effect. Up to 2 months, no colonies were found in drug treated wells, while vehicle treated cells formed abundant colonies on average 13 colonies per imaged field, not significantly different than what was observed in BRAF^{V600E}; p53$^{-/-}$ cells infected with PIK3CA^{H1047R} or AKT^{myr} (Fig. 3-11C).

DISCUSSION

The PI3'K pathway is often deregulated in human tumors through activating mutations in the *PIK3CA* gene or loss of the negative regulator, PTEN. A recent study found that 2% of human lung adenocarcinoma harbor mutations in the *PIK3CA* gene which codes for the p110α catalytic subunit of PI3'K. Furthermore, AKT, the most studied effector of PI3'K, is often found to be over-expressed or amplified in a variety of human tumors (10). PI3'K signaling is important for the initiation of KRAS-driven tumors, as mice with a mutation in *Pik3ca* that prevents binding and activation by RAS have decreased tumorigenesis driven by endogenous $KRAS^{G12D}$ (45). Furthermore, using inhibitors of PI3'K, it has been shown that PI3'K signaling is important for initiation of $KRAS^{G12D}$-driven tumors in lung cancer mouse models (46).

Unlike *BRAF*, *PIK3CA* mutations are not mutually exclusive with *KRAS*, particularly in colon cancer (47). One study analyzed a variety of human tumors and found individuals with mutations in *KRAS* or *BRAF* had a higher frequency of *PIK3CA* mutations than individuals with wild type *KRAS* of *BRAF* (48). Another study focusing on human lung adenocarcinoma found that 70% of tumors with *PIK3CA* mutations had a co-occuring mutation in *KRAS* (62%), *EGFR* (19%), and *BRAF*, *MEK1*, *or ALK* (6%) (9). Such findings suggest an additional function for PI3'K pathway activation which may confer a growth advantage to tumors. We have already established that RAF/MEK/ERK signaling is necessary for $KRAS^{G12D}$ induced lung tumorigenesis and is sufficient in tumor initiation independent of KRAS. Using a conditional model for the mutational activation of *Pik3ca*, we sought to determine if the PI3'K signaling pathway had these same properties. The conditional *Pik3ca*^{latH1047R} mouse contains a Cre- inducible allele that allows for the controlled expression of p110α^{H1047R}, a constitutively active catalytic domain mutant. This

oncoprotein phosphorylates the PI(4,5)P2 to generate PI(3,4,5)P3 despite lack of upstream activator status (49).

We first tested the ability of the PIK3CA^{H1047R} to initiate lung tumorigenesis on its own and found that it is insufficient to induce tumors in the lung even up to one year after infection with high titers of AdCre. Although this mutation is found in a significant number of lung cancers, it is likely not a driver mutation in these tumors. Loss of PTEN along with expression of PIK3CA^{H1047R} leads to hyperplasias in the airways that are positive for pAKT. This agrees with the original report of the conditional PIK3CA^{H1047R} mouse, in which the *Pik3ca* mutation lead only to mild hyperplasia in the ovarian follicle, while in combination with PTEN loss, large tumors were observed (40). Other groups have also demonstrated that hyperactive PI3'K signaling through loss of PTEN fails to induce lung tumorigenesis (44). The inability of PIK3CA^{H1047R} to drive tumorigenesis is important to note due to the interest in targeting PI3'K and its downstream effectors in clinical trials (50).

We next wanted to determine if parallel mutational activation of RAF/MEK/ERK and PI3'K pathways would phenocopy tumor progression observed in KRAS^{G12D} driven lung tumors in order to assess the relative role that each effector pathway plays in terms of KRAS tumor initiation and progression. Activation of PIK3CA^{H1047R} greatly enhances the formation of tumors driven by both BRAF^{V600E} and KRAS^{G12D} in a manner that is dependent on AKT. At early and later time points, compound mutant mice had a greater tumor burden which decreased survival relative to littermates expressing only BRAF^{V600E}. Interestingly, parallel activation of both RAF/MEK/ERK and PI3'K pathways did not phenocopy KRAS in terms of tumor initiation. We found that expression of PIK3CA^{H1047R} greatly enhanced tumor initiation driven by BRAF^{V600E}. As shown in Chapter 2, KRAS^{G12D}- induced tumors tend to form later and at a smaller multiplicity than BRAF^{V600E}- induced tumors, but our findings

demonstrate that this is likely not due to activation of PI3'K signaling, as activation of this pathway greatly enhanced tumorigenesis in both models. Furthermore, we have previously shown that activation of both $KRAS^{G12D}$ and $BRAF^{V600E}$ decreases tumor multiplicity relative to $BRAF^{V600E}$ alone. Though PI3'K signaling is activated by KRAS and likely plays an important role in $KRAS^{G12D}$ tumor initiation, it is possible that negative feedback driven by oncogenic KRAS or alternate effector pathways of KRAS are actively inhibiting tumor initiation. Another possiblilty is that hyperactivation of PIK3CA in the context of $KRAS^{G12D}$ tumorigenesis drives proliferation in an additional subset of cells, though we could not readily detect differences in cell type marker expression (data not shown).

After observing such striking cooperation in terms of tumor initiation, we wanted to determine if dual activation of RAF/MEK/ERK and PI3'K pathways could drive tumor progression in $BRAF^{V600E}$- driven tumors which normally do not progress beyond benign adenomas. PI3'K signaling through loss of PTEN in benign nevi initiated by $BRAF^{V600E}$ drives progression to aggressive and invasive lesions in the mouse model for melanoma (51). We hypothesized that we could drive progression in benign lung adenomas driven by $BRAF^{V600E}$ through expression of $PIK3CA^{H1047R}$. A subset of KRAS- driven tumors are found to have progressed to adenocarcinoma at later stages, and it is possible that this is due to engagement of the PI3'K signaling pathway (41). We infected mice with low titers of AdCre and aged them out to assess this. We found that compound mutant mice had only benign adenomas 20 weeks after AdCre infection. Lack of progression in $BRAF^{V600E}$; $PIK3CA^{H1047R}$ tumors demonstrates that KRAS driven tumors are not simply engaging RAF/MEK/ERK and PI3'K signaling to cause progression. Indeed, since only a fraction of KRAS- driven tumors progress, a likely scenario is that alternate pathways must be activated stochastically in order to drive progression in these tumors. One potential alternative

effector pathway is through RAC-1, which has been shown to play a role in initiation of $KRAS^{G12D}$- driven tumors (52).

Since $PIK3CA^{H1047R}$ activation did not appear to drive progression in $BRAF^{V600E}$ tumors, we wanted to determine if its activation would accelerate progression in $BRAF^{V600E}$; $p53^{-/-}$ tumors. We conditionally activated $BRAF^{V600E}$ and $PIK3CA^{H1047}$ and prevented expression of *TRP53* in the mouse lung to determine if we could promote tumors to progress beyond what is normally observed in $BRAF^{V600E}$; p53 null tumors. Not only were there significantly more lesions in $BRAF^{V600E}$; $PIK3CA^{H1047R}$; $p53^{-/-}$ mice, the majority of tumors found in this mouse four weeks after AdCre infection were advanced lesions that were determined to be undergoing epithelial to mesenchymal transition (EMT), a hallmark in the progression of advanced and potentially invasive lesions (53). This finding suggests that activation of PI3'K signaling not only enhances tumor initiation, but accelerates the progression of tumors lacking p53.

We used a conditional mouse model for loss of PTEN to further demonstrate cooperation between PI3'K signaling and $BRAF^{V600E}$. Though cooperation was not as striking as in $BRAF^{V600E}$; $PIK3CA^{H1047R}$ lung tumorigenesis, $BRAF^{V600E}$; $PTEN^{-/-}$ mice had a significantly higher tumor burden than mice expressing $BRAF^{V600E}$ alone. Loss of PTEN is a common event in human cancer and serves a number of tumor suppressive functions besides directly antagonizing PI3'K signaling through its phosphatase activity (54), though the dramatic cooperation previously observed with $BRAF^{V600E}$ and $PIK3CA^{H1047R}$ suggests that loss of PTEN cooperates through activation of PI3'K> AKT signaling. $BRAF^{V600E}$; $PTEN^{-/-}$ tumors still express wild type PIK3CA and are thus sensitive to regulation at the level of upstream activators such as receptor tyrosine kinases, which may explain the diminished cooperation in these mice.

PIK3CA mutations are often found in tumors with KRAS mutations. Since it is known that KRAS engages PI3'K signaling, it would seems redundant to have both KRAS and PI3'K mutationally activated. Thus, it is likely that in tumors with only KRAS mutated, KRAS is not fully activating normal PI3'K signaling, and additional activation of this pathway can confer a growth advantage to tumor cells. We found a striking cooperation in tumor initiation when both $KRAS^{G12D}$ and $PIK3CA^{H1047R}$ were both activated in the mouse lung. Since KRAS has a relatively long latency to tumor formation, these results were more significant that the cooperation observed with $BRAF^{V600E}$. We previously found that dual activation of $BRAF^{V600E}$ and $KRAS^{G12D}$ depressed tumorigenesis, indicating the KRAS signaling was actively preventing tumor initiation. This could potentially be through suppression of PI3'K, as mutational activation of PIK3CA greatly enhanced tumorigenesis driven by KRAS. Furthermore, $PIK3CA^{H1047R}$ could be actively suppressing a growth inhibitory pathway engaged by $KRAS^{G12D}$. These findings support the notion of using combined targeting therapy against RAF/MEK/ERK and PI3'K signaling in human tumors with KRAS mutated, as inhibiting the PI3'K signaling arm may prevent as additional growth advantage to tumor cells driven by KRAS.

One potential mechanism for increased tumor burden when PIK3CA is activated is the ability to evade apoptosis. KRAS or BRAF expression may induce a subset of cells to undergo programmed cell death, and hyperactivation of PI3'K signaling may actively repress this by the AKT mediated phosphorylation and inhibition of pro-apoptotic proteins such as BAD. In our *in vivo* studies we did not observe any obvious signs of apoptosis in $KRAS^{G12D}$ or $BRAF^{V600E}$ expressing lungs through cleaved Caspase 3 staining or TUNEL assays. It is possible that apoptotic cells are eliminated by macrophages patrolling the lung. Another scenario is that hyperactivation of PI3'K signaling prevents engagement of oncogene-induced

senescence (OIS) in a subset of cells expressing $BRAF^{V600E}$ or $KRAS^{G12D}$. Past studies using primary human fibroblasts have demonstrated that senescence induced by hyperactive RAS or RAF in a subset of cells was dependent of the suppression of PI3'K>AKT signaling (55). One mechanism that senescence could be achieved in these cells is through the activation of FOXO transcription factors. FOXO proteins are known tumor supressors that exert their function in the nucleus. Active AKT phosphorylates FOXO resulting in its export to the cytoplasm where it cannot function (56). In vivo data demonstrated that senescent cells with depressed PI3'K>AKT signaling had active FOXO in the nucleus (55). Mutational activation of PIK3CA likely overrides global negative feedback mechanisms that promote senescence through the activation of FOXO proteins as well as Rb and p53 pathways. This may be an explanation for the cooperation observed when $PIK3CA^{H1047R}$ is expressed with $BRAF^{V600E}$ and $KRAS^{G12D}$ in the lung epithelium. When staining our tissue sections from compound mutant mice for phospho-FOX01, we found high cytoplasmic signals in a subset of cells in regions of epithelial hyperplasias, implying that inactivation of FOX01 may contribute to enhanced tumor initiation (data not shown).

Other mechanisms of cooperation between the RAS/RAF/MEK/ERK and PI3'K> AKT pathways may directly impact cell cycle machinery. In NIH 3T3 cells, conditional activation of RAF induced G1 cell cycle arrest, but activation of both RAF and AKT strongly promoted S phase progression by the induction of Cyclin D and repression of $p27^{KIP1}$, a negative regulator of the cell cycle (57).

It was difficult to assess the levels of signal pathway activation downstream of PI3'K using standard immunohistochemistry techniques on tumor sections. Indeed, we were unable to detect phospho-AKT in any compound mutant adenomas using this technique. Whole lung lysates taken from mice with full tumor burden did,

however, show elevated pAKT in compound mutant mice when compared to $BRAF^{V600E}$ expressing littermates, but whole lung lysates contain protein from non-transformed cells which complicates analysis (data not shown). In order to understand the mechanism of cooperation we observed *in vivo*, we turned to cell lines isolated from tumor bearing mice. The isolation of cells from tumors lacking TRP53 allowed for an *in vitro* interrogation of signal pathway activation.

Baseline lysates of cells growing in culture showed enhanced signaling downstream of PI3'K in cells carrying the $PIK3CA^{H1047R}$ mutation. In all compound mutant clones, pAKT was increased as well as phosphorylation of PRAS40. PRAS40 is a negative regulator of mTORC1, and when phosphorylated by AKT, this inhibition is relieved to promote cell growth. Increased phosphorylation of FOX01 was also found in cells expressing $PIK3CA^{H1047R,}$ further validating active PI3'K>AKT signaling in this system.

Cells with both $BRAF^{V600E}$ and $PIK3CA^{H1047R}$ were sensitive to the combined effects of MAPK and PI3'K/AKT signaling. Cells displayed sensitivity to individual MEK and ERK inhibition, as expected due to the observation that compound mutant tumors remain sensitive to MEK inhibitor PD0325901 *in vivo*. While PI3'K inhibition by GDC-0941 had an effect as well, AKT inhibition by MK-2206 only appeared to have minimal cytostatic effect even at high concentrations. AKT inhibition prevented cooperation in tumor formation by $BRAF^{V600E}$ and $PIK3CA^{H1047R}$ *in vivo*, but did cause regression of pre-existing tumors, which may explain the minimal effects of MK-2206 *in vitro*. Combining MEK and ERK inhibitors with PI3'K and AKT inhibitors was the most effective in preventing cell proliferation as well as inducing cell death. Lysates taken cells treated for 24 hours with individual drugs or combinations reflected the anti-growth effects of combinatorial treatment. Cyclin D was most strongly repressed when combining pathway inhibition as well as decreases in CDK2 and CDK4.

Induction of growth arrest upon drug treatment was likely mediated through expression of BIM, as it was most strongly expressed in cells treated with PD0325901, GDC-0941, and PD/GDC and SCH/MK combination treatment which had the strongest effects of cell growth. Furthermore, $p27^{KIP1}$ was elevated in these treatments as well. The ability for combination treatment to induce growth arrest likely occurred through destabilization of cyclin D and expression of $p27^{KIP1}$, in agreement with previous studies using fibroblasts (57). Finally, combination treatment resulted many floating cells as well as an increase in Cleaved- Caspase 3 expression. This finding suggests that inhibition of both MAPK and PI3'K signaling in cells with both pathways activated is sufficient to prevent growth and induce cell death, supporting the notion of combined therapy in the clinic.

We found a clear-cut difference in the ability to form colonies in soft agar when comparing cells with $BRAF^{V600E}$ and both $BRAF^{V600E}$ and $PIK3CA^{H1047R}$ mutations. While $BRAF^{V600E}$; $PIK3CA^{H1047R}$ mutant cells are readily able to grow in an anchorage independent manner that depends of PI3'K>AKT signaling, $BRAF^{V600E}$ expressing cells were consistently unable to do so. Ectopic expression of $PIK3CA^{H1047R}$ and myristoylated AKT allowed for these cells to grow in soft agar, however. This observation agrees with past findings that demonstrated activation of PI3'K prevents anoikis upon detachment from the extracellular matrix in cells transformed by Ras (58).

Overall, tumors with activating mutations in both *BRaf* or *KRas* and *Pik3ca* had a much higher efficiency of initiation. Long term studies to determine if $PIK3CA^{H1047R}$ influences progression of $KRAS^{G12D}$ tumors remains to be conducted, but it appears that $PIK3CA^{H1047R}$ does not drive progression of tumors driven by $BRAF^{V600E}$. Despite this, the development of adenocarcinoma in $BRAF^{V600E}$- driven tumors that lack p53 is greatly enhanced when $PIK3CA^{H1047R}$ is expressed. Thus, it is likely that this

mutation will speed up the development of adenocarcinoma in tumors driven by KRAS. Despite being an active effector of KRAS which is involved in tumorigenesis, it appears as if PI3'K signaling remains rate limiting in terms of $KRAS^{G12D}$ tumor initiation. Our studies, as well as the presence of both KRAS and PIK3CA activating mutations in human patients indicate combined PI3'K pathway and MAPK targeting remains a viable option for treatment of such tumors. Further studies using long term combined treatment with MAPK and PI3'K signaling in mice harboring $BRAF^{V600E}$ or $KRAS^{G12D}$ along with $PIK3CA^{H1047R}$ are currently underway. We know that compound $BRAF^{V600E}$; $PIK3CA^{H1047R}$ tumors remain sensitive to PD0325901, and additional experiments show that $KRAS^{G12D}$; $PIK3CA^{H1047R}$ tumors are also sensitive (data not shown). Using $BRaf^{CA}$ and $KRas^{LSL}$ mice, we know that PD0325901 treatment is not an effective cure for KRAS driven tumors, as tumor burden is quickly re-established after drug removal. It may be possible to prevent this by combining a MEK inhibitor with a PI3'K or AKT inhibitor, as the importance of PI3'K signaling in $KRAS^{G12D}$ driven tumors has been established.

Figure 3-1. Activation of PIK3CA^{H1047R} on its own fails to initiate tumorigenesis in the mouse lung.

PIK3CA$^{lat\text{-}H1047R/lat\text{-}H1047R}$ and *PIK3CA$^{lat\text{-}H1047R/lat\text{-}H1047R}$; PTEN$^{flox/flox}$* mice were infected with 10^7pfu and aged to six months.

A. H and E stains showing normal lungs in *PIK3CA$^{lat\text{-}H1047R/lat\text{-}H1047R}$* and small epithelial hyperplasias in *PIK3CA$^{lat\text{-}H1047R/lat\text{-}H1047R}$; PTEN$^{flox/flox}$* mice at six months post AdCre.

B. phosho-AKT (Ser 473) and KI67 immunofluorescent stains *PIK3CA$^{lat\text{-}H1047R/lat\text{-}H1047R}$* and *PIK3CA$^{lat\text{-}H1047R/lat\text{-}H1047R}$; PTEN$^{flox/flox}$* mice showing an increase in phospho- AKT signal in epithelial hyperplasia when PTEN is lost.

Figure 3-2. Activation of PIK3CA^{H1047R} enhances tumorigenesis driven by BRAF^{V600E}.

BRaf^{CA} and *BRaf^{CA};Pik3ca$^{lat\text{-}H1047R}$* mice were infected with 10^7 pfu AdCre and euthanized three weeks later. Tumor number, size, and percent burden were quantified. Bar represents 100μm.

Figure 3-3. Survival of BRaf$^{CA/+}$ and BRaf$^{CA/+}$; Pik3ca$^{lat\text{-}H1047R}$ mice following AdCre infection.

BRaf^{CA} and *BRaf^{CA}; Pik3ca$^{lat\text{-}H1047R}$* mice were infected with $5x10^6$ pfu AdCre and aged out until heavy tumor burden necessitated euthanasia. Percent of animals alive was determined each day after infection until all animals were euthanized.

Figure 3-4. Inhibition of PI3'K signaling does not effect the development of BRAF^{V600E}- driven lung tumors.

BRaf^{CA} mice were infected with 10^6 pfu AdCre to initiate BRAF^{V600E}- driven tumorigenesis. Five weeks later mice were dosed with 120 mg/kg of AKT inhibitor MK-2206 or vehicle control.

A: H and E staining of lungs from treatment and vehicle groups and quantification of percent tumor burden. Bar represents 500μM.

B. Western blot of whole lobe lysates probed with antibodies against phospho-AKT (Ser 463) and phospho-ERK 1/2 (Thr 202/Tyr 204) demonstrating effectiveness of AKT inhibitor MK-02206.

Figure 3-5. Inhibition of AKT signaling prevents cooperation between BRAF^{V600E} and PI3'K^{H1047R}

BRaf^{CA}; Pik3ca$^{lat\text{-}H1047R}$ mice were infected with 10^6 pfu AdCre and five weeks later dosed with 120 mg/kg MK-2206, 12.5 mg/kg PD0325901, or vehicle. *BRaf^{CA}* mice were infected with 10^6 pfu AdCre and five weeks later mice were dosed with vehicle.

A. H and E staining of lungs. Bar represents 500μM.

B. Western blots of whole lobe lysates probed with antibodies against phospho-AKT (Ser 473) and phospho- ERK 1/2 (Thr 202/Tyr 204), demonstrating effectiveness of AKT inhibitor MK-2206 and MEK inhibitor PD0325901.

C. Quantification of tumor number, size, and percent burden of AdCre infected *BRaf$^{CA;}$Pik3ca$^{lat\text{-}H1047R}$* mice treated with MK-2206, PD0325901, or vehicle, and *BRaf^{CA}* mice treated with vehicle.

Figure 3-6. Activation of PIK3CA^{H1047R} does not cause BRAF^{V600E}-driven tumors to progress to adenocarcinoma.

BRaf^{CA} and BRaf^{CA}; Pik3ca$^{lat\text{-}H1047R}$ mice were infected with 10^3 pfu AdCre and aged out to 20 weeks. H and E staining of representative tumors show lack of progression in both genotypes.

Figure 3-7. Activation of PIK3CA^{H1047R} accelerates the development of adenocarcinoma in BRAF^{V600E}; p53$^{-/-}$ tumors.

BRaf$^{CA/+}$; Trp53$^{flox/flox}$ and *BRaf$^{CA/CA}$; Trp53$^{flox/flox}$; Pik3ca$^{lat\text{-}H1047R}$* mice were infected 10^7 pfu AdCre and aged out to four weeks.

A. H and E staining of lungs from both genotypes with high magnification of two different tumors from the *BRaf$^{CA/CA}$; Trp53$^{flox/flox}$; Pik3ca$^{lat\text{-}H1047R}$* mouse showing anaplastic cells and epithelial to mesenchymal transition (EMT).

B. Immunohistochemical staining of a high-grade tumor from the *BRaf$^{CA/CA}$; Trp53$^{flox/flox}$; Pik3ca$^{lat\text{-}H1047R}$* mouse. Loss of TTF-1 and expression of Vimentin indicate EMT. High expression of phospho-S6 (Ser 235/236) and KI67 indicate the highly proliferative and progressed state of this lesion.

Figure 3-8. Loss of PTEN cooperates with BRAF^{V600E} in lung tumorigenesis.

BRaf^{CA}, BRaf^{CA}; Pik3ca$^{lat\text{-}H1047R}$, and *BRaf^{CA}; PTEN$^{flox/flox}$* mice were infected with 10^6 pfu AdCre and euthanized four weeks later.

A. Immunohistochemical stain against PTEN demonstrating loss of expression in tumors initiated in *BRaf^{CA}; PTEN$^{flox/flox}$* mice.
B. H and E staining of lungs from each genotype and quantification of percent tumor burden. Bars represent 100μM.

Figure 3-9. Activation of PI3'K^{H1047R} enhances tumorigenesis driven by KRAS^{G12D}.

KRas^{LSL} and *KRas$^{LSL;}$Pik3ca$^{lat\text{-}H1047R}$* mice were infected with 10^7 pfu AdCre and euthanized five weeks later. Tumor burden was measured as percent tumor area of total lung area. Bar represents 500μM.

Figure 3-10. Cell lines isolated from BRAF^{V600E}; PIK3CA^{H1047R}- driven TRP53$^{-/-}$ tumors are sensitive to the combined effects of MAPK and PI3'K pathway inhibition.

A. Cells were isolated from an AdCre infected *BRaf$^{CA/CA}$; Trp53$^{flox/flox}$; Pik3ca$^{lat\text{-}H1047R}$* mouse and baseline signaling in lysates was compared to cells isolated from a *BRaf^{CA}; Trp53$^{flox/flox}$* mouse. Lysates from clones isolated from cells with the PIK3CA^{H1047R} mutation show higher baseline signaling of PI3'K and downstream effectors.
B. BRAF^{V600E}; PIK3CA^{H1047R}; p53$^{-/-}$ clone 5 cells were treated with 1 μM PD0325901, 5 μM GDC-0941, 1 μM SCH772984, 5μM MK-2206, or a combination of PD0325901 and GDC-0941 and SCH772984 and MK-2206 for 72 hours. Cell viability was measured in luminescence using the CellTitre-Glo assay (Promega).
C. Images of BRAF^{V600E}; PIK3CA^{H1047R}; p53$^{-/-}$ cells after 24 hour treatment with 1μM PD0325901 and SCH772984 and 5 μM GDC-0941 and MK-2206 and combinations.
D. Western blots of lysates prepared from cells shown in Figure 3-10C, treated for 24 hours with each drug and combinations of PD0325901 + MK-2206 and SCH772984 + MK-2206

Figure 3-11. Hyperactivation of PIK3CA signaling confers anchorage independent growth to cells isolated from BRAF^{V600E}; p53$^{-/-}$ tumors.

Tumor cells were isolated from an AdCre infected *BRaf*^{CA}*; Trp53*$^{flox/flox}$ mouse and then stably infected with retrovirus expressing mCherry, PI3'K p110α^{H1047R}, and HA-tagged, myrisolated AKT (AKT^{myr}).

A. Cells were plated in soft agar and cultured for three weeks. Numbers of colonies were quantified.

B. Western blots of lysates from cells probing for downstream effectors of PIK3CA activation.

C. Cells were isolated from an AdCre infected *BRaf*$^{CA/CA}$*; Trp53*$^{flox/flox}$*; Pik3ca*$^{lat\text{-}H1047R}$ mouse (clone 5) and plated in soft agar containing vehicle, 5μM MK-2206, 5 μM GDC-0941, and 1 μM PD0325901. Colony numbers were quantified.

Fig. 3-1

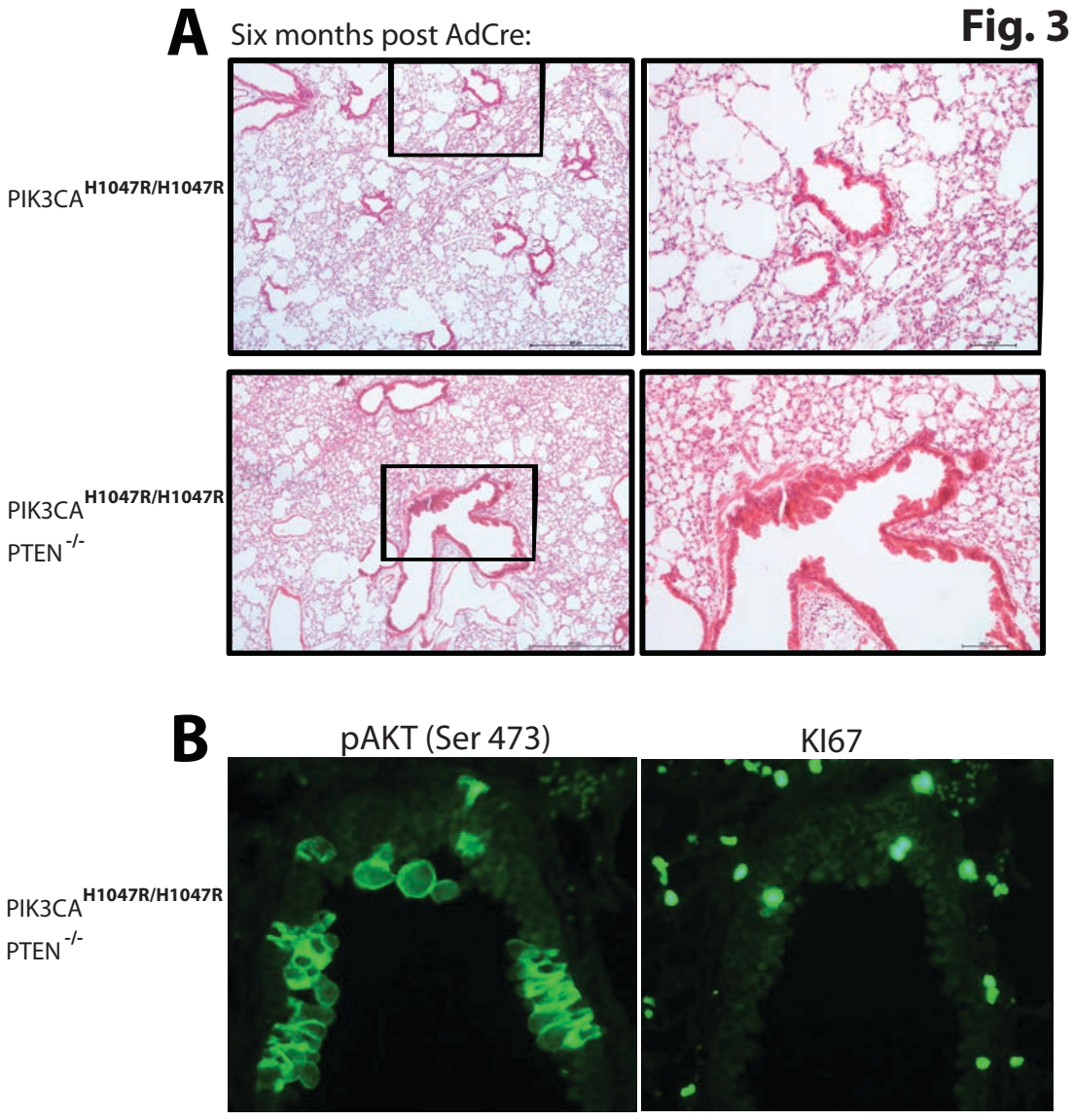
A
Six months post AdCre:
PIK3CA H1047R/H1047R
PIK3CA H1047R/H1047R
PTEN -/-
B
pAKT (Ser 473)
KI67
PIK3CA H1047R/H1047R
PTEN -/-

Fig. 3-2

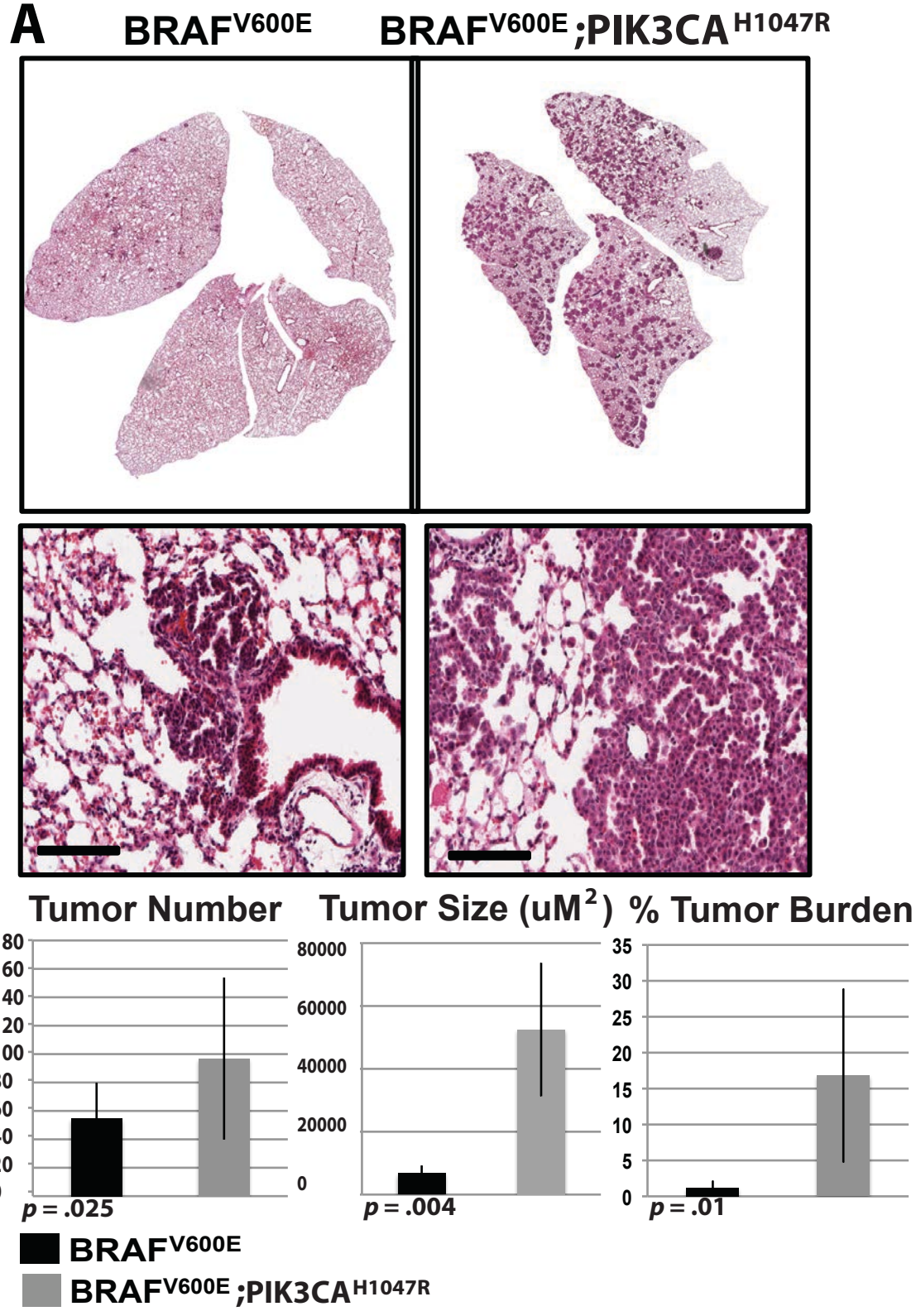
A
BRAFV600E
BRAFV600E;PIK3CAH1047R
Tumor Number
Tumor Size (uM2)
% Tumor Burden
180
160
140
120
100
80
60
40
20
0
80000
60000
40000
20000
0
35
30
25
20
15
10
5
0
p = .025
p = .004
p = .01
BRAFV600E
BRAFV600E;PIK3CAH1047R

Fig. 3-3

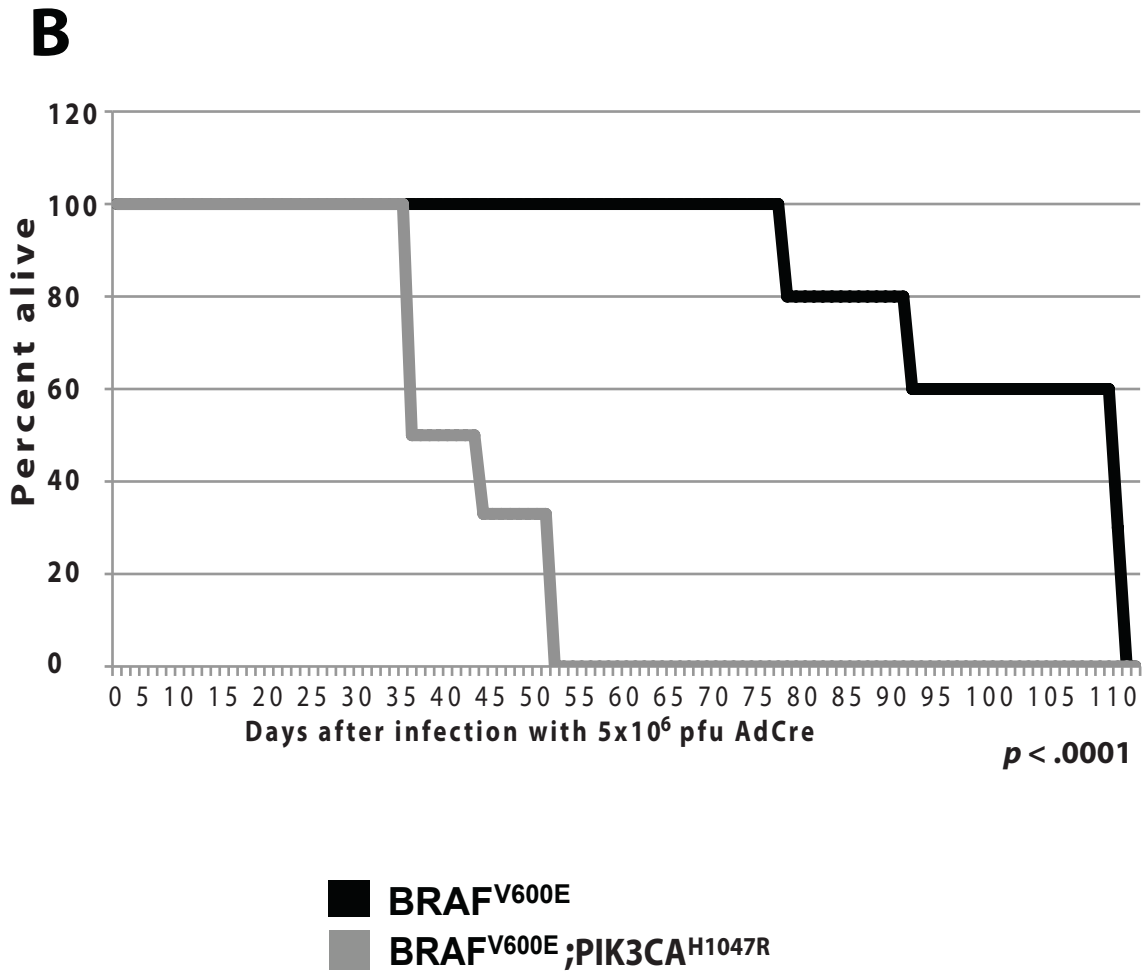
B
120
100
80
60
40
20
0
Percent alive
0 5 10 15 20 25 30 35 40 45 50 55 60 65 70 75 80 85 90 95 100 105 110
Days after infection with 5x10^6 pfu AdCre
p < .0001
BRAF^V600E
BRAF^V600E;PIK3CA^H1047R

Fig. 3-4

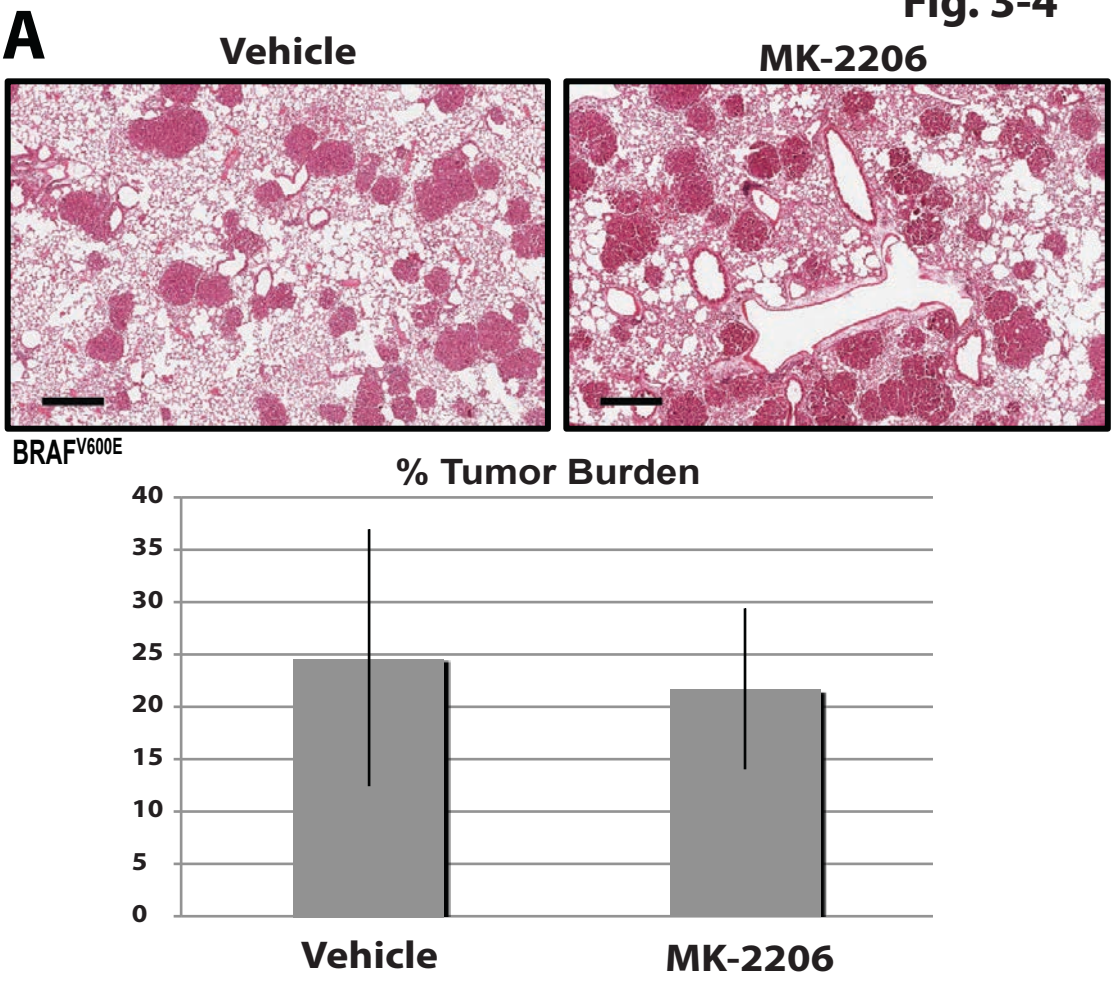
A
Vehicle
MK-2206
BRAF V600E
% Tumor Burden
40
35
30
25
20
15
10
5
0
Vehicle
MK-2206
B
Vehicle
MK-2206
pAKT (Ser 473)
pERK 1/2
(Thr 202/204)
AKT (total)
ERK 1/2 (total)

Fig. 3-5

A

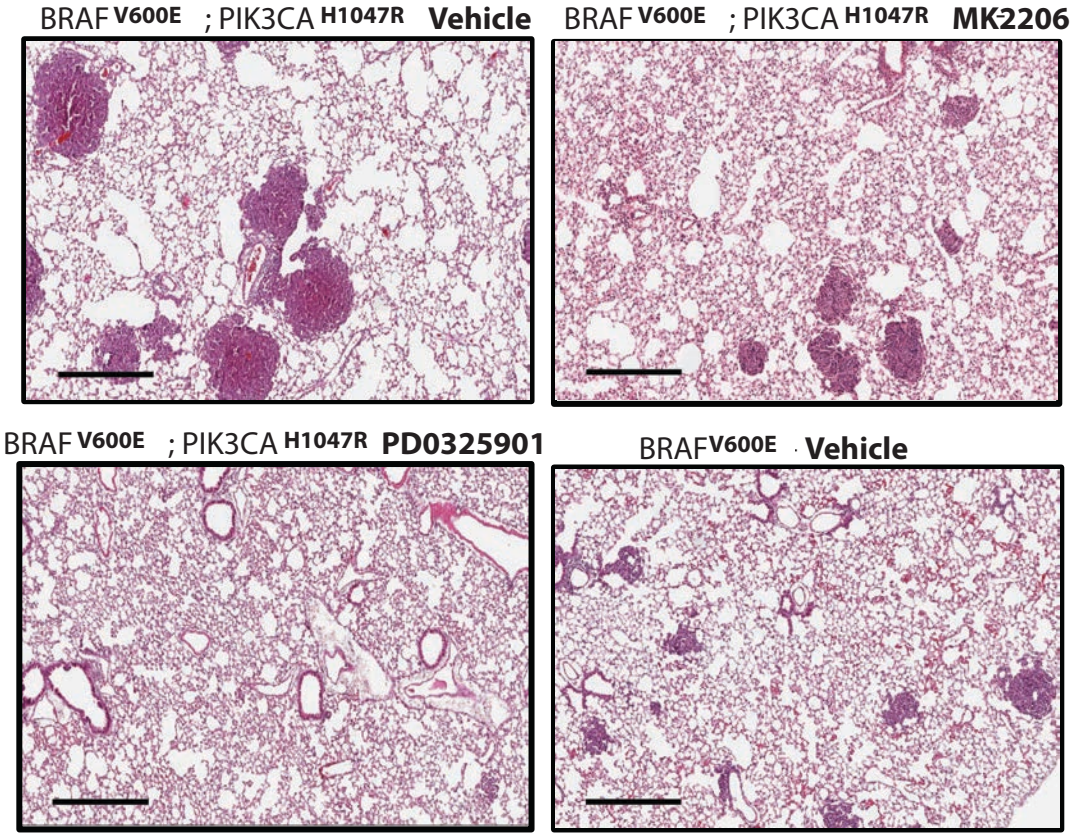
BRAF V600E ; PIK3CA H1047R Vehicle
BRAF V600E ; PIK3CA H1047R MK-2206
BRAF V600E ; PIK3CA H1047R PD0325901
BRAF V600E Vehicle

B

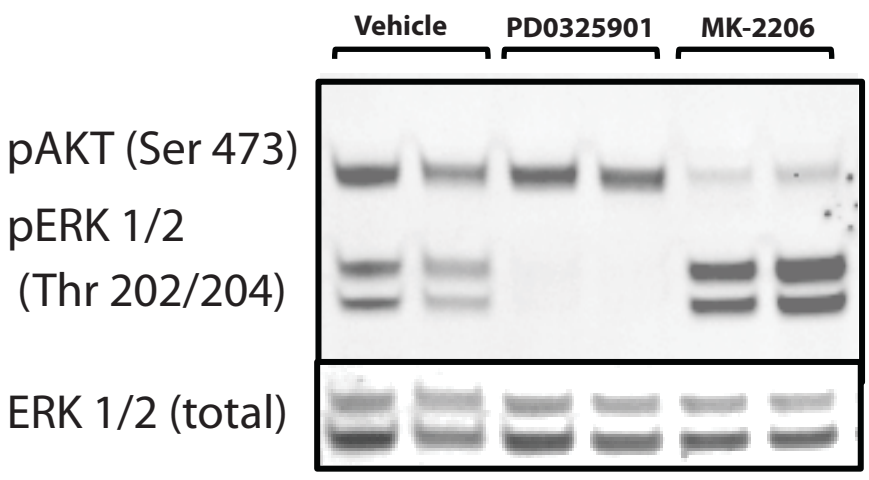
Vehicle
PD0325901
MK-2206
pAKT (Ser 473)
pERK 1/2
(Thr 202/204)
ERK 1/2 (total)

Fig. 3-5

C

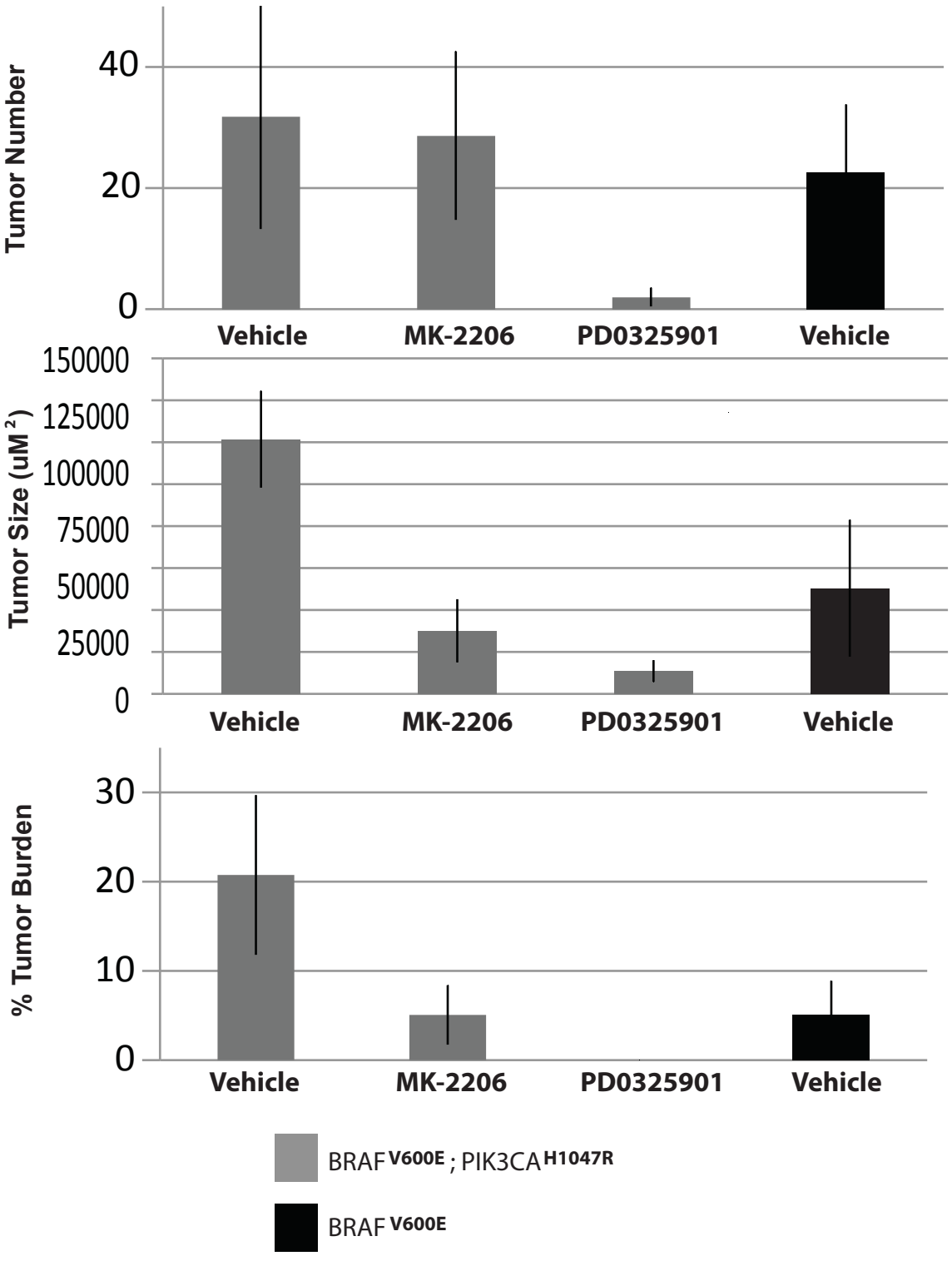
Tumor Number
40
20
0
Vehicle
MK-2206
PD0325901
Vehicle
Tumor Size (uM 2)
150000
125000
100000
75000
50000
25000
0
Vehicle
MK-2206
PD0325901
Vehicle
% Tumor Burden
30
20
10
0
Vehicle
MK-2206
PD0325901
Vehicle
BRAF V600E ; PIK3CA H1047R
BRAF V600E

Fig. 3-6

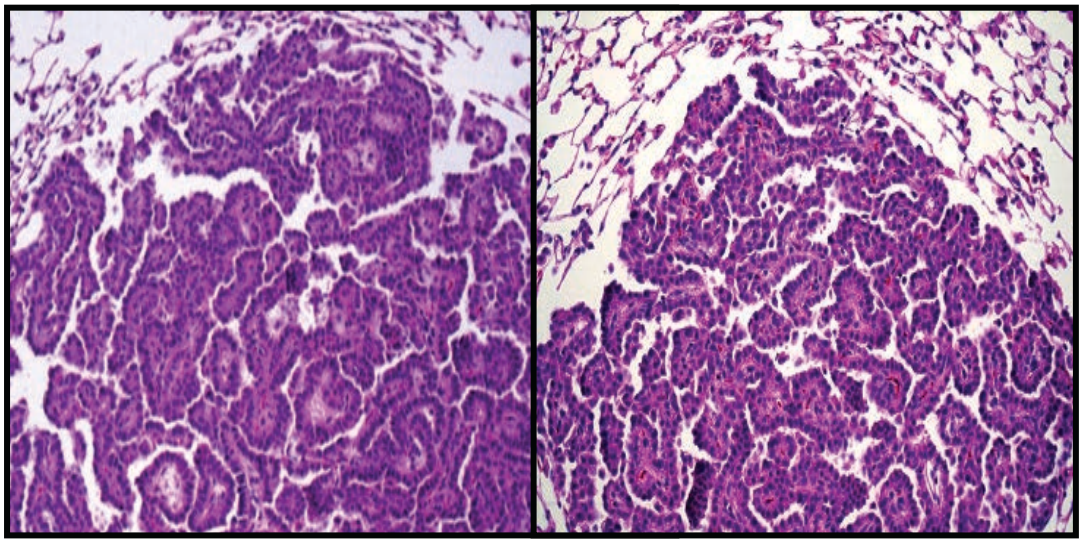

$BRAF^{V600E}$

$BRAF^{V600E;}$
$PIK3CA^{H1047R}$

A

Fig. 3-7

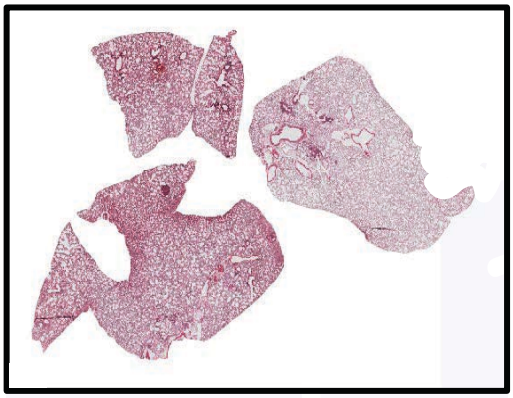

BRAF ^{V600E} ; TRP53 $^{-/-}$

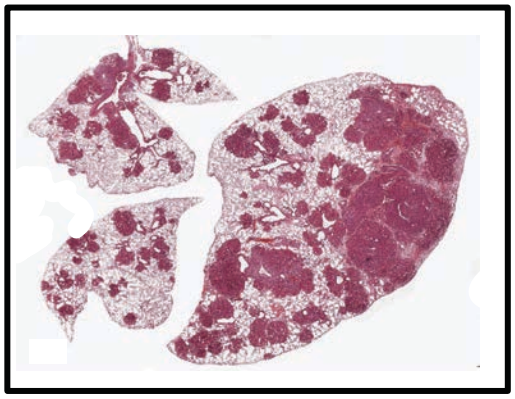

BRAF ^{V600E} ; TRP53 $^{-/-}$;
PIK3CA ^{H1047R}

BRAF ^{V600E} ; TRP53 $^{-/-}$;
PIK3CA ^{H1047R}

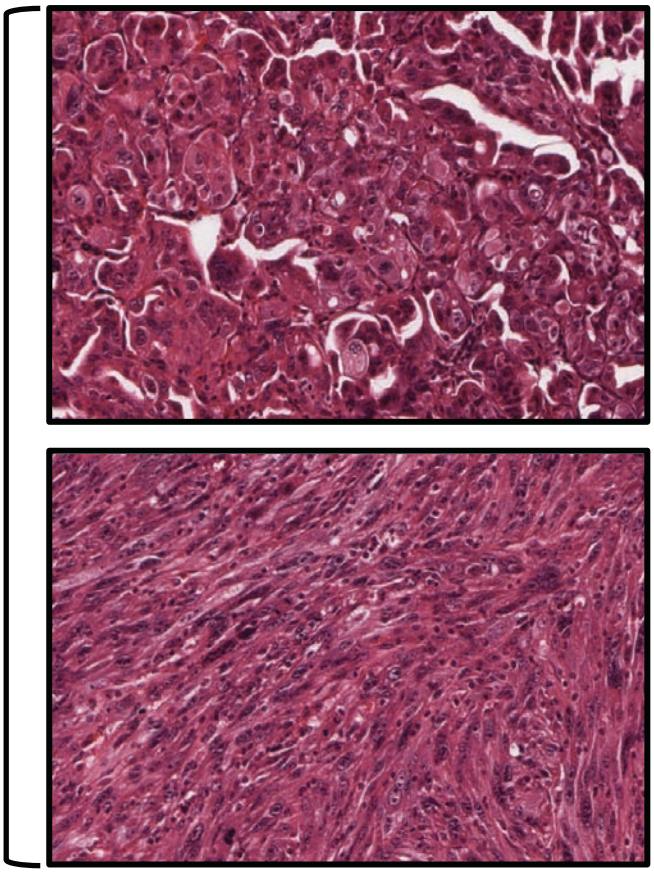

B

Fig. 3-7

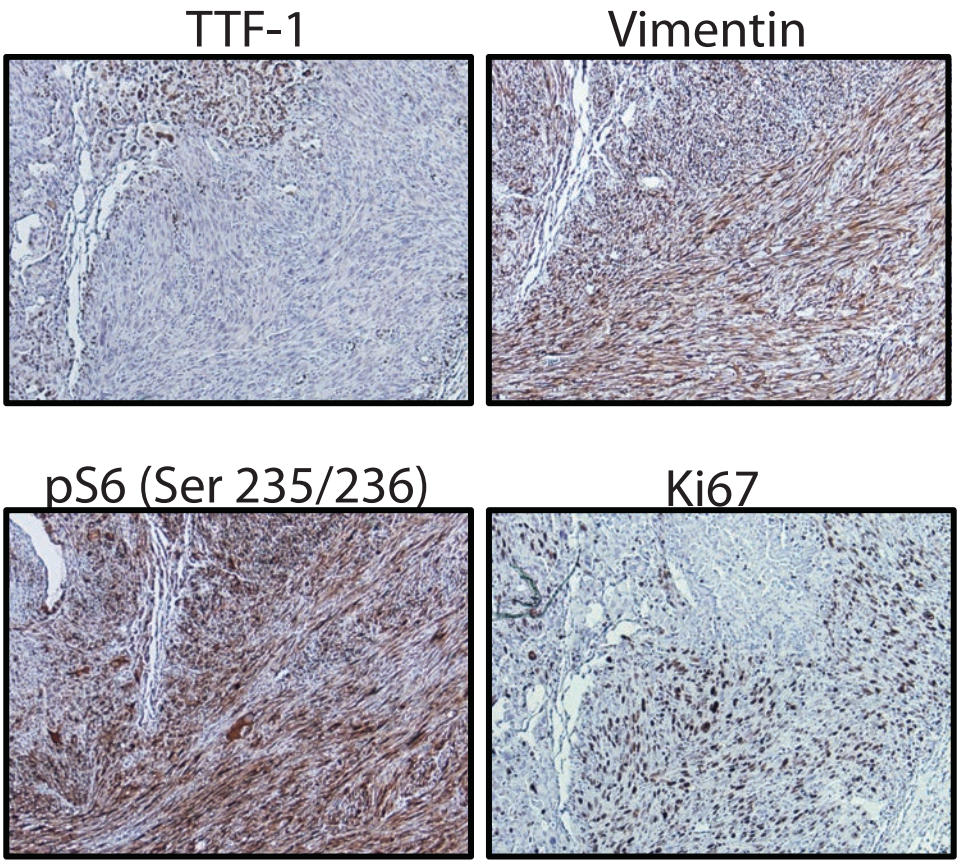

A

Fig. 3-8

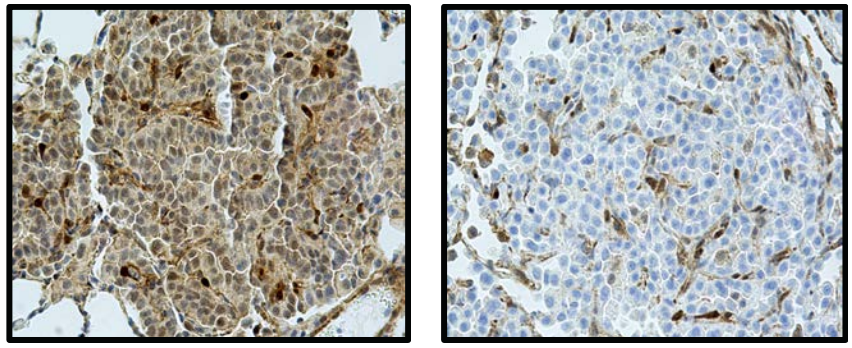
PTEN
BRAF V600E
BRAF V600E; PTEN -/-

B

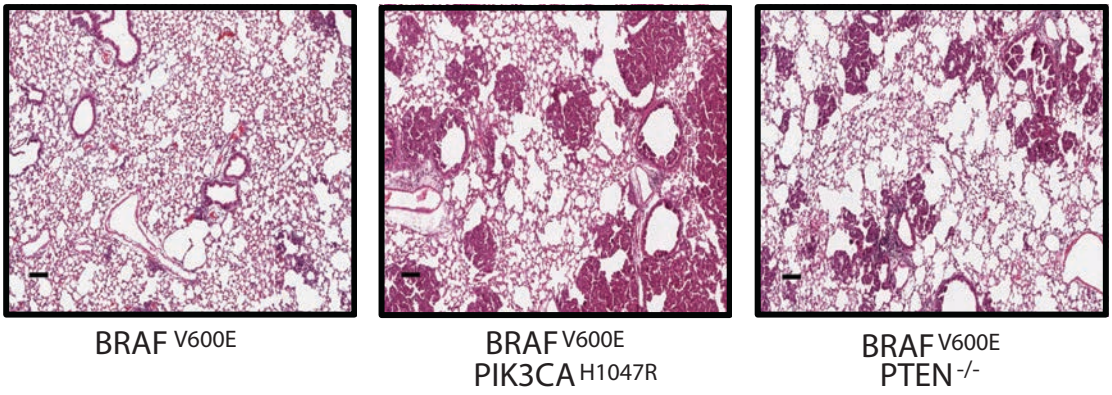
BRAF V600E
BRAF V600E PIK3CA H1047R
BRAF V600E PTEN -/-

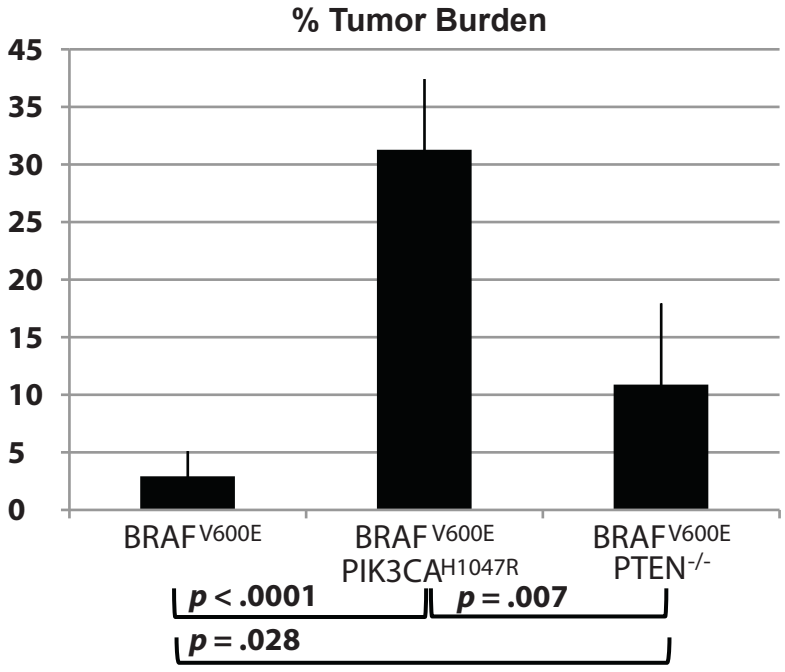
% Tumor Burden
45
35
30
25
20
15
10
5
0
BRAF V600E
BRAF V600E PIK3CA H1047R
BRAF V600E PTEN -/-
p < .0001
p = .007
p = .028

Fig. 3-9

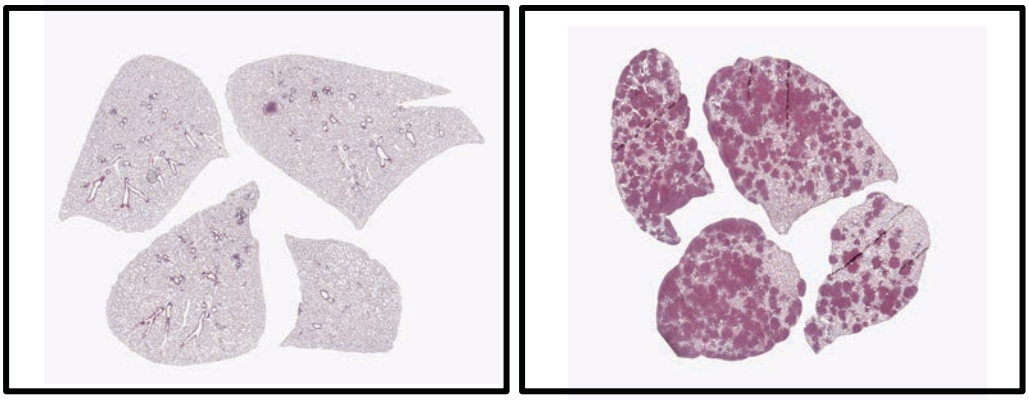

KRAS G12D

KRAS G12D ; PIK3CA H1047R

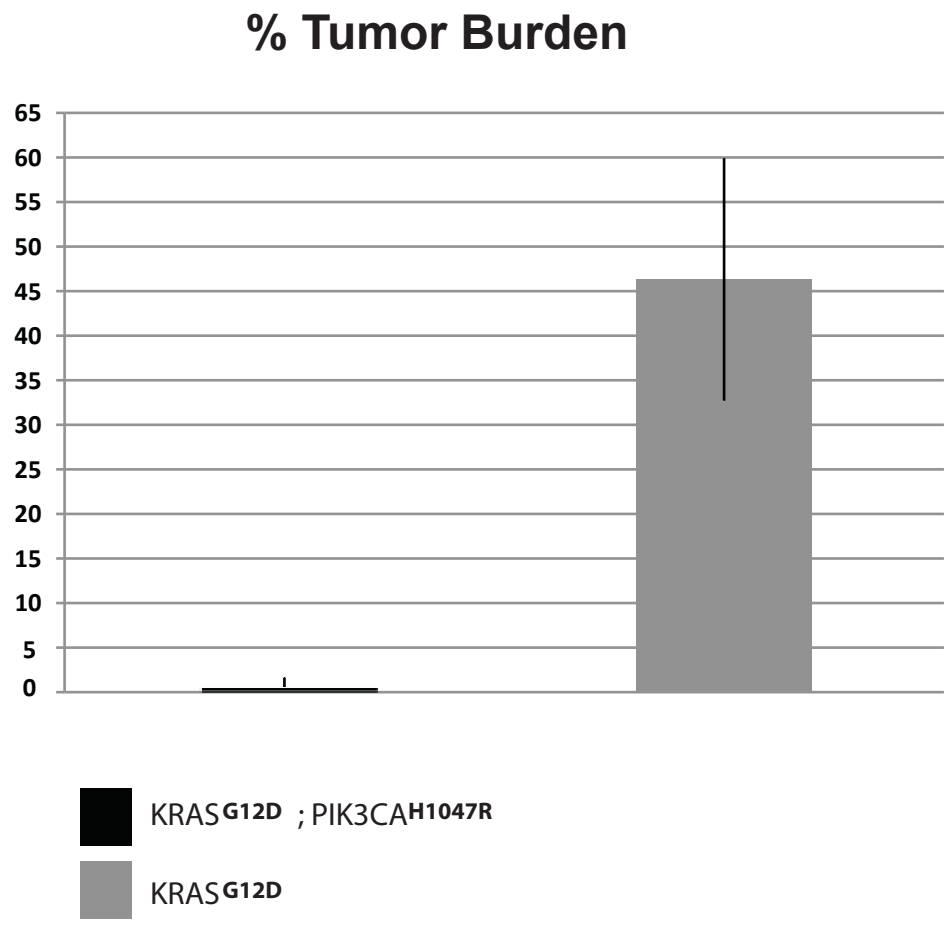

A

Fig. 3-10

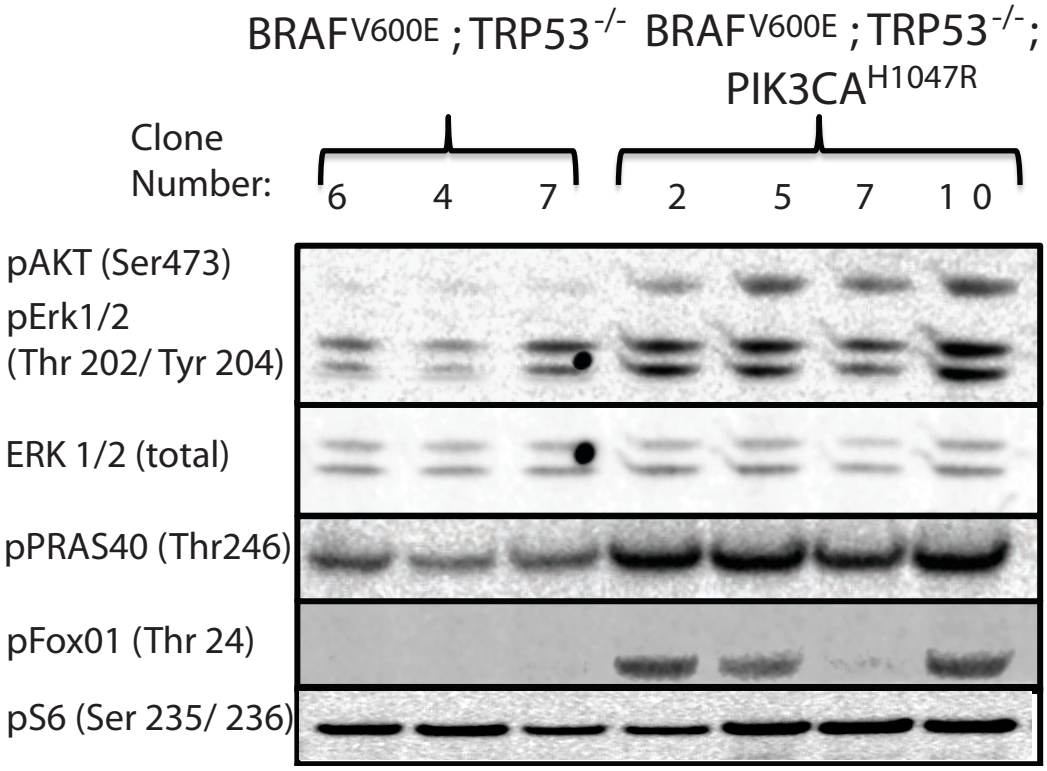
BRAF V600E ; TRP53 -/-
BRAF V600E ; TRP53 -/- ; PIK3CA H1047R
Clone Number:
6
4
7
2
5
7
1 0
pAKT (Ser473)
pErk1/2 (Thr 202/ Tyr 204)
ERK 1/2 (total)
pPRAS40 (Thr246)
pFox01 (Thr 24)
pS6 (Ser 235/ 236)

Fig. 3-10

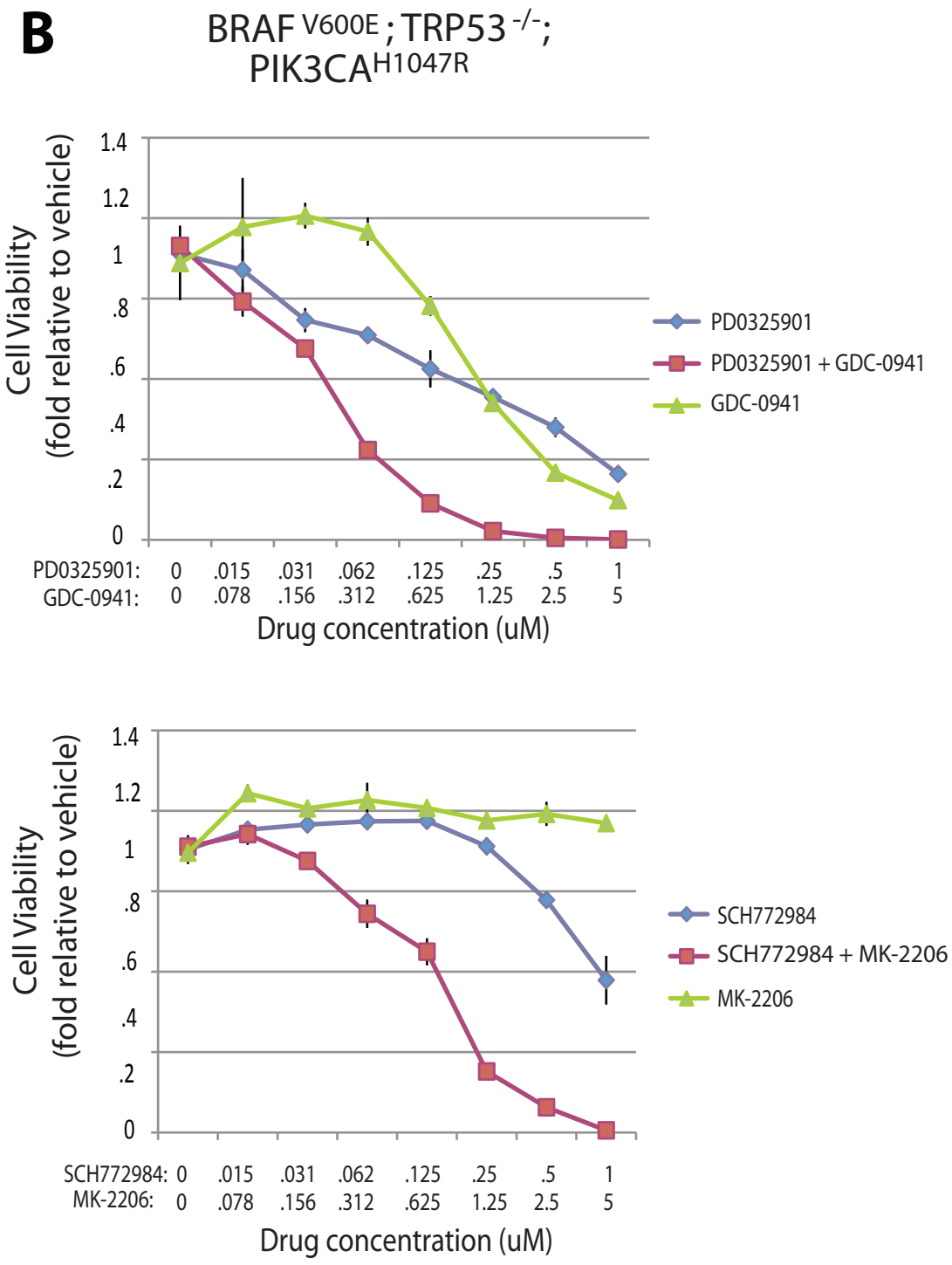
B
BRAF V600E ; TRP53 -/-;
PIK3CA H1047R
Cell Viability
(fold relative to vehicle)
1.4
1.2
1
.8
.6
.4
.2
0
PD0325901:
GDC-0941:
0
0
.015
.078
.031
.156
.062
.312
.125
.625
.25
1.25
.5
2.5
1
5
Drug concentration (uM)
PD0325901
PD0325901 + GDC-0941
GDC-0941
Cell Viability
(fold relative to vehicle)
SCH772984:
MK-2206:
Drug concentration (uM)
SCH772984
SCH772984 + MK-2206
MK-2206

C

Fig. 3-10

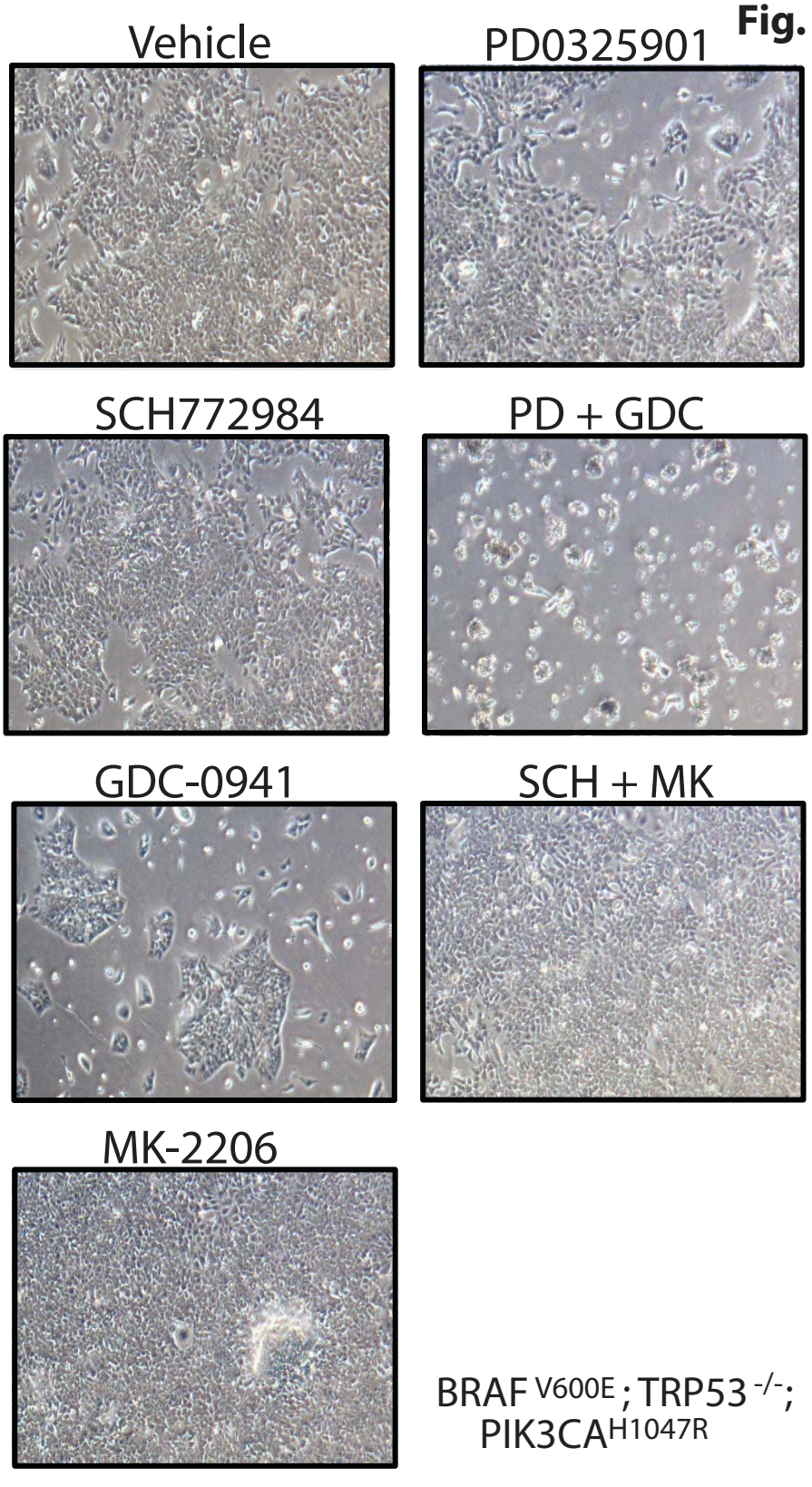
Vehicle
PD0325901
SCH772984
PD + GDC
GDC-0941
SCH + MK
MK-2206
BRAF V600E ; TRP53 -/- ;
PIK3CA H1047R

Fig. 3-10

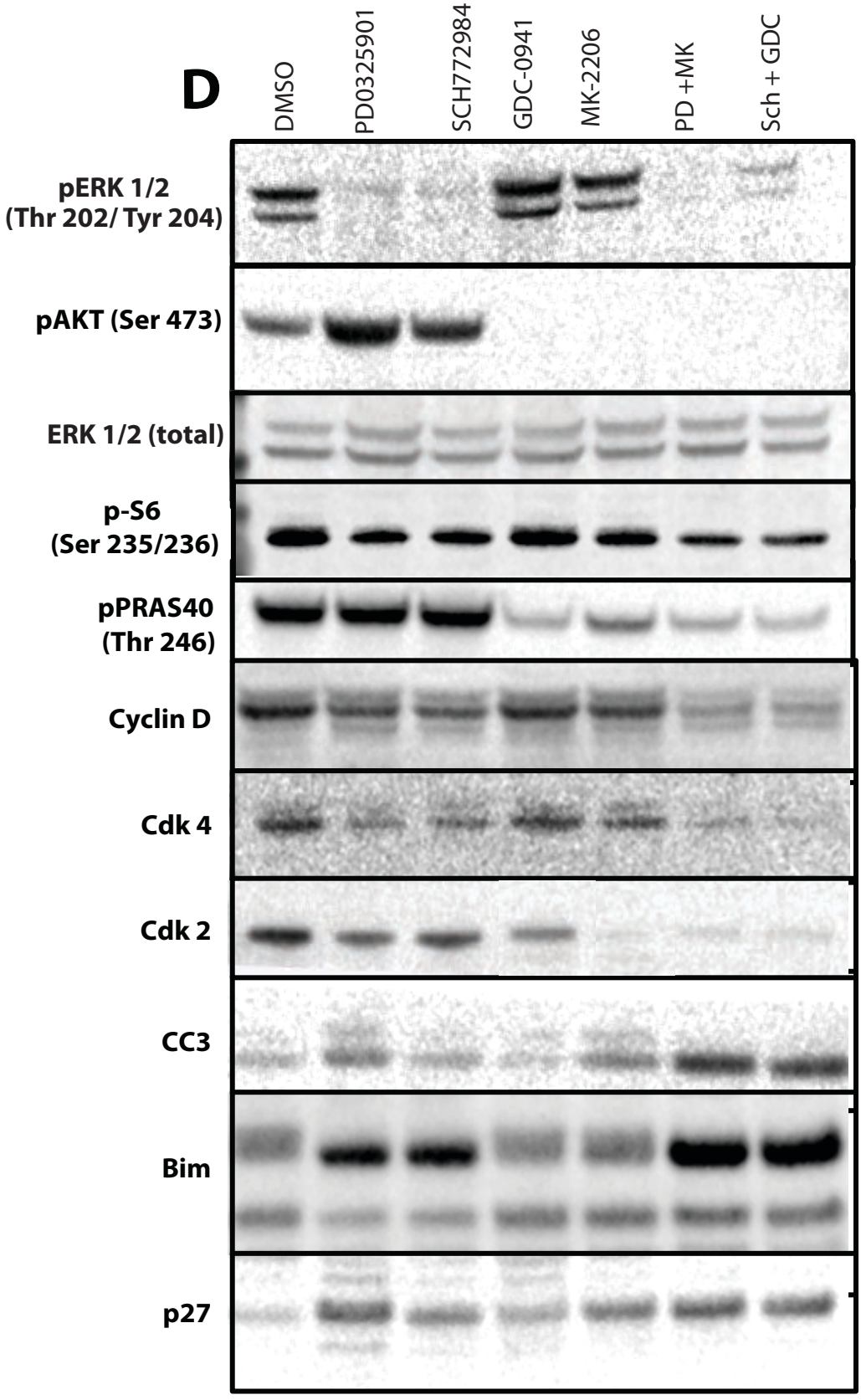
D
DMSO
PD0325901
SCH772984
GDC-0941
MK-2206
PD +MK
Sch + GDC
pERK 1/2
(Thr 202/ Tyr 204)
pAKT (Ser 473)
ERK 1/2 (total)
p-S6
(Ser 235/236)
pPRAS40
(Thr 246)
Cyclin D
Cdk 4
Cdk 2
CC3
Bim
p27

Fig. 3-11

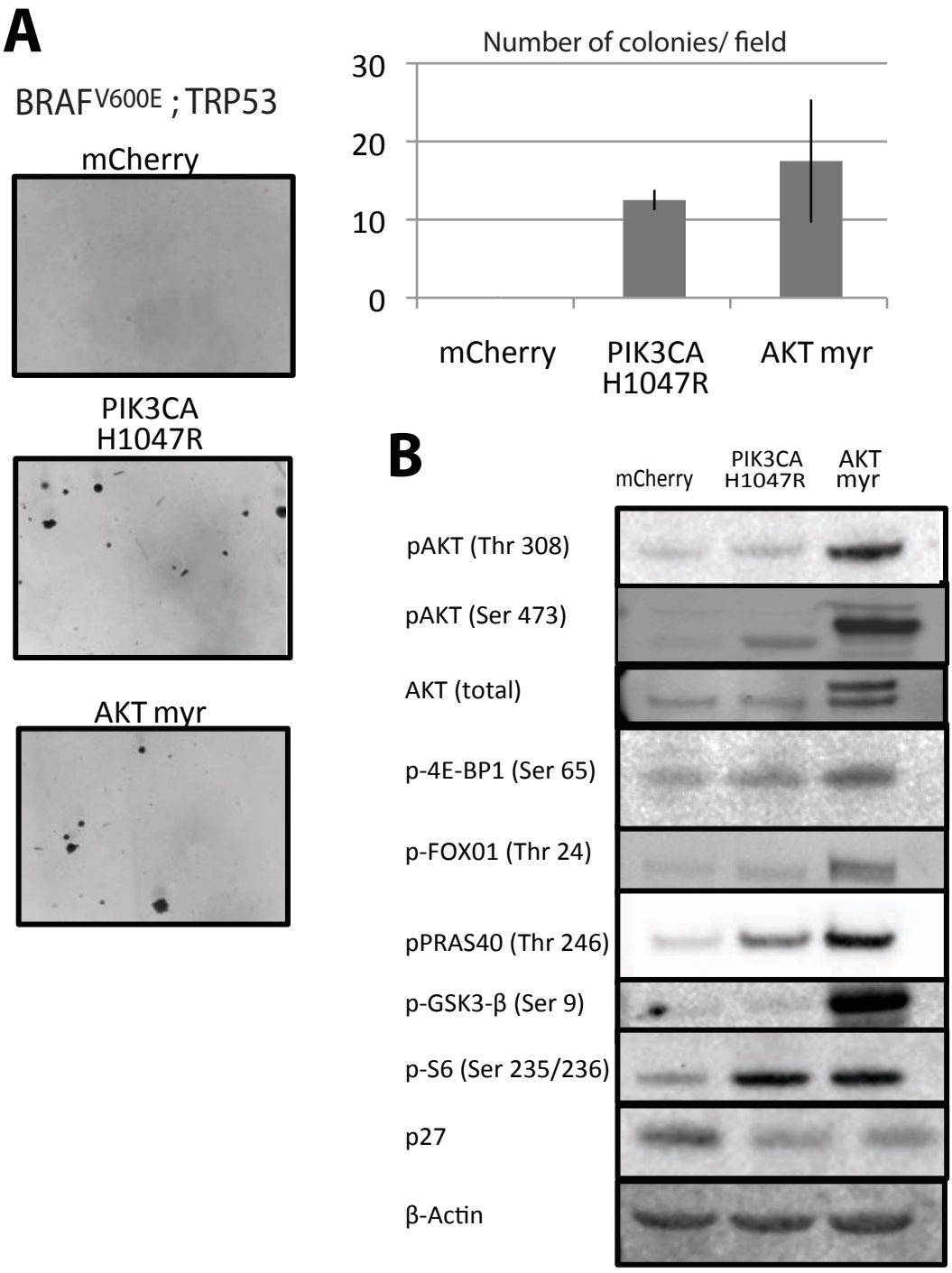
A
BRAF V600E ; TRP53
mCherry
PIK3CA H1047R
AKT myr
Number of colonies/ field
30
20
10
0
mCherry
PIK3CA H1047R
AKT myr
B
mCherry
PIK3CA H1047R
AKT myr
pAKT (Thr 308)
pAKT (Ser 473)
AKT (total)
p-4E-BP1 (Ser 65)
p-FOX01 (Thr 24)
pPRAS40 (Thr 246)
p-GSK3-β (Ser 9)
p-S6 (Ser 235/236)
p27
β-Actin

Fig. 3-11

C

BRAF ^{V600E}; TRP53 $^{-/-}$; PIK3CA ^{H1047R}

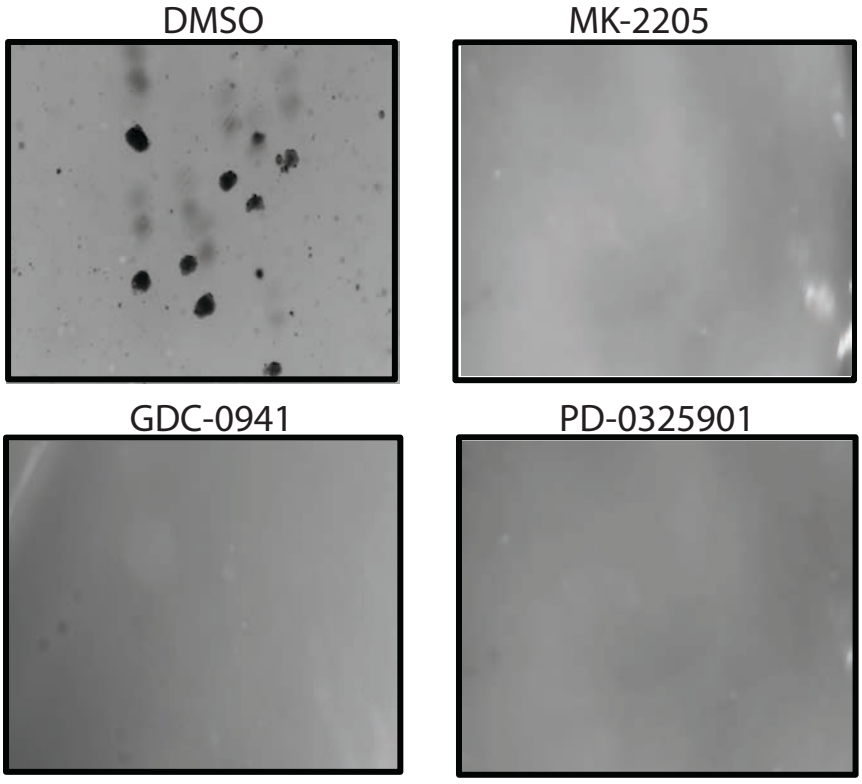

CHAPTER 4: Induction of pulmonary inflammation in $BRAF^{V600E}$- driven tumorigenesis

We hypothesized that a pro-inflammatory response could be elicited by oncogenic $KRAS^{G12D}$ that does not occur with $BRAF^{V600E}$, and such an alteration of the microenvironment due to the production of chemokines and presence of tumor infiltrating cells may cause the progression of $KRAS^{G12D}$- driven tumors that is not observed with $BRAF^{V600E}$. To test this hypothesis, we chose to induce inflammation in $BRAF^{V600E}$ driven tumors in an attempt to drive tumor progression in this model. We obtained a knock-out mouse for the β6 subunit of integrin αVβ6, which is expressed in epithelial cells and plays a role modulating the inflammatory response following injury. Mice homozygous for this mutation display inflammation of the lungs characterized by activated lymphocytes (59). We crossed this mouse to the $BRaf^{CA}$ mouse to generate littermates that were $BRaf^{CA}$; $\beta6^{-/-}$ or $BRaf^{CA}$; $\beta6^{+/+}$. Mice were aged to 6 weeks and infected with $5x10^6$ pfu AdCre or AdβGal, then aged out for an additional 10 weeks. Lungs were then removed and fixed for histological analysis. As expected, mice infected with AdβGal had no visible lesions. There was, however, notable degree of inflammation in the lungs of $\beta6^{-/-}$ mice compared to their $\beta6^{+/+}$ littermates. Specifically, $\beta6$ knock out mice had an abundance of resting lymphocytes, often located at the bronchioalveolar duct junction. All mice infected with AdCre developed an abundance of tumors and overall tumor burden did not seem to differ greatly between $\beta6^{-/-}$ mice compared to their $\beta6^{+/+}$ littermates. There was a difference in the grade of tumors present, however.

Tumors of $BRaf^{CA}$; $\beta6^{+/+}$ were characterized as grade 1 or 2, with papillary structures made up of uniformly sized, well polarized cells with a normal cytoplasm to nucleus ratio. In contrast, the tumors of $BRaf^{CA}$; $\beta6^{-/-}$ mice were frequently advanced

to grade 3 or 4 with some regions of anaplastic adenocarcinoma (Fig 4-1A). Cells within these tumors contained pleopmorphic nuclei, with hyperchromatic chromatin, irregular nuclear contours, multiple nucleoli (white circles), increased nuclear size (yellow circles) and mitotic activity (black circles) (Fig 4-2B). Infiltrating lymphocytes were also present within these tumors.

The previous experiment to induce inflammation in the *BRaf*^{CA} mouse lung involved using a tissue wide knock-out mouse. The loss of Integrin signaling and the various cellular pathways and cellular responses that it governs could affect the tumor cells or microenviroment in a number of ways that could influence tumor phenotype. We next sought an alternative way to induce inflammation that was independent of cellular genotype. For this purpose, we took use of well-established protocols involving environment- induced inflammation.

Ovalbumin sensitization in mice is one of the best charcterized models for allergic asthma, in which a robust immune response is induced. Following sensitization, wild type mice challenged with an antigen in the respiratory tract exhibit eosinophilic infiltration, airway hyper-responsiveness, increased IgE in the serum, and at later stages, airway remodeling (60). We sought to determine if this particular type of inflammation could potentially drive progression of adenomas in the *BRaf*^{CA} mouse model. We took appropriately aged *BRaf*^{CA} mice and primed them with intraperitoneal injection of 50 µg Ovalbumin every two days for one week to induce the production of antigen-specific antibodies. Mice were then infected with $1x10^7$ pfu AdCre or AdβGal. Two weeks later, mice were split into two groups and intranasally challenged with either 100µg Ovalbumin or saline control once a week for nine weeks to elicit an adaptive immune response in the lung (Fig 4-2A). 11 weeks after AdCre infection, following the final intranasal challenge, all mice were euthanized and lung histology was assessed. At this time point, a number of mice were

displaying signs of respiratory stress such as rapid breathing and weight loss.

Surprisingly, Ovalbumin challenged mice had a significantly lower tumor burden than their saline challenged littermates. Overall, mice challenged with Ovalbumin had a tumor burden of 7%. This is lower than the average tumor burden usually observed in these mice at this titer and time point, indicating a protective effect by Ovalbumin challenge. Mice challenged with saline had an average tumor burden of 25.8%, greater than 3 fold higher than ovalbumin challenged mice (p = >.001, Fig 4-2B). The greater tumor burden was due to a higher overall number of individual lesions, however the number of single lesions in saline challenged mice was difficult to quantify due to confluent tumors. The grade of individual lesions was not significantly different between the two groups, and no lesions were found progressed beyond grade 1 or 2.

Discussion

Reports have shown that mutational activation of $KRAS^{G12D}$ leads to a pro-inflammatory response. When the $KRas^{LSL}$ mouse model was crossed to a mouse expressing CCA- specific Cre, a robust inflammatory response was found among and within tumors characterized by alveolar macrophages and neutrophils. Bronchioalveloar lavage revealed the presence of chemokines involved in inflammatory cell recruitment, and cell lines isolated from this model produced inflammatory chemokines that attract neutrohpile and macrophages such as CXL- 1, 2, and 5, and CCL 2,3, and 4. (61) Furthermore, it was previously found that IL-8 is a transcriptional target of RAS signaling, and that this response was required for tumor associated inflammation (62). This led us to hypothesize that induction of inflammation could be a possible mechanism for progression to high-grade lung tumors in this model.

Inflammation is known to support tumor growth and progression through remodeling of the extracellular matrix and promoting angiogenesis. The presence of tumor- associated macrophages (TAMs) has been correlated to poor prognosis in human patients through their positive effect of tumor growth (63).

Mice lacking the β6 subunit of Integrin αVβ6 mice have pulmonary inflammation due to the inability to activate latent TGF-β. These mice have increased numbers of macrophages that secrete high levels of Matrix Metalloproteinases as well as an increase in alveolar size. At late ages, these mice present with a lung phenotype that is similar to what is found in patients with chronic obstructive pulmonary disease (COPD) (59).

We hypothesized that pulmonary inflammation could cause $BRAF^{V600E}$– driven tumors to progress to adenocarcinoma similar to what is observed in $KRAS^{G12D}$-

driven tumors. By crossing *BRaf*^{CA} to *Int*β*6*$^{-/-}$ mice, we found that loss of intact Integrin αVβ6 signaling caused BRAF^{V600E}- driven tumors to progress to high-grade, anaplastic adenocarcinoma. The advanced grade of tumors found in *BRaf*^{CA}*;* β*6*$^{-/-}$ mice could be a result of non-autonomous effects such as modulation of the tumor microenvironment due to the presence of infiltrating cells which would support the idea that a pro-inflammatory microenvironment may be driving KRAS^{G12D} tumor progression. This observation is complicated by the fact that these mice are null for β*6* in the tumor cells as well. The effect of advanced tumor grade could potentially be due to loss of Integrin αVβ6 in the tumor cells themselves, and not modulation of the tumor microenvironment through lack of TGFβ activation. A mouse model with conditional inactivation of the β*6* subunit would address this, however in either case it appears as if αVβ6 serves as a tumor suppressor in this model.

Our findings are somewhat supported by past studies revealing that cigarette smokers with COPD have increased risk of lung cancer, and cell specific expression of KRAS^{G12D} drove COPD- like pulmonary inflammation (64). To determine whether the tumor microenvironment or loss of TGFβ signaling promoted tumor progression in *BRaf*^{CA}*;* β*6*$^{-/-}$ mice, further analysis is required.

Using Ovalbumin challenge to induce pulmonary inflammation, we found that mice challenged with the antigen had a significantly lower tumor burden compared to saline-challenged littermates. We were surprised by these findings since we hypothesized that an inflammatory response may be pro-tumorigenic in this model. One possibility for the protective effect of ovalbumin challenge may be the type of inflammatory response that it elicits. In general, ovalbumin sensitization and challenge usually causes a two-fold increase in macrophages with much larger increases in eosinophils, lymphocytes, and neutrophils. In the lungs of ovalbumin

challenged mice, patches of eosinophils were abundant, particularly near tumors or bronchio-alveolar duct junctions. Past studies involving the study of human tumors in various tissue types have reported that tumor associated eosinophilia correlates with a positive prognostic value (28), (65). This effect is due to the presence of cytotoxic T cells. We did not conduct an analysis on the specific type of T cells present in our samples, or the specific type of cytokines.

Another fact that is at odds with our observation is that individuals with asthma, which Ovalbumin challenge is a model for, do not have lower rates of lung cancer. In fact, studies suggest that patients with asthma may have an increased risk of lung cancer even among non-smokers (66). This discrepancy may be due to the fact that Ovalbumin challenge cannot recapitulate the discreet phases of human asthma that involve the recruitment of a wide variety of cell types.

Figure 4-1 Tumorigenesis in BRAF^{V600E}; Integrin $\alpha V\beta 6^{-/-}$ mice.

BRaf^{CA}; $\beta 6^{-/-}$ or *BRaf^{CA} ; $\beta 6^{+/+}$.* Mice were aged to 6 weeks and infected with 5x10^6 pfu AdCre or AdβGal, then aged out for an additional 10 weeks.

A. H and E stains showing progressed tumorigenesis in a *BRaf^{CA}; $\beta 6^{-/-}$* tumor.

B. High magnification of a tumor from *BRaf^{CA}; $\beta 6^{-/-}$* mouse showing irregular nucleii (white circles), increased nuclear size (yellow circles) and mitotic activity (black circles).

4-2 BRAF^{V600E} tumorigenesis in lungs challenged with Ovalbumin.

BRaf^{CA} mice were primed with intraperitoneal injection of 50 µg Ovalbumin every two days for one week then infected with 1x10^7 pfu AdCre or AdβGal. Two weeks later, mice were split into two groups and intranasally challenged with either 100µg Ovalbumin or saline control once a week for nine weeks.

A. Schematic of experimental design.

B. H and E staining of lungs to show difference in tumor multiplicity.

C. Quantification of tumor burden in infected *BRaf$^{Ca/+}$* mice challenged with Ovalbumin or saline.

Fig. 4-1

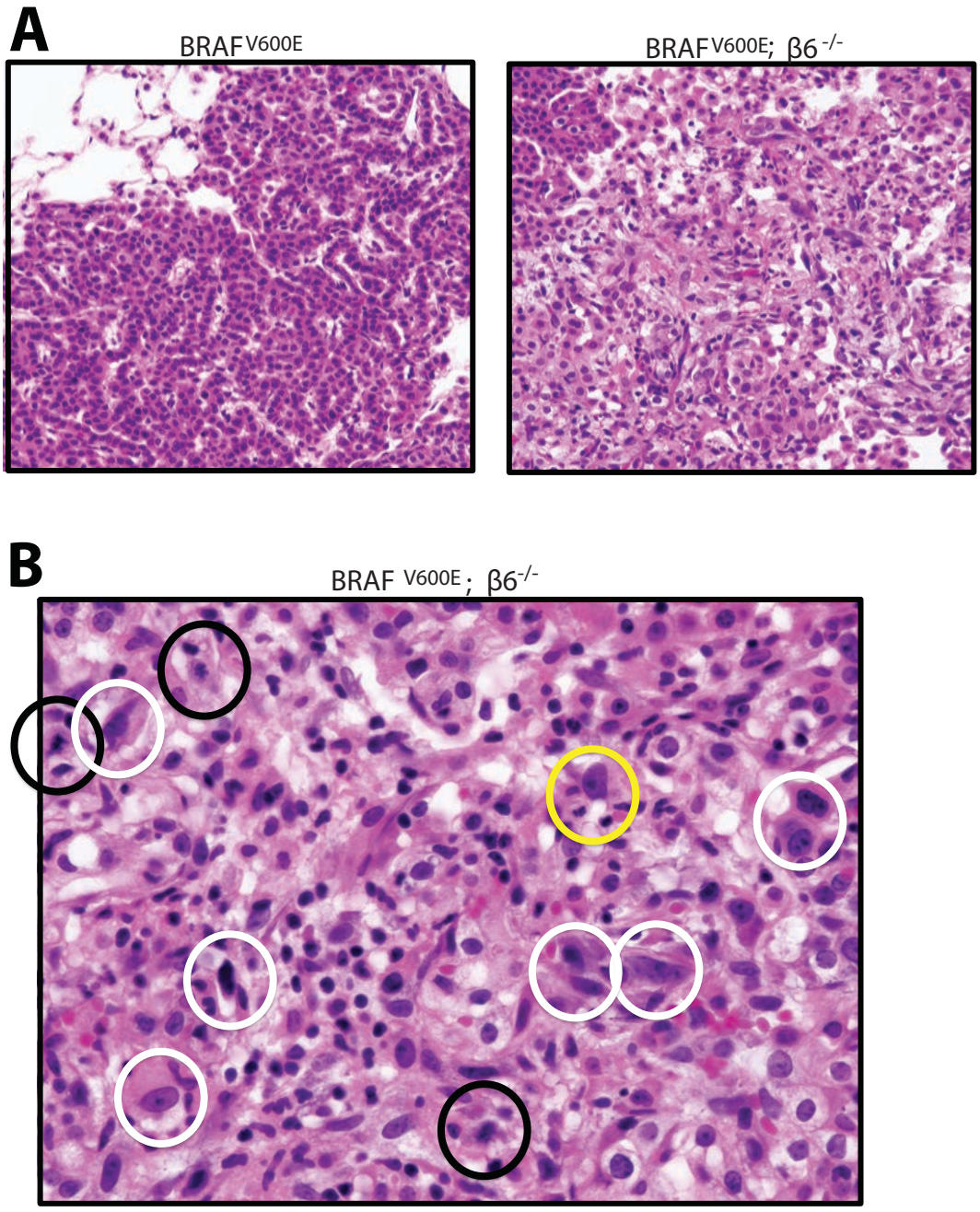

Fig. 4-2

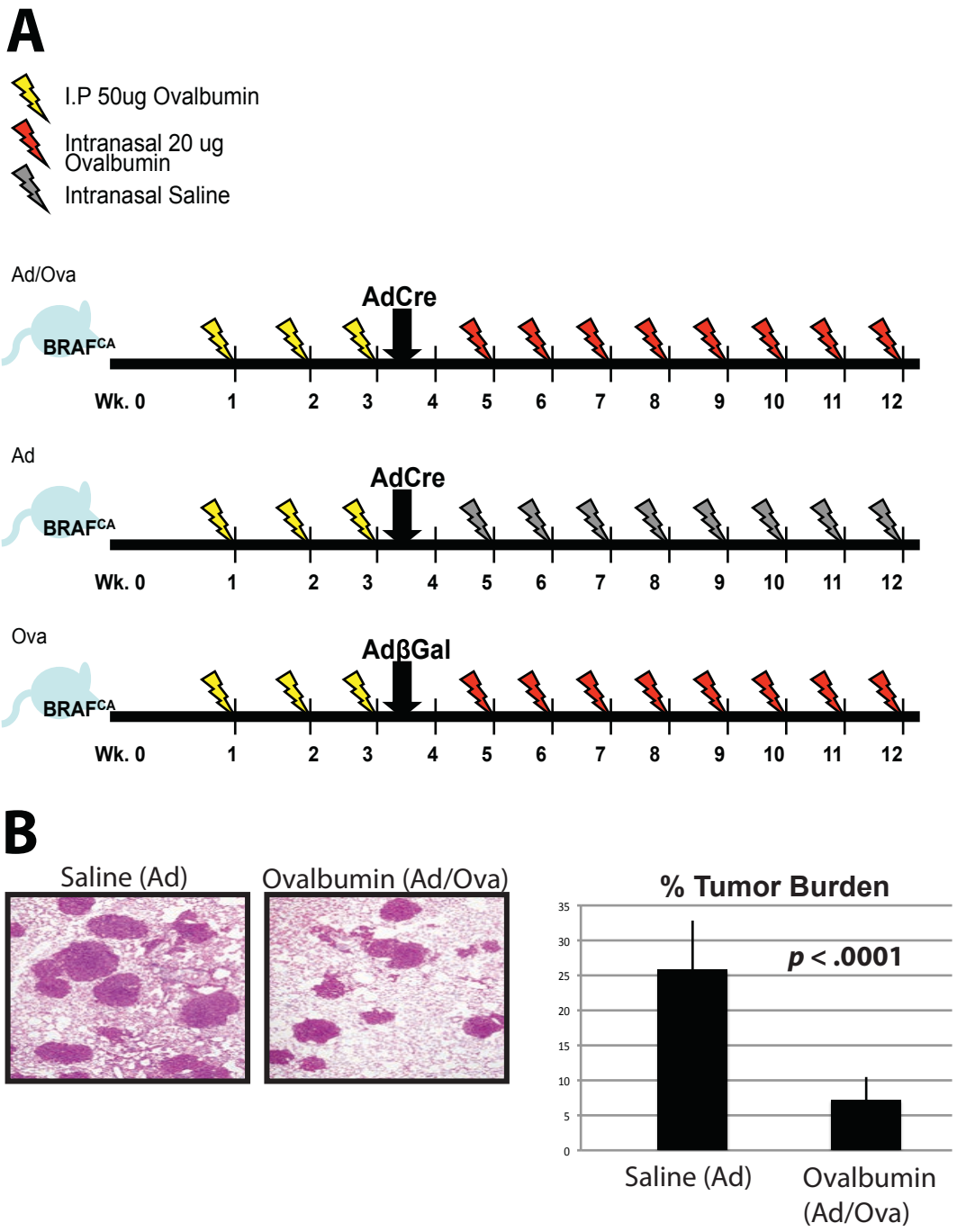
A
I.P 50ug Ovalbumin
Intranasal 20 ug Ovalbumin
Intranasal Saline
Ad/Ova
AdCre
BRAFCA
Wk. 0 1 2 3 4 5 6 7 8 9 10 11 12
Ad
AdCre
BRAFCA
Wk. 0 1 2 3 4 5 6 7 8 9 10 11 12
Ova
AdβGal
BRAFCA
Wk. 0 1 2 3 4 5 6 7 8 9 10 11 12
B
Saline (Ad)
Ovalbumin (Ad/Ova)
% Tumor Burden
p < .0001
35
30
25
20
15
10
5
0
Saline (Ad)
Ovalbumin (Ad/Ova)

Chapter 5: Conclusion

The purpose of this work was to determine the relative importance of KRAS effector pathways in order to better develop strategies to target cancer driven by this oncogene in the clinic. Observations made from the use of mouse models and small molecule inhibitors as genetic and biochemical tools have demonstrated the ability of genes in the MAPK and PI3'K pathways (both frequently altered in human cancer) to regulate the development of lung tumors. These findings also provide a framework for further analysis which can be conducted using additional systems, experiments that I did not have time to complete in my course of study.

I have established that RAF/MEK/ERK signaling is both necessary and sufficient for $KRAS^{G12D}$- driven tumor formation. Furthermore, I have shown that despite similarities at early stages, $KRAS^{G12D}$ and $BRAF^{V600E}$ oncogenes differ in their ability to initiate tumors and drive progression to high grade lesions, with KRAS forming fewer but overall more malignant tumors. Differences in tumor multiplicity may be attributed to different cell types being stimulated to proliferate in each model. No difference was found in the expression of cell type markers used in this study, but the range of these markers was limited. Further analysis should employ a wider range of cell-type specific markers, including those of lung progenitor cells. If different cells of origin are initiating tumors in these models, this may also explain the differences in tumor progression. A good approach to study cell of origin in these models would be to employ a fluorescent reporter mouse to sort out tumor initiating cells at early time points. A number of such mice exist which express fluorescent reporters upon Cre-mediated recombination, allowing for FACS sorting of cells that also express $KRAS^{G12D}$ or $BRAF^{V600E}$. Simply crossing the conditional mouse to a reporter may risk false positive or negatives if expression of the reporter is disconnected from that

of the oncogene. The development of a mouse that expresses a fluorescent reporter and $BRAF^{V600E}$ from the same promoter is currently underway in our lab. Mouse embryonic stem cells containing the *BRaf*^{CA} allele are being targeted through homologous recombination to contain an internal ribosomal entry site (IRES) separating mutated exon 15 and a fluorescent reporter construct. Upon Cre-mediated recombination, $BRAF^{V600E}$ will be expressed with the reporter in a bicistronic manner. This will allow for isolation of only cells that express $BRAF^{V600E}$.

The lack of progression in $BRAF^{V600E}$- expressing tumors may be due to either active engagement of a growth arrest response, or the inability to active alternate pathways which drive progression. Since only a fraction of $KRAS^{G12D}$ tumors progress to high-grade, it is possible that KRAS tumors engage specific signaling pathways at late time points in a stochastic manner. This may be due to loss of genomic stability due to persistent cell divisions, the release of negative feedback loops, or a response to changes in the microenviroment. Interrogating protein expression beyond immunostaining techniques would better address the mechanism of KRAS progression. Laser-capture microscopy serves as a potential means to do this. mRNA levels can be assessed in a manner that compares malignant and benign tumors. Tumors undoubtedly contain normal cells, however, and tumors form at different times, so at any given time, gene expression may be highly variable between tumors of one mouse. Indeed, this analysis has been conducted on BRAF tumors in our lab and a great degree of variability was uncovered, complicating analysis.

Another similarity between $KRAS^{G12D}$- and $BRAF^{V600E}$- driven tumors is the response to MEK1/2 inhibition. Interfering with MAPK signaling in this manner prevented formation and caused regression of both tumor types, unequivocally demonstrating the importance of this pathway in tumor initiation and maintenance.

Upon drug removal, tumor burden was quickly re-established, however. This could be due to 1) late forming tumors that were initiated after drug removal, 2) a population of initiating cells within tumors that is resistant to MEK inhibition but prevented from proliferating by the drug, or 3) the effects of MEK inhibition being non-autonomous, and the presence of the drug having an effect of normal cells that don't express $BRAF^{V600E}$ or $KRAS^{G12D}$ but are vital to the maintenance of tumors. Such cells may exist in the microenvironment, such as endothelial cells. Inhibition of MAPK could prevent signaling from VEGF, which is necessary for blood vessel establishment and maintenance. Large networks or blood vessels are present in both BRAF and KRAS tumors, and their loss may cause the tumors to shrink to a size that does not require a large endothelial network. Removal of drug might then allow these tumors to re-grow.

The simplest approach to begin to understand which if these factors is at play would be a short term drug treatment of mice with an established tumor burden, followed by extensive immunohistochemistry involving the co-staining of markers for apoptotic and endothelial cells. More complicated systems would be required to determine if scenario 1) or 2) is responsible for tumor re-establishment. One such system that is currently being optimized using the $BRaf^{CA}$ mouse is ex-vivo culture of lungs. Lungs are removed from mice and cut into 150 μm sections that can be maintained in a culture dish with media. Our lab has established that tumors can grow in ex-vivo sections and these are sensitive to MEK1/2 inhibition, providing an experimental platform to address the mechanism of drug action.

The development of a mouse for the conditional expression of $PIK3CA^{H1047R}$ was an ideal complement to the $BRaf^{CA}$ and $KRas^{LSL}$ mice to study the role of this pathway in $KRAS^{G12D}$- mediated tumorigenesis. We originally hypothesized that engagement of PI3'K signaling may drive progression in $BRAF^{V600E}$ tumors. Indeed,

phospho-S6 levels were greatly increased in $KRAS^{G12D}$ tumors of high grade. We have found that by itself, PI3'K activation does not initiate tumors. This is important due to the current efforts to target the PI3'K pathway in the clinic. Patients with *PIK3CA* mutations may benefit from such therapy, but there also might be additional mutations that serve as drivers of tumor growth. AKT inhibition has no effect on BRAF driven tumorigenesis, and studies conducted by others show that PI3'K signaling plays no role in maintenance of KRAS driven tumors. Such work supports the use of combined therapy in the clinic.

Though it was not apparent that $PIK3CA^{H1047R}$ activation drove progression of $BRAF^{V600E}$ tumors, combining constitutive PI3'K signaling through mutational activation of PIK3CA or loss of PTEN (to a lesser degree) greatly enhanced the onset of tumors driven by $BRAF^{V600E}$ an effect dependent on signaling through AKT. The mechanism of such cooperation is of great interest. Cell lines isolated from mice have served as an initial means to interrogate this mechanism, and have shown that cells expressing $PIK3CA^{H1047R}$ have elevated levels of pro-growth and survival pathways as well as the ability to grow in soft agar. Though this system provides insights into mechanism of cooperation, additional in vivo experiments are needed to validate such observations.

Cooperation between $KRAS^{G12D}$ and $PIK3CA^{1047R}$ is a better system to study mechanism due to its clinical relevance. Initially, a better characterization of this cooperation will need to be conducted to the extent of what has been done with $BRAF^{V600E}$. First and foremost, it should be determined if this cooperation depends on AKT or if $PIK3CA^{1047R}$ expression has an influence of progression of KRAS tumors. Cell lines should also be isolated to determine relative expression levels, response to small molecule inhibitors, and the ability to grow in an anchorage independent manner. Further analysis of signal pathway activation in $KRAS^{G12D}$;

PIK3CA^{H1047R} tumors could provide candidates to further explore both in vitro and in vivo using shRNA techniques and small molecule inhibitors. Such strategies would determine if regulation of specific candidates is necessary or sufficient for the cooperation between PIK3CA^{H1047R} and KRAS^{G12D}. Crossing single and compound mutant mice with fluorescent reporters would allow for the isolation of individual tumor cells to determine if specific cell types or relative signal pathway activation levels determine cooperation. Such studies would provide invaluable insights into the initiation and progression of non-small cell lung cancer driven by KRAS^{G12D} and perhaps aid in the development of strategies to target this disease in human patients.

This work has also established that inflammation has an effect of BRAF^{V600E} induced tumorigenesis in the mouse lung. Interestingly, an inflammatory response brought on by loss of TGFß signaling enhanced tumor progression while Ovalbumin challenge decreased tumor multiplicity. These studies left open a number of questions that I unfortunately did not have time to address. Indeed, a great deal of further analysis is required to determine exactly what role inflammation plays. Initially, a better characterization of the inflammatory response used in each system is required to make any conclusions. Such experiments can also be repeated using *KRas*^{LSL} mice, which show evidence of tumor-associated inflammation and do progress to high-grade. Finally, further experiments involving induction of more specific types of inflammation could be conducted. This work is indeed important due to the various environmental insults encountered by people everyday that may cause pulmonary inflammation. Targeting inflammation in cancer patients may also serve as a viable source of cancer therapy.

CHAPTER 6: Materials and Methods

Mice and Adenovirus delivery

All experiments involving mice were conducted in accordance with protocols approved by the UCSF Institutional Animal Care and Use Committee (IACUC). *BRaf*^{CA} (*Braf*^{tm1Mmcm}), *KRas*^{LSL} (*Kras*^{tm4Tyj}), *Aqp5*$^{-/-}$, *LucRep* (*Tg(Actb-GFP-Luc*), *Trp53*^{flox} (*Trp53*^{tm1Brn}), *PIK3CA*$^{lat-1047R}$, *Pten*^{floxed} , and *ß6*$^{-/-}$ mice were bred and genotyped as previously described (17, 19, 25, 27, 40, 59, 67, 68). Stocks of Adenovirus encoding Cre recombinase (Ad-Cre) and AdβGal were purchased from Viraquest (North Liberty, IA) and intranasal instillation for infection of the mouse lung epithelium was performed as previously described (69). BrdU (Sigma) was administered at 10 mg/kg by intra-peritoneal injection either 4 or 20 hours prior to euthanasia.

For ovalbumin challenge studies, mice were sensitized with i.p. injection of 50μg ovalbumin (Sigma) and later challenged with intranasal instillation of 100 μg ovalbumin or phosphate-buffered saline (PBS).

Histology and quantitation of lung tumor burden

Lungs were removed and fixed in zinc buffered formalin and stored in 70% (v/v) ethanol prior to paraffin embedding. 5μm sections were cut and slides were Hematoxylin and Eosin (H&E) stained. H&E stained slides were scanned with the Aperio ScanScope scanner. Quantification was performed using Aperio Spectrum ImageScope viewing software. Tumor number and size were measured per lobe and

overall tumor burden was calculated as (area of lung lobe occupied by tumor)/ (total area of lobe) in μm^2.

Electron Microscopy of BRAF^{V600E}-induced lung tumors

Tumor bearing lungs from initiated *BRaf$^{CA/+}$* mice were removed 11 weeks after Ad-Cre infection and fixed in 2%(v/v) glutaraldehyde, 1%(v/v) paraformaldehyde in 0.1M Sodium Cacodylate buffer at pH 7.4. Following fixation, samples were incubated in 2%(v/v) Osmium Tetroxide in the same buffer. Samples were then stained in 2%(v/v) aqueous Uranyl Acetate, dehydrated in acetone, infiltrated and then embedded in LX-112 resin (Ladd Research Industries, Burlington, VT). Toluidine blue stained semi-thin sections were made to locate the areas of interest. Samples were ultrathin sectioned on a Reichert Ultracut S ultramicrotome and counter stained with 0.8% lead citrate. Grids were examined on a JEOL JEM-1230 transmission electron microscope (JEOL USA, Inc., Peabody, MA) and photographed with a Gatan Ultrascan 1000 digital camera and Digital Micrograph software (Gatan Inc., Warrendale, PA).

In vivo Drug treatments and bioluminescent imaging

In vivo studies: PD0325901 (Hansun Trading Co.) was formulated in 0.5%(w/v) Hydroxy-Propyl-Methylcellulose (HPMT, Sigma) and administered by oral gavage at 12.5 mg/kg per mouse once per day. MK-2206 (Merck) was formulated in 30% (w/v) Captisol (Ligand Technology, La Jolla, Ca.) and mice were dosed at 120 mg/mg. Mice carrying the *LucRep* transgene were injected with Firefly D-Luciferin (Gold Biotechnology) intra-peritoneally and were imaged 10 minutes later using the Xenogen IVIS 100 bioluminescent imaging system. Bioluminescent signal measured

in photons/second (p/s) was quantified using Live Image software (Caliper Life Sciences).

Immunostaining of mouse lung tissue and immunoblotting

Mouse lungs were fixed in formaldehyde overnight, processed, embedded in paraffin, cut into 5μm sections and mounted on glass slides. Citrate-mediated antigen retrieval was performed and then the following antibodies were used for detection: TTF-1, anti-SP-C; anti-RAGE, anti-gp38 (Santa Cruz); anti-AQP5 (Calbiochem); anti-BrdU (Roche); anti-Ki67 (abcam); anti-phospho-ERK1/2 (Thr202/ Tyr 204), anti-Vimentin, anti-phospho-AKT (Ser 473), anti-phospho-S6 (Ser235/ 236), and anti-PTEN (Cell signaling technology).

50μg aliquots of cell extract were analyzed by conventional immunoblotting using antisera against the following proteins: phospho-MEK1/2 (Ser 221), phospho-ERK1/2 (Thyr 202/ Thr204), total ERK1/2, Cleaved caspase 3, Cyclin D, phospho-AKT (Ser473), total AKT, phospho-PRAS 40 (Thr 246), phospho-FOX01 (Thr 24), phospho-S6 (Ser 235/236), phospho 4E-BP1 (Ser 65), phospho- GSK3ß (Ser 9), p27, ß-Actin (Cell Signaling Technology); BIM (Epitomics); Cdk2, and Cdk 4 (Santa Cruz). Immunoblots were visualized using the Odyssey FC system (Li-Cor) and Image Studio software.

Lung tumor cell isolation, culture and analysis

Lungs of tumor bearing mice were perfused with dispase (BD) and individual lobes were minced and incubated with 2 mg/mL dispase/ collagenase (Roche). Cell suspensions were then filtered and cultured in DMEM with 10%(v/v) normal calf serum. Recombination of the conditional *BRaf*^{CA} allele was verified using established genotyping protocols (2). Cells were selected for in DMEM containing

200μg G418. Cell proliferation assays were performed using Alamar Blue (Invitrogen) and CellTitre-Glo (Promega) Luminescence was detected using the Glo-Max microplate reader (Promega). Cell cycle analysis was conducted by propidium-iodide (PI) uptake and detection and FACS sorting using the FACSCalibur machine (Becton Dickinson). The pBabe Puro vector encoding bovine PIK3CA $p110\alpha^{H1047R}$ was provided by Dr. Frank McCormick (UCSF). The pBabe puro vector encoding HA tagged- AKT^{myr} was purchased from Adgene (Cambidge, MA.). The pBabe mcherry vector was provided by Xiaolin Nan from Oregon Health Sciences University (HSU). Ecotropic virus was produced by collection and filtration of supernatant derived from transiently transfected Plat-E cells. Soft agar colony formation was performed using 1.4% SeaPlaque low melting temperature agarose (Cambrex, Rockland, ME.) Colony counts were performed using a standard dissecting microscope. PD0325901 (Hansun Trading Co.), MK-2206 (Merck), GDC-0941 (Genentech), SCH772984 (Schering-Plough) were all dissolved in dimethyl sulfoxide (DMSO).

REFERENCES CITED

1. Herbst RS, Heymach JV, Lippman SM. Lung cancer. N Engl J Med 2008;359:1367-80.
2. Herbst RS, Lippman SM. Molecular signatures of lung cancer--toward personalized therapy. N Engl J Med 2007;356:76-8.
3. Lynch TJ, Bell DW, Sordella R, et al. Activating mutations in the epidermal growth factor receptor underlying responsiveness of non-small-cell lung cancer to gefitinib. N Engl J Med 2004;350:2129-39.
4. Choi YL, Soda M, Yamashita Y, et al. EML4-ALK mutations in lung cancer that confer resistance to ALK inhibitors. N Engl J Med;363:1734-9.
5. Heist RS, Engelman JA. SnapShot: non-small cell lung cancer. Cancer Cell;21:448 e2.
6. Pao W, Miller V, Zakowski M, et al. EGF receptor gene mutations are common in lung cancers from "never smokers" and are associated with sensitivity of tumors to gefitinib and erlotinib. Proc Natl Acad Sci U S A 2004;101:13306-11.
7. Schubbert S, Shannon K, Bollag G. Hyperactive Ras in developmental disorders and cancer. Nat Rev Cancer 2007;7:295-308.
8. Brose MS, Volpe P, Feldman M, et al. BRAF and RAS mutations in human lung cancer and melanoma. Cancer Res 2002;62:6997-7000.
9. Chaft JE, Arcila ME, Paik PK, et al. Coexistence of PIK3CA and other oncogene mutations in lung adenocarcinoma-rationale for comprehensive mutation profiling. Mol Cancer Ther;11:485-91.
10. Altomare DA, Testa JR. Perturbations of the AKT signaling pathway in human cancer. Oncogene 2005;24:7455-64.
11. Virmani AK, Fong KM, Kodagoda D, et al. Allelotyping demonstrates common and distinct patterns of chromosomal loss in human lung cancer types. Genes Chromosomes Cancer 1998;21:308-19.
12. Gysin S, Salt M, Young A, McCormick F. Therapeutic strategies for targeting ras proteins. Genes Cancer 2011;2:359-72.
13. Davies H, Bignell GR, Cox C, et al. Mutations of the BRAF gene in human cancer. Nature 2002;417:949-54.
14. Hollander MC, Blumenthal GM, Dennis PA. PTEN loss in the continuum of common cancers, rare syndromes and mouse models. Nat Rev Cancer;11:289-301.
15. Zhu J, Woods D, McMahon M, Bishop JM. Senescence of human fibroblasts induced by oncogenic Raf. Genes Dev 1998;12:2997-3007.
16. Spyridopoulos I, Isner JM, Losordo DW. Oncogenic ras induces premature senescence in endothelial cells: role of p21(Cip1/Waf1). Basic Res Cardiol 2002;97:117-24.

17. Jackson EL, Willis N, Mercer K, et al. Analysis of lung tumor initiation and progression using conditional expression of oncogenic K-ras. Genes Dev 2001;15:3243-8.
18. Jackson EL, Olive KP, Tuveson DA, et al. The differential effects of mutant p53 alleles on advanced murine lung cancer. Cancer Res 2005;65:10280-8.
19. Dankort D, Filenova E, Collado M, Serrano M, Jones K, McMahon M. A new mouse model to explore the initiation, progression, and therapy of BRAFV600E-induced lung tumors. Genes Dev 2007;21:379-84.
20. Ohren JF, Chen H, Pavlovsky A, et al. Structures of human MAP kinase kinase 1 (MEK1) and MEK2 describe novel noncompetitive kinase inhibition. Nat Struct Mol Biol 2004;11:1192-7.
21. Winslow MM, Dayton TL, Verhaak RG, et al. Suppression of lung adenocarcinoma progression by Nkx2-1. Nature 2011;473:101-4.
22. Shaw AT, Meissner A, Dowdle JA, et al. Sprouty-2 regulates oncogenic K-ras in lung development and tumorigenesis. Genes Dev 2007;21:694-707.
23. Rooney SA, Young SL, Mendelson CR. Molecular and cellular processing of lung surfactant. FASEB J 1994;8:957-67.
24. Yousem SA, Nikiforova M, Nikiforov Y. The histopathology of BRAF-V600E-mutated lung adenocarcinoma. Am J Surg Pathol 2008;32:1317-21.
25. Ma T, Song Y, Gillespie A, Carlson EJ, Epstein CJ, Verkman AS. Defective secretion of saliva in transgenic mice lacking aquaporin-5 water channels. J Biol Chem 1999;274:20071-4.
26. Engelman JA, Chen L, Tan X, et al. Effective use of PI3K and MEK inhibitors to treat mutant Kras G12D and PIK3CA H1047R murine lung cancers. Nat Med 2008;14:1351-6.
27. Lyons SK, Meuwissen R, Krimpenfort P, Berns A. The generation of a conditional reporter that enables bioluminescence imaging of Cre/loxP-dependent tumorigenesis in mice. Cancer Res 2003;63:7042-6.
28. Lowe D, Jorizzo J, Hutt MS. Tumour-associated eosinophilia: a review. J Clin Pathol 1981;34:1343-8.
29. Albanese C, Johnson J, Watanabe G, et al. Transforming p21ras mutants and c-Ets-2 activate the cyclin D1 promoter through distinguishable regions. J Biol Chem 1995;270:23589-97.
30. Schmid K, Oehl N, Wrba F, Pirker R, Pirker C, Filipits M. EGFR/KRAS/BRAF mutations in primary lung adenocarcinomas and corresponding locoregional lymph node metastases. Clin Cancer Res 2009;15:4554-60.
31. Slebos RJ, Kibbelaar RE, Dalesio O, et al. K-ras oncogene activation as a prognostic marker in adenocarcinoma of the lung. N Engl J Med 1990;323:561-5.
32. Bos JL. ras oncogenes in human cancer: a review. Cancer Res 1989;49:4682-9.
33. Feldser DM, Kostova KK, Winslow MM, et al. Stage-specific sensitivity to p53 restoration during lung cancer progression. Nature 2010;468:572-5.
34. Miller KA, Yeager N, Baker K, Liao XH, Refetoff S, Di Cristofano A. Oncogenic Kras requires simultaneous PI3K signaling to induce ERK activation and transform thyroid epithelial cells in vivo. Cancer Res 2009;69:3689-94.

35. Charles R-P, Iezza G, Amenodola E, Dankort D, McMahon M. Mutationally activated BRAF(V600E) elicits papillary thyroid cancer in the adult mouse. Cancer Res 2011:In Press.
36. Kim CF, Jackson EL, Woolfenden AE, et al. Identification of bronchioalveolar stem cells in normal lung and lung cancer. Cell 2005;121:823-35.
37. Sebolt-Leopold JS. MEK inhibitors: a therapeutic approach to targeting the Ras-MAP kinase pathway in tumors. Curr Pharm Des 2004;10:1907-14.
38. Ji H, Wang Z, Perera SA, et al. Mutations in BRAF and KRAS converge on activation of the mitogen-activated protein kinase pathway in lung cancer mouse models. Cancer Res 2007;67:4933-9.
39. Tsavachidou D, Coleman ML, Athanasiadis G, et al. SPRY2 is an inhibitor of the ras/extracellular signal-regulated kinase pathway in melanocytes and melanoma cells with wild-type BRAF but not with the V599E mutant. Cancer Res 2004;64:5556-9.
40. Kinross KM, Montgomery KG, Kleinschmidt M, et al. An activating Pik3ca mutation coupled with Pten loss is sufficient to initiate ovarian tumorigenesis in mice. J Clin Invest;122:553-7.
41. Trejo CL, Juan J, Vicent S, Sweet-Cordero A, McMahon M. MEK1/2 inhibition blocks development of autochthonous lung tumors induced by KRASG12D or BRAFV600E. Cancer Res.
42. Halilovic E, She QB, Ye Q, et al. PIK3CA mutation uncouples tumor growth and cyclin D1 regulation from MEK/ERK and mutant KRAS signaling. Cancer Res;70:6804-14.
43. Wee S, Jagani Z, Xiang KX, et al. PI3K pathway activation mediates resistance to MEK inhibitors in KRAS mutant cancers. Cancer Res 2009;69:4286-93.
44. Iwanaga K, Yang Y, Raso MG, et al. Pten inactivation accelerates oncogenic K-ras-initiated tumorigenesis in a mouse model of lung cancer. Cancer Res 2008;68:1119-27.
45. Gupta S, Ramjaun AR, Haiko P, et al. Binding of ras to phosphoinositide 3-kinase p110alpha is required for ras-driven tumorigenesis in mice. Cell 2007;129:957-68.
46. Yang Y, Iwanaga K, Raso MG, et al. Phosphatidylinositol 3-kinase mediates bronchioalveolar stem cell expansion in mouse models of oncogenic K-ras-induced lung cancer. PLoS One 2008;3:e2220.
47. Yeang CH, McCormick F, Levine A. Combinatorial patterns of somatic gene mutations in cancer. FASEB J 2008;22:2605-22.
48. Janku F, Lee JJ, Tsimberidou AM, et al. PIK3CA mutations frequently coexist with RAS and BRAF mutations in patients with advanced cancers. PLoS One;6:e22769.
49. Kang S, Bader AG, Vogt PK. Phosphatidylinositol 3-kinase mutations identified in human cancer are oncogenic. Proc Natl Acad Sci U S A 2005;102:802-7.
50. Engelman JA. Targeting PI3K signalling in cancer: opportunities, challenges and limitations. Nat Rev Cancer 2009;9:550-62.

51. Dankort D, Curley DP, Cartlidge RA, et al. Braf(V600E) cooperates with Pten loss to induce metastatic melanoma. Nat Genet 2009;41:544-52.
52. Kissil JL, Walmsley MJ, Hanlon L, et al. Requirement for Rac1 in a K-ras induced lung cancer in the mouse. Cancer Res 2007;67:8089-94.
53. Thiery JP, Acloque H, Huang RY, Nieto MA. Epithelial-mesenchymal transitions in development and disease. Cell 2009;139:871-90.
54. Song MS, Carracedo A, Salmena L, et al. Nuclear PTEN regulates the APC-CDH1 tumor-suppressive complex in a phosphatase-independent manner. Cell;144:187-99.
55. Courtois-Cox S, Genther Williams SM, Reczek EE, et al. A negative feedback signaling network underlies oncogene-induced senescence. Cancer Cell 2006;10:459-72.
56. Greer EL, Brunet A. FOXO transcription factors at the interface between longevity and tumor suppression. Oncogene 2005;24:7410-25.
57. Mirza AM, Gysin S, Malek N, Nakayama K, Roberts JM, McMahon M. Cooperative regulation of the cell division cycle by the protein kinases RAF and AKT. Mol Cell Biol 2004;24:10868-81.
58. Khwaja A, Rodriguez-Viciana P, Wennstrom S, Warne PH, Downward J. Matrix adhesion and Ras transformation both activate a phosphoinositide 3-OH kinase and protein kinase B/Akt cellular survival pathway. EMBO J 1997;16:2783-93.
59. Huang XZ, Wu JF, Cass D, et al. Inactivation of the integrin beta 6 subunit gene reveals a role of epithelial integrins in regulating inflammation in the lung and skin. J Cell Biol 1996;133:921-8.
60. Kumar RK, Herbert C, Foster PS. The "classical" ovalbumin challenge model of asthma in mice. Curr Drug Targets 2008;9:485-94.
61. Ji H, Houghton AM, Mariani TJ, et al. K-ras activation generates an inflammatory response in lung tumors. Oncogene 2006;25:2105-12.
62. Sparmann A, Bar-Sagi D. Ras-induced interleukin-8 expression plays a critical role in tumor growth and angiogenesis. Cancer Cell 2004;6:447-58.
63. Joyce JA, Pollard JW. Microenvironmental regulation of metastasis. Nat Rev Cancer 2009;9:239-52.
64. Ochoa CE, Mirabolfathinejad SG, Ruiz VA, et al. Interleukin 6, but not T helper 2 cytokines, promotes lung carcinogenesis. Cancer Prev Res (Phila);4:51-64.
65. Costello R, O'Callaghan T, Sebahoun G. [Eosinophils and antitumour response]. Rev Med Interne 2005;26:479-84.
66. Brown DW, Young KE, Anda RF, Giles WH. Asthma and risk of death from lung cancer: NHANES II Mortality Study. J Asthma 2005;42:597-600.
67. Jonkers J, Meuwissen R, van der Gulden H, Peterse H, van der Valk M, Berns A. Synergistic tumor suppressor activity of BRCA2 and p53 in a conditional mouse model for breast cancer. Nat Genet 2001;29:418-25.
68. Trotman LC, Niki M, Dotan ZA, et al. Pten dose dictates cancer progression in the prostate. PLoS Biol 2003;1:E59.

69. Fasbender A, Lee JH, Walters RW, Moninger TO, Zabner J, Welsh MJ. Incorporation of adenovirus in calcium phosphate precipitates enhances gene transfer to airway epithelia in vitro and in vivo. J Clin Invest 1998;102:184-93.

Publishing Agreement

It is the policy of the University to encourage the distribution of all theses, dissertations, and manuscripts. Copies of all UCSF theses, dissertations, and manuscripts will be routed to the library via the Graduate Division. The library will make all theses, dissertations, and manuscripts accessible to the public and will preserve these to the best of their abilities, in perpetuity.

Please sign the following statement:

I hereby grant permission to the Graduate Division of the University of California, San Francisco to release copies of my thesis, dissertation, or manuscript to the Campus Library to provide access and preservation, in whole or in part, in perpetuity.

Author Signature

7/9/2012

Date